AD NUMBER

AD486617

LIMITATION CHANGES

TO:

Approved for public release; distribution is unlimited. Document partially illegible.

FROM:

**Distribution authorized to U.S. Gov't. agencies and their contractors;
Administrative/Operational Use; JUN 1966. Other requests shall be referred to Rome Air Development Center (EMATE), Griffiss AFB, NY 13440. This document contains export-controlled technical data.**

AUTHORITY

USAF per ltr, 17 Sep 1971

HIGH POWER MICROWAVE COMPONENTS IN OVERSIZED WAVEGUIDE

John P. Quine
Cousby Younger
J. J. Jarek

AFLC, GAFB, N.Y., 29 Jul 66-71

FOREWORD

This interim report was prepared by John P. Quine, Cousby Younger, and J.J. Jarek of General Electric Co., Schenectady, New York, under Contract AF 30(602)-3682, project no. 4506, task no. 450602. Period covered 17 September 65 to 17 March 66. RADC project engineer was Vincent C. Vannicola(EMATE).

Release of subject report to the general public is prohibited by the Strategic Trade Control Program, Mutual Defense Assistance Control List (revised 6 January 1965) published by the Department of State.

This report has been reviewed and is approved.

Vincent C. Vannicola

Approved: VINCENT C. VANNICOLA
Project Engineer
Electron Devices Section

Approved: ARTHUR J. FROHLICH
Chief, Techniques Branch
Surveillance & Control Division

Abstract

The purpose of this investigation is to develop components for oversized waveguide configurations for which a/λ and b/λ are in the range of 1.5 - 2.25 for the TE_{10} mode in rectangular waveguide and where D/λ is at least 1.7 for the TE_{01} mode in circular waveguide. The components considered shall include E- and H-plane bends, mode absorbers, 3 db directional couplers, pressure windows, resonant rings and rotary joints. Where necessary, the theoretical and computer studies shall be verified before design data is finalized. These components may be developed through whatever design concepts are necessary to assure high peak and high average power.

The present report presents experimental results at X-band for -3 db multi-hole side wall directional couplers. These couplers employ tapers along the coupling region to reduce the waveguide width from 2.800" to 2.050". The reduction in width is necessary in order to increase the coupling per unit length. In this way a -3 db coupler having a length equal to 45" can be obtained. A method is described for cancelling the mode conversion caused by the tapers by means of metal and dielectric wedges placed on the side walls.

Experimental results are presented for an X-band mode absorber in which the TE_{30} mode in the 2.800" wide oversized waveguide is coupled to 0.933" wide waveguide by means of side wall slots. Experimental results are also presented for a mode absorber for the TE_{mn}, TM_{mn} degenerate mode pairs. In this case a length of waveguide having an hexagonal cross section is employed to remove the degeneracy.

TABLE OF CONTENTS

1.0 INTRODUCTION

The purpose of this program is the development of components for oversized waveguide having high power handling capability. Components for both rectangular and circular waveguides will be considered; however, emphasis will be placed on rectangular waveguide components. Both waveguide dimensions for the rectangular waveguide components will range between 1.5 to 2.25 free space wavelengths, and the diameter of the circular waveguide components will be at least 1.7 free space wavelengths. The design objective is to develop components capable of carrying 5 megawatts of peak power and 100 kilowatts of average power, and which can operate over at least a 5% bandwidth at X band, with spurious mode levels below -20db.

Highest priority will be given to the development of a -3 db multi-hole directional coupler, mode absorbers, resonant rings, and pressure windows. E-plane bends, quasi-optic couplers, transducers from the rectangular waveguide $TE_{10}^{\square}$ mode to the circular waveguide TE_{01}° mode, non-hybrid power dividers, and E-plane bends will also receive attention.

2.0 MULTI-HOLE SIDE WALL DIRECTIONAL COUPLERS IN OVERSIZED RECTANGULAR WAVEGUIDES

In Reference 2 the problem of obtaining the relatively large values of coupling per unit length required for a - 3 db coupler of reasonable length (44") was considered. One approach investigated was the use of hole spacings of the order of $3\lambda/4$. It had been hoped that such spacings would allow the use of large apertures, and would result in high values of coupling per unit length along with high directivity. Theoretical and experimental results were presented, however, which showed that the spacings of the coupling holes must be less than $\lambda/2$ in order to prevent resonances in the coupling characteristics, associated with the formation of "grating waves".

A second approach which was investigated was to decrease the waveguide width from 2.800" to 2.050" in order to obtain greater coupling per unit length for a given hole size and spacing. Experimental results for this approach are presented in the following sections.

2.1 EXPERIMENTAL RESULTS WITH WIDTH REDUCTION TAPERS

A design for a 22" variable curvature taper for reducing the waveguide width from 2.800" to 2.050" was described in Section 2.43 of Reference 2. In the past period fabrication and testing of this taper were completed. Figure 2.1 shows the measured values of the spurious mode voltages for the taper alone. These data were obtained using the directional coupler test assembly shown in Figures 2.15a and b of Reference 2. In this case a pair of the 22" tapers were assembled along one of the side walls and the common side wall normally containing the coupling apertures was replaced by a solid conducting wall. It is seen that the measured values of the spurious mode voltages for the two tapers in cascade are unexpectedly high. The theoretical value for a single taper had been estimated to be less than - 30 db. (See Section 2.43 of Reference 2.)

Figure 2.2 shows measured values of the spurious mode voltages in Port 3 (the coupled port) for a - 3.4 db (at 9.0GHz) directional coupler employing the variable curvature taper and a constant hole spacing d = 0.600", constant strip widths W = 0.050" and constant strip thickness t = 0.100". These relatively poor results were attributed to a poor distribution function for the coupling along the coupling region. Since constant strip widths and spacings were employed, the distribution of the coupling was determined solely by the variation of the waveguide width along the coupling region.

Calculations were performed to determine how the strip widths should be varied along the coupling region in order to obtain a desirable distribution function for the coupling. It was found that with the variable curvature tapers, a satisfactory distribution of the coupling could not be obtained as a result of the relatively rapid decrease of waveguide width in the region near the center of the coupler. In this region the coupling is not required to change very rapidly in the case of typical desirable coupling distributions that may be employed.

Experiments were also carried out with straight tapers as shown in Figure 2.3. Figure 2.4 shows spurious mode voltages measured for a pair of straight tapers each having a length T = 10.112" separated by a straight section having width = 2.050" and length S = 23.776". It is seen that the spurious mode voltages generated by these tapers alone is below -25 db in a narrow frequency band centered near 8.7GHz. Figures 2.5 and 2.6 show the spurious mode voltages for a -2.5 db (at 9.0GHz) directional coupler employing these tapers. In this case a 44" uniform grating having W = 0.075, t = 0.100" and d = 0.600" was employed. It is seen that the values of the spurious mode voltages measured for the directional coupler are somewhat higher than the values measured with the taper alone.

Figures 2.7 and 2.8 show the measured spurious mode voltages for a -2.7 db (at 9.0GHz) directional coupler employing the same straight tapers as described above, but with a tapered hole distribution designed to produce a coupling distribution, $k_{101}^{102}(z)$ given by* $0.0121 \sin \frac{\pi z}{L} + 0.0026$, where z is the distance measured along the coupling region of length L = 44.6" (75 coupling holes). By comparing Figures 2.5 and 2.7 and Figures 2.6 and 2.8, it can be concluded that the spurious mode voltages obtained with the tapered hole distribution are not significantly lower than those obtained with the uniform hole distribution. It appears that the principal effect of the change in the coupling distribution has been to shift the frequencies at which maximum and minimum values of spurious mode voltages occur. This led to the conclusion that the discrete discontinuities in the width reduction taper were the principal sources of mode conversion.

As a result of the above conclusion it was decided to try a longer straight taper. Figure 2.9 shows the measured spurious mode voltage obtained with a pair of straight tapers each of length, T = 15.600" and separated by a section of

*k_{101}^{102} is defined as the coupling between the TE_{10} modes in the two coupled waveguides 1 and 2.

straight waveguide of length S = 15.600". This combination of S and T resulted when a minimum strip width of 0.050" at the center of the coupling region and a monotonic variation of coupling along the coupling region were specified. A strip width of 0.050" was considered the minimum allowable value as a result of considerations of high CW power.

The data in Figure 2.9 for the 15.600" tapers should be compared with the data shown in Figure 2.4 for the 10.112" tapers. Both sets of data were obtained in the same way. Since mode conversion for each discontinuity in a straight taper is inversely proportional to the taper length;* it had been expected that the average spurious mode level with the 15.6" tapers would be roughly 3 db lower than with the 10.112" tapers. It is seen that this expectation was certainly not borne out in the case of the TE_{20} mode. Apparently, the spurious mode voltages produced at the four discrete taper discontinuities in the 15.600" tapers added constructively at frequencies around 9.1GHz to produce a - 14 db value for the ratio TE_{20}/TE_{10}. The measured values for a - 2.7 db (at 9.0GHz) directional coupler employing these tapers are shown in Figures 2.10 and 2.11. Inspection of these data again leads to the conclusion that the tapers produce a major part of the mode conversion in the directional coupler.

The poor results obtained with both the variable curvature taper and with the straight taper configurations led to the conclusion that it would be difficult to design tapers having low mode conversion over reasonably broad frequency band widths by employing several discrete taper discontinuities. In such tapers one must rely on a cancellation of the spurious mode voltages from the several taper discontinuities, with cancellation being required in both output ports. The problem of predicting the frequencies at which cancellations occur is made difficult by the fact that coupling holes affect the modal propagation constants. A change in the coupling distribution would therefore

* See Appendix 1.

upset the taper design, and a change in the taper of course affects the coupling.

For these reasons it was decided to investigate techniques for compensating each of the discrete taper discontinuities individually by means of compensating devices. By placing the compensating device close to the discontinuity one should be able to achieve low spurious mode voltages over a broad frequency bandwidth. Two approaches for compensating the individual taper discontinuities are described in the next section.

2.2 EXPERIMENTAL RESULTS WITH COMPENSATED TAPERS

Figure 2.12 shows the transmission characteristics of the coupler whose predominately TE_{20} spurious mode conversion characteristics are presented in Figures 2.10 and 2.11. The swept frequency test signal was fed into port 1 through a low mode converting taper from WR112 waveguide to the 2.800" x 2.500" oversized waveguide. The signal was removed from the port under test through a second taper from oversized to WR112 waveguide. The other ports were terminated in multimode loads. This resulted in some trapping and resonating of the spurious mode energy particularly when measuring port 1 to port 2 transmission characteristics as can be seen by the rather severe spurious TE_{20} mode resonance absorption dips in Figure 2.12. Thus the swept frequency transmission characteristics of the coupler were used as a qualitative measure of the magnitude of the total spurious mode conversion coefficients. The purpose of the compensating devices described in the following was to minimize the TE_{20} spurious mode conversion without excessive excitation of other spurious modes.

Since it had been concluded that the directional coupler width tapers were the major cause of the excessive TE_{20} spurious mode levels (see Sect. 2.1), it was reasoned that a first order compensation might be made by working with the tapers alone, i. e., with the coupling hole grating replaced with a solid wall. Four discrete discontinuities, consisting of abrupt changes of side wall direction are seen to exist. The experimental procedure was simplified by eliminating the TE_{20} mode discontinuities at transverse planes I and IV by canting the input and output waveguides through one-half the ramp angle, θ, as shown in Figure 2.13. This in effect changes the input junctions from assymmetrical H-plane tapers which excite predominantly the TE_{20} mode to symmetrical H-plane tapers which excite predominantly the TE_{30} mode. With a 15.6" long

symmetrical taper the TE_{30} mode generation was very low.

Having eliminated generation of the TE_{20} mode at planes I and IV, efforts were concentrated on experimentally compensating the tapers at planes II and III with dielectric wedges. The use of dielectric and metal wedges to compensate the TE_{20} mode is discussed in more detail in Appendix 1. Briefly, however, the dielectric wedge, at plane II for example, serves to slow down one side of the cylindrical phase fronts approaching from the left in Figure 2.13 so that they became more nearly planar and perpendicular to the axis of the guide when they are launched into the uniform width section of guide beyond plane II. Wedges are considered a better approach to TE_{20} mode compensation than a complete lens for this particular application from the standpoint of power handling ability. The wedge obviously can be more readily cooled than a lens, and therefore should handle more average power. To prove the feasibility of dielectric wedge compensation, polystyrene wedges and rectangular parallelepipeds of various b, h, and ℓ dimensions were inserted at planes II and III and the swept frequency transmission characteristics were recorded. The parameters b, h and ℓ were adjusted until the TE_{20} spurious mode absorption resonances were essentially eliminated. This corresponded to the parameter combination: ' = 1", h = 1/8", 1 = 1/8".

Once the tapers alone were compensated the coupling grating and the secondary arm of the coupler were installed. Polystyrene wedges identical to those in the primary arm were installed in the secondary arm. Figure 2.14a shows the transmission characteristics with this first order compensation. An improvement was noted when compared to Figure 2.12, but further second order adjustments were still needed. In comparing Figures 2.12 and 2.14a it should be noted that the coupling aperture distribution was changed from $k_{101}^{102} = 0.0026 + 0.0121 \sin \frac{\pi Z}{L}$ for Figure 2.12 to $k_{101}^{102} = 0.147 \sin \frac{\pi Z}{L}$ for Figure 2.14a. This

change was made in order to adjust the coupling to - 3 db near 9.0 GHz.

Figure 2.15 shows the result of one second order adjustment. In this case the canted waveguides formerly attached to ports 1 and 2 were replaced with straight sections and compensation at planes I and IV was made using both dielectric and metal wedges. Dielectric wedges were used on the side wall containing the coupling aperture and metal wedges were used on the exterior side walls. The dielectric wedge tends to slow down the portion of the phase front passing near it while the metal wedge tends to speed up the portion of the phase front in its vicinity. The result is that the wave is launched into the taper region with a tilted plane phase front which more nearly approximates the cylindrical phase fronts characteristic of the tapered region.

Figures 2.16 and 2.17 show the measured spurious mode conversion at ports 2 and 3, respectively, for the straight tapered coupler with all wedge compensation as indicated in Figure 2.15. It will be noted that the TE_{20} mode conversion was less than - 22 db over the frequency band from 7.5 to 9.0 GHz. This should be compared to the value of - 16 db obtained in the frequency band from 7.5 to 8.7 GHz for the same taper without compensation (see Figures 2.10 and 2.11).

Tests were also performed with the input waveguides at ports 1 and 2 canted by an angle = $\theta/2$ (Figure 2.13) in order to acomplish partial compensation at these ports. Further compensation was then obtained with metal and polystyrene wedges added at planes I and IV. The compensation at ports 3 and 4 was not changed from that of Figure 2.15. Figure 2.18 shows the measured coupling characteristics, and Figures 2.19 and 2.20 show the measured spurious mode conversion at ports 2 and 3, respectively. The overall results are substantially the same as when wedge compensation alone was employed (Figure 2.15 - 2.17).

The results described above represent only the first attempt at reducing the spurious mode conversion in the - 3 db directional couplers. It is believed that more refined adjustments of the wedge compensators can result in further reductions in the mode conversion. In order to expedite these more refined adjustments mode selective directional couplers have been constructed. These are now being calibrated and will be described in the next report. Use of these couplers will make possible a rapid adjustment of the wedge compensators to their optimum configuration. Thus, the spurious mode levels at the output ports will be monitored as a function of frequency (with a pen recorder or an oscilloscope) as the compensating wedges are adjusted.

3.0 MODE ABSORBER DEVELOPMENT

Previous work on mode absorbers is described in Section 6 of Reference 1 and Section 3 of Reference 2. During the past period this development was continued and results are presented in the following sections.

3.1 TE_{30} MODE ABSORBER

A detailed description for this mode absorber is given in Section 3.1 of Reference 2. The following characteristics were measured during the past period:

a. Reflection coefficient for desired TE_{10} mode in main waveguide.

b. Coupling from TE_{10} mode in main waveguide to TE_{10} mode in side waveguides.

c. Spurious mode conversion in main waveguide.

d. Overall insertion loss for desired TE_{10} mode in main waveguide.

e. The Q of the main waveguide for the TE_{10} mode was also measured, from which the TE_{10} mode attenuation constant was calculated. This was a check of d. above.

f. Spurious mode absorption for the TE_{20}, TE_{30} and TE_{40} modes.

The measured reflection coefficient for the TE_{10} mode in the main waveguide was below - 40 db over the frequency range between 7.5 to 10 GHz. The measured coupling from the TE_{10} mode in the main waveguide to the TE_{10} mode in the side waveguides was below - 45 db in the frequency range between 7 and 10 GHz. This measurement was made by means of a 12" taper from the 2.500" x 0.930" side waveguide to 1.122" x 0.497" standard waveguide.

The spurious mode conversion in the main waveguide was measured by probing the field[3] on the top wall at the output of the mode absorber with a pure TE_{10} mode applied at the input port of the mode absorber and with the mode

absorber terminated in a multi-mode matched load. The results of these measurements indicated that the spurious mode conversion was below - 30 db for the TE_{20}, TE_{30} and TE_{40} modes in the frequency range between 8 and 10.0 GHz except at 9.5 GHz where the measured value of mode conversion for the TE_{30} mode was - 29 db. It should be noted that a mode conversion loss of - 30 db corresponds to an insertion loss of approximately 0.0045 db to the desired TE_{10} mode.

The overall insertion loss for the TE_{10} mode in passing through the TE_{30} mode absorber was determined by simply measuring the difference in the transmission between a generator and a detector with and without the mode absorber inserted. The insertion loss determined in this way was lower than 0.05 db over the frequency range between 7 and 10 GHz. The results of the Q measurements indicated that the TE_{10} mode attenuation in the mode absorber is approximately 0.03 db. This should be compared with a theoretical value of 0.01 db for an equal length of aluminum waveguide having the same cross sectional dimensions as the main waveguide in the mode absorber. Further tests are planned to determine whether the 0.03 db attenuation measured for the mode absorber is caused by the reduced effective conductivity of the slotted side walls. It should be noted that this may turn out to be the case, since the side walls were formed with brass strips clamped between aluminum top and bottom wall plates. (See Figure 3.1 of Reference 2.)

The absorption of the spurious modes was measured by an insertion loss method. The equipment employed for these measurements is shown in Figure 3.1. Spurious TE_{no} modes were generated at the abrupt discontinuity between the 1.800" x 2.500" and the 2.800" x 2.500" oversized waveguides. The absorption loss was determined by measuring with the top wall probe the level of the spurious modes with and without the mode absorber in place.

With the 1.800" dimension centered on the 2.800" dimension, only the TE_{30} spurious mode is generated at the discontinuity. Figure 3.2 shows the results obtained in this case. The quantity E_{30}/E_{10} is the ratio of the TE_{30} mode voltage to the TE_{10} mode voltage. It is seen that the mode conversion caused by the centered H-plane step alone is relatively independent of frequency and has a value of approximately - 8.5 db. The relative frequency independence of the measured mode conversion results partly from the fact that very low back scattering in any mode occurs when the junction is fed from the small waveguide side.

The TE_{30} mode absorption is the difference between E_{30}/E_{10} with and without the mode absorber, and it is seen that this is a decreasing function of frequency which has a value of 6.0 db at approximately 8.8 GHz. A mode absorption of 6.0 db represents an absorption of 75% of the incident TE_{30} mode power.

The mode absorber was actually designed (see Section 3.1 of Reference 2) to have an infinite mode absorption (100% absorption of the incident TE_{30} mode power) at frequencies centered about 9.0 GHz. A study of the possible reasons for the discrepancy between the theoretical and measured value of mode absorption disclosed that an error was made in the original theoretical analysis. Just below equation 3.2 in Reference 2 it is stated that the coupling with a slot on each side wall is equal to twice the coupling obtained with a single slot. This statement is in error, because the coupling with the two slots is actually only $\sqrt{2}$ times the coupling with a single slot. Thus, with the slot dimensions employed the total coupling is less than the value required for complete power transfer between an incident TE_{30} mode in the main waveguide and the TE_{10} modes in the two side waveguides. For complete power transfer a value of integrated coupling of $\pi/2$ is required. Assuming a value of integrated coupling equal to $\frac{\pi}{2\sqrt{2}}$ instead, one calculates a value of - 7 db

for the mode absorption, which agrees reasonably well with the measured value.

The mode absorption was also measured for the TE_{20} and TE_{40} modes. In order to generate these modes the axes of the 1.800" and 2.800" waveguides were offset in the H-plane. Figures 3.3, 3.4, and 3.5 show results obtained with a 0.500" offset. Figure 3.3 shows that in this case the ratio of TE_{20}/TE_{10} is approximately - 2 db, and is essentially the same with or without the mode absorber. The mode absorption for the TE_{20} mode is therefore very small. Figure 3.4 shows similar results for the TE_{40} mode. Note, however, that the level of the TE_{40} mode generated by the step discontinuity is of the order of -20 db. Figure 3.5 shows that with a 0.500" offset the generated TE_{30} mode is well below -20 db relative to the TE_{10} mode. Although the mode absorption for the TE_{30} mode can also be calculated from these data, the results would be much less accurate than those given in Figure 3.2.

Figure 3.6 shows the levels of the spurious modes that are generated when a 0.250" offset is employed. In this case substantial power is obtained in all of the spurious modes. This adjustment would be convenient to use, because a single set of measurements can yield accurate absorption data for all of the spurious modes.

3.2 MODE ABSORBER FOR THE TE_{mn}, TM_{mn} DEGENERATE MODE PAIRS

A theoretical description of a mode absorber for the TE_{mn}, TM_{mn} degenerate mode pairs employing oversized waveguide of hexagonal cross section was given in Section 6 of Reference 1 and Section 3.2 of Reference 2. During the past period fabrication of this mode absorber was completed and electrical tests were carried out.

The results of these tests show that more efficient mode absorption can be obtained by employing unslotted hexagonal waveguide in conjunction with short lengths of slotted rectangular waveguide. This configuration has important advantages over the configuration previously proposed (References 1 and 2) which employs slotted hexagonal waveguide.

3.2.1 RECTANGULAR TO HEXAGONAL WAVEGUIDE TRANSITIONS

Aluminum mandrels for gradual transitions from rectangular to hexagonal waveguide are shown in Figure 3.4 of Reference 2. The dimensions for these transitions are shown in Figure 3.7 of the present report. Two each of these transitions having lengths equal to 7.0" and 10.0" were electroformed. These are shown in Figure 3.8.

The spurious mode conversion produced by these transitions was measured using the Klinger method.[4] Figures 3.9 and 3.10 show measured values of the spurious mode conversion for single 7" and 10" long transitions. These data were obtained by employing a moveable short circuit in the hexagonal waveguide. The short circuit was of the non-contacting choke type; the dimensions of the chokes were the same as for the rectangular waveguide short circuit shown in Figure 2 of Reference 5. In making these measurements the transition was fed from the rectangular waveguide side by a 24" variable curvature taper which transformed the standard size rectangular waveguide (1.112" x 0.497") to the oversized rectangular waveguide (2.800" x 2.500"). Spurious mode conversion for this taper has been measured to be below - 35 db in the frequency range of interest (see Section 3.2 of Reference 1).

Inspection of the data in Figures 3.9 and 3.10 shows that the TE_{12} and TM_{12} modes are the strongest spurious modes. This was expected from considerations based on the symmetry of the transition. It was also expected that the TE_{30} mode would be excited by the transitions. The data indicate, however, that the level of this mode is quite low.

As is usually done in the measurement of spurious mode conversion by the Klinger[4] method, the spurious modes were identified by their wavelength. The TE_{mn} and TM_{mn} modes form a degenerate mode pair, each member of the pair having the same wavelength. For this reason it is not possible to distinguish between

the individual modes of a degenerate pair in rectangular waveguide by noting the positions of the moveable plunger which cause resonance. In the case of hexagonal waveguide, however, the modes corresponding to the TE_{mn}, and TM_{mn} in rectangular waveguide are not degenerate, and it is, therefore, possible to distinguish these modes from one another by noting the resonant positions of the moveable plunger. For instance by extrapolating data calculated under Contract AF30(602)-2990 (Reference 1) by H. Meinke, one obtains $\lambda c/a = 1.185$ for the TE_{11} (HEX) and $\lambda c/a = 0.75$ for the TE_{12} (HEX). Using these values for $\lambda c/a$, the hexagonal waveguide wavelengths were calculated as a function of frequency. Measured values of the wavelengths for the TE_{11} (HEX) and the TE_{12} (HEX) modes were found to agree in most cases to within 1% of the calculated values.

Figures 3.11 and 3.12 show data for 7" and 10" transitions tested in pairs with the hexagonal ends connected together. The Klinger measurement was performed with a non-contacting choke type moveable shorting plunger in the rectangular waveguide following the second transition. Inspection of the data in Figures 3.11 and 3.12 shows that the TE_{12} and TM_{12} are the strongest spurious modes when the transitions are tested in pairs; this was also the case for the single transitions. When tested in pairs, the TE_{12} spurious modes generated by each of the transitions appear to add constructively near 8.6 GHz to produce approximately 4 db more mode conversion than for a single transition. The total mode conversion for two transitions was below - 25 db for the 7" transitions and below - 30 db for the 10" transitions over the frequency range from 7.4 to 9.8 GHz.

The measured results obtained with the two lengths of transition show that a 10" transition length is required to insure that the spurious mode conversion produced by the pair of transitions is less than - 30 db. It should be recalled,

however, that no analysis was performed to determine the optimum transition shape which leads to a minimum transition length for a given mode conversion. The results obtained above apply for transitions having a $\sin^2 \frac{\pi z}{2L}$ variation for the angle of the hexagon (see Figure 3.7). A future analysis may reveal that substantially shorter lengths of transitions can result, if a different transition shape is employed.

3.2.2 ABSORPTION BY RESONANT SLOTS IN RECTANGULAR WAVEGUIDE

According to the theory developed in Section 6.2b of Reference 1, maximum spurious mode absorption occurs in the hexagonal waveguide with slotted side walls when the attenuation constant per unit length, α of the side wall composite modes (horizontally polarized) has a value equal to 2k. In this case k is the coupling per unit length between the horizontally and vertically polarized composite modes. It was also pointed out in the above references that exact satisfaction of the condition, $\alpha = 2k$ is not necessary, since the mode absorption does not vary rapidly as a function of α near the maximum value. Experiments were carried out to determine the validity of the theory developed in References 1 and 2. The results of these investigations show that the slotted hexagonal waveguide is not the optimum mode absorber configuration. Instead, the optimum configuration now appears to be a length of unslotted hexagonal waveguide used in conjunction with short lengths of slotted rectangular waveguide.

The value of α produced by resonant slots in oversized rectangular waveguide carrying the TE_{10} mode was measured. In this case transverse slots were centered on both the top and bottom walls, in order to obtain maximum coupling to the longitudinal current of the TE_{10} mode. It was reasoned that when operation is far above cutoff, the value of α measured in this way would be very nearly the same as the values of α for the TE_{1n}, TM_{1n} modes in hexagonal waveguide of similar size having slots centered on both side walls.

Figures 3.13 and 3.14 show the slotted rectangular waveguide with the absorbing loads employed to absorb the energy radiated by the slots. As can be seen in the photograph, thin brass dividers were used to decouple the individual slots from one another. Tight electrical contact between the dividers and the waveguide wall was obtained by applying pressure to the individual dividers through a rubber gasket and an aluminum pressure plate. Each slot in

this case radiates into a parallel plate region. The absorbing material* was shaped in the form of wedges as shown in order to provide a gradual matched termination for the parallel plate medium, and to prevent energy leakage from the open sides of the parallel plates. The parts for the absorbing load assembly were constructed so that they could be used either with the rectangular waveguide with slots on top and bottom walls for attenuation measurements, or with hexagonal waveguide with slots on the side walls to form a mode absorber.

Figure 3.15 shows the slot dimensions. These were designed to be resonant at 9.0 GHz using a formula derived for a single slot radiating into free space.(7) Measurements were made with 25, 50, and 75 slot pairs, each pair consisting of a slot on the top and bottom walls. The total absorption was very nearly proportional to the total number of slot pairs, and was equal to approximately 0.96 db per slot pair at the slot resonant frequency. Figure 3.16 shows the results for 25 slot pairs. It is seen that the resonant frequency is approximately 8.0 GHz instead of 9.0 GHz as calculated for the single slot in free space. Evidently, the slot has a lower resonant frequency in the environment of the parallel plate medium.

The value of α required to satisfy the condition $\alpha = 2k$ can be determined from equation 6.9 of Reference 1. Thus,

$$\alpha = 2k = 0.4 \left(\frac{b_c - b_s}{b} \right) \pi \frac{\lambda}{a^2} \qquad 3.1$$

The value of the ratio $(b_c - b_s)/ b$ is equal to 0.4 for the hexagonal waveguide dimensions shown in Figure 3.7 ($b_c = 3.000"$, $b_s = 2.000"$, $b = 2.500"$).

* The absorbing material employed is Radite 75, supplied by Radar Design Corporation, Syracuse, New York.

Letting d = the slot spacing, one obtains

$$\alpha d = 0.16\,\pi\,\frac{\lambda d}{a^2} \qquad 3.2$$

Letting

$\lambda = 1.313"$ (9.0 GHz)

$d = 0.400"$

$a = 2.800"$

There results

$\alpha d = 0.341$ nepers

$\alpha d(db) = 8.686 \times 0.0341 = 0.296$ db

This value of α should be compared with the measured value of approximately 0.96 db given above for resonant slots in rectangular waveguide.

It is also interesting to compare the measured value with the value of α calculated for a single slot radiating into free space. The following formula can be used to calculate the normalized series resistance introduced by a single half wave resonant slot centered on the broad wall of a rectangular waveguide[7]

$$\frac{R}{Z_{10}} = 0.523 \left(\frac{\lambda 10}{\lambda}\right)^3 \left(\frac{\lambda^2}{ab}\right) \cos^2 \frac{\pi\lambda}{4a} \qquad 3.3$$

where all symbols have their usual meanings. The attenuation for a pair of such slots on opposite broad walls is given by

$$\alpha d = \frac{R}{Z_{10}} \qquad 3.4$$

where d is the slot spacing.

Letting

$f = 8.0$ GHz, $\lambda = 1.48"$

$a = 2.8"$ $b = 2.5"$,

the calculated value of αd is 0.869 db. This is unexpectedly close to the measured value of 0.96 db given above for a pair of slots radiating into parallel plate medium.

In Section 3.22 of Reference 2 a short discussion is given of experimental results reported in Reference 8 for centered transverse slots radiating from the broad wall of a WR-284 waveguide into a secondary WR-137 waveguide. In these experiments the axes of the two waveguides were 90° apart to form a slot coupled E-plane T-junction. Slots having lengths equal to 1.00" and 0.75" resonated at approximately 6.4 GHz and 8.0 GHz, respectively, and the resulting coupling values from the WR-284 to the WR-137 waveguides were - 10 db and - 12 db, respectively, at the resonant frequencies. These values of coupling correspond to coupling losses of 0.45 db and 0.28 db, respectively. The corresponding values of $\frac{R}{Z_{10}}$ are 0.0259 and 0.0161, respectively. Use of equation 3.3 yields $\frac{R}{Z_{10}} = 0.11$ for the 1" slot resonated at 6.4 GHz; it is seen that this is approximately four times the measured value of 0.0259 reported in Reference 7 for the 1" slot coupling the WR-284 and WR-137 waveguides.

It appears, therefore, that it is reasonable to conclude from the above results that equation 3.3 produces fairly accurate results when applied to slots radiating into free space, or into a parallel plate medium. However, too high a value of $\frac{R}{Z_{10}}$ is obtained from this equation when the slot is radiating into a narrow width secondary waveguide. Apparently, the fact that the narrow width secondary waveguide has only a single propagating mode causes the total power radiated from the slot to be less than in the case of radiation into free space or into a parallel plate medium. In the latter two cases the energy from the slot radiates into a continuous spectrum of propagating modes.

Some further conclusions concerning the properties of waveguide slots should be mentioned. In Reference 8 it is shown that the attenuation obtained with several slots is very nearly equal to the attenuation obtained with a single slot multiplied by the total number of slots. This implies that the

effect of neighboring slots on the leakage from any one slot is small. The reflection coefficient from an array of many slots can also be fairly small. For example, with the array of 100 slot pairs described above the reflection coefficient for the TE_{10} mode was below - 26 db over the frequency range from 7.0 to 9.5 GHz.

3.2.3 EXPERIMENTAL RESULTS WITH SLOTTED HEXAGONAL WAVEGUIDE MODE ABSORBER

Figure 3.17 shows two 4' lengths of electroformed hexagonal waveguides. On one of these the side walls have been machined to a uniform thickness equal to 0.090", and a total of 100 slots have been cut along the center of each side wall, with a spacing equal to 0.400". The slot dimensions are the same as shown in Figure 3.15, except that the 0.583" dimension was decreased to 0.500". This was done in order to shift the resonant frequency from 8.0 GHz to approximately 9.0 GHz. Figure 3.18 shows the slotted hexagonal waveguide assembled with the absorbing loads.

Measurements were performed to determine the reflection coefficient and insertion loss for the TE_{10} mode, and the absorption of the spurious modes. The reflection coefficient experienced by the TE_{10} mode was below - 36 db in the frequency band between 7.5 and 10.0 GHz. The measured insertion loss experienced by the TE_{10} mode was below 0.05 db in this same frequency range.

The absorption of the spurious modes was measured by an insertion loss method. For this purpose, use was made of the E-plane wedge shown in Figure 3.19. The wedge was placed at the output of a 24" long taper from standard 1.122" x 0.497" waveguide to 2.800" x 2.500" oversized waveguide. With a TE_{10} mode incident on the wedge, the TE_{10} mode and the TE_{1m}, TM_{1m} degenerate mode pairs are transmitted beyond the wedge, with very little energy reflected in any mode. The measured TE_{10} mode reflection produced by the wedge was below - 36 db from 7.0 to 10.0 GHz. An approximate theoretical calculation of the amplitudes of the spurious modes generated by the wedge is given in Appendix 2.

The TE_{1m} and TM_{1m} modes in each of the degenerate mode pairs generated by the wedge have just the right amplitudes to cause the cross polarized component of the electric field of each pair to be zero everywhere in the transverse plane. The

degenerate mode pairs generated by the wedge are, therefore, the vertically polarized composite mode pairs described in Section 6 of Reference 1. These modes have longitudinal currents along the top and bottom walls, but none along the side walls. It is these modes that the hexagonal waveguide mode absorber must be designed to absorb.

The mode absorption was determined by probing the field along the top wall of the waveguide beyond the wedge with and without the mode absorber inserted between the wedge and the probe. The field was probed along an existing 36" long section of 2.800" x 2.500" waveguide having a "holey" top wall as shown in Figure 3.20. The longitudinal hole spacing is 0.200". One line of holes is located along the center of the top wall. Other lines of holes are located at distances equal to $\pm$ a/6 and $\pm$ a/4 from the center of the waveguide where a is the waveguide width. As a result of the symmetry of the system only the TE_{1m}, TM_{1m} modes are present in significant amounts. It was therefore necessary to probe along only the center line of holes. This was done using an electric field probe with a bolometer detector. The probe was detuned to obtain stability. For these measurements the "holey" waveguide was terminated in a multi-mode matched load. By plotting the variation of the probe voltage along the length of the "holey" waveguide section, it was possible to calculate the relative amplitudes of the spurious modes relative to the TE_{10} mode. The mode absorption produced by the mode absorber was taken as the difference between the calculated spurious mode levels with and without the mode absorber in place.

Figure 3.21 shows the result obtained at 8.8 GHz without the mode absorber. Measurements were made at every 10th hole along the 36" length of "holey" waveguide. The strong beat between the TE_{10} and the vertically polarized TE_{11}, TM_{11}

spurious mode pair is clearly evident. Note that the points for minimum and maximum probe voltage are separated by $\lambda_{b11}/2$ where λ_{b11} = 36" at 8.8 GHz is the beat wavelength between the TE_{10} mode and the TE_{11}, TM_{11} mode pair. The small ripple on the curves can be readily identified as a superimposed beat between the TE_{10} and the TE_{12}, TM_{12} spurious mode pair. The beat wavelength λ_{b12} between these modes is equal to 8.3" at 8.8 GHz.

One can determine the ratio of the amplitudes of the spurious modes from the ratio of the minimum to the maximum probe voltage. This ratio has been termed the $(VSWR)_{mn}$ (because of the analogy with standing wave phenomena). Figure 3.21 shows that $(VSWR)_{11}$ is approximately 19.5 db. This corresponds to an amplitude of - 1.8 db for the TE_{11}, TM_{11} mode relative to the TE_{10} mode. Values of - 2.3, - 2.2, - 2.3, and - 2.0 db were obtained at f = 8.4, 8.6, 9.0, and 9.2 for this ratio. The relative constancy of this ratio as a function of frequency was expected from consideration of the properties of the thin wedge (see Appendix 2). As expected, the amplitudes of the TE_{12}, TM_{12} modes were low, and of the order of - 20 db relative to the TE_{10} mode.

Figure 3.22 shows the results obtained at 8.8 GHz when the mode absorber with 100 slot pairs was inserted between the wedge and the holey waveguide probe section. It is seen that the effect of inserting the mode absorber was to reduce the value of $(VSWR)_{11}$ from 19.5 db to 9.2 db. Since a value of the $(VSWR)_{11}$ = 9.2 db corresponds to a value of - 6.3 db for the ratio of the TE_{11}, TM_{11} mode relative to the TE_{10} mode, the mode absorption is equal to 6.3 - 1.8 or 4.5 db.

Figure 3.23 shows the results obtained when 50 of the 100 slot pairs were covered with aluminum foil from the outside of the waveguide, rendering them dissipationless. The value of the $(VSWR)_{11}$ in this case is only 1.6 db, corresponding to a value of - 21 db for the ratio of the TE_{11}, TM_{11} mode relative to the TE_{10} mode. The mode absorption in this case is 21 - 1.8 = 19.2 db.

Figure 3.24 shows the results of more extensive measurements made in the frequency band between 8.4 and 9.2 GHz. Inspection of these data shows that a maximum in the mode absorption is obtained when approximately 50 of the slot pairs are covered, rendering them dissipationless. These results cannot be explained by the theoretical considerations given in previous sections of this report or in References 1 and 2. An explanation will be given in the following section.

3.2.4 INTERPRETATION OF THE EXPERIMENTAL RESULTS

The data in Figure 3.24 show that much higher values of mode absorption can be obtained when some of the slots are covered with aluminum foil. From these results it was concluded that a new and more efficient mode of operation for the hexagonal waveguide mode absorber can be obtained through the use of unslotted or lossless hexagonal waveguide.

When lossless hexagonal waveguides are used the vertically and horizontally polarized composite TE_{mn}, TM_{mn} modes are essentially degenerate, and are coupled to one another. In Section 6.28 of Reference 1 the coupling coefficient k_{mn} between the vertically and horizontally polarized composite modes was shown to be equal to $\Delta\text{-}B/2$ where $\Delta\text{-}B$ is the difference in propagation constant between the TE_{mn} and the TM_{mn} modes comprising the composite modes. Thus,

$$k_{mn} = \frac{\pi}{\lambda}\left[\sqrt{1 - \left(\frac{\lambda}{\lambda_c}\right)^2_{TE_{mn}}} - \sqrt{1 - \left(\frac{\lambda}{\lambda_c}\right)^2_{TM_{mn}}}\right] \qquad (3.5)$$

Values of λ_c calculated by Meinke were given in Reference 1 for the case of a hexagonal waveguide having the ratio $b/a = 0.9$ where b is the average height and a is the width of the hexagonal waveguide. Measured values of λ_c are given below in Table 3.1 for the hexagonal waveguide dimensions employed in the present experiments. For this waveguide $b = (b_c + b_s)/2 = 2.500"$, $a = 2.800"$, $b_c = 3.000$, $b_s = 2.000$, $(b_c - b_s)/2 = 0.4$.

Table 3.1

Cutoff Wavelengths for Modes in Hexagonal Waveguide

Mode	λ_c/a	Mode	λ_c/a
TE_{11}	1.185	TE_{12}	0.75
TM_{11}	1.373	TM_{12}	0.86

Using the data in Table 3.1 in Equation 3.5 values of 0.066 and 0.1855 result for $k_{11}\lambda$ and $k_{12}\lambda$, respectively at a frequency of 9.0 GHz.

It can be seen that a hexagonal waveguide transforms energy from an incident vertically polarized composite mode to a horizontally polarized composite mode. Assuming that a vertically polarized composite mode of unit amplitude is incident on the lossless hexagonal waveguide at the point $z = 0$, the normalized voltage amplitudes E_v and E_h of the vertically and horizontally polarized composite modes are given by [9]

$$|E_v| = \cos k_{mn} z \tag{3.6}$$

$$|E_h| = \sin k_{mn} z \tag{3.7}$$

Thus at $z = 0$ there results $|E_v| = 1$, and $|E_h| = 0$; at $z = \pi/2k_{mn}$ there results $|E_v| = 0$, and $|E_h| = 1.0$. Once the power which is incident in the vertically polarized mode has been converted to the horizontally polarized composite mode, it can be dissipated by means of side wall slots. These slots can be placed on the side walls of the rectangular waveguide following the transition from hexagonal to rectangular waveguide.

The above mode of operation of the mode absorber which employs lossless hexagonal waveguides can be compared to the previously considered mode of operation which employs slotted hexagonal waveguides. The solution to the coupled line equations for the slotted waveguide case must consider the loss which is present[9]. These solutions, however, take on relatively simple forms when one assumes that the slots introduce loss only to the horizontally polarized composite mode, and that the attenuation constant α for this mode is equal to $2k_{mn}$. It should be recalled that the condition $\alpha = 2k_{mn}$ results in the most efficient mode absorption when a slotted hexagonal waveguide is employed. Thus, for a wave of unit amplitude incident in the vertically polarized mode, the solutions are

*Equation 3.5 is derived in Section 6.2b of Reference 1.

$$|E_v| = e^{-k_{mn} z} \left[1 + k_{mn} z\right] \tag{3.8}$$

$$|E_h| = k_{mn} z e^{-k_{mn} z} \tag{3.9}$$

Values of the composite mode voltages for z = L calculated from equation 3.6, 3.8 and 3.9 are shown plotted in Figure 3.25. Inspection of these curves show that $|E_v|$ for $\alpha = 0$ obtained from equation 3.6 is a periodic function of $k_{mn}L$ with period equal to $\pi/2$, whereas $|E_v|$ for $\alpha = 2k_{mn}$ decreases monotonically with increasing values of $k_{mn}L$. It should be noted that for values of $k_{mn}L$ less than approximately 2.0, $|E_v|$ for $\alpha = 0$ is less than $|E_v|$ for $\alpha = 2k_{mn}$.

The experimental results shown in Figure 3.24 can be compared to the theoretical data shown in Figure 3.25 by considering Figure 3.26. This shows the dimensions of the components employed in the experiments. It is now desired to calculate the mode absorption that should be expected for the several experimental conditions for which data is given in Figure 3.24. Consider first the amount of mode absorption that should be expected under optimum conditions with the slotted hexagonal waveguide mode of operation ($\alpha = 2k_{mn}$). From equation 3.5 a value of 0.066 was calculated for $k_{11}\lambda$ at 9.0 GHz. This result can be expressed as

$$k_{11}L = 0.066\ L/\lambda \tag{3.10}$$

at 9.0 GHz. For L = 40", λ = 1.313" one obtains $k_{11}L = 2.01$. Referring to the curve labeled $|E_v|$ ($\alpha = 2k_{mn}$) in Figure 3.25, it is seen that the theoretical maximum mode absorption under optimum conditions ($\alpha = 2k_{11}$) is equal to approximately 8 db. This should be compared to the measured value of approximately 4.5 db obtained with no slots covered (Figure 3.24). However, the measured value of 4.5 db with no slots covered resulted from the combined effects of the 40" slotted section and the sections of unslotted hexagonal waveguides contained in the system.

The mode absorption produced by the unslotted hexagonal waveguide will now be calculated. First, it can be easily shown that the 10" transition in which the angle of the hexagonal cross section (Figure 3.7) varies gradually according to $\sin^2 \frac{\pi Z}{2L}$ has an effective coupling length which is equivalent to that of a 5" length of hexagonal waveguide having $(b_c - b_s)/b = 0.4$. It can be seen from Figure 3.26, therefore, that the effective length of lossless hexagonal waveguide on either side of the slotted waveguide is equal to 10". The value of $k_{11}L$ at 9.0 GHz for each of these 10" effective lengths can be determined from equation 3.10, and is equal to 0.502. The value of the mode absorption produced by each of these 10" effective lengths of lossless hexagonal waveguide can be determined from the curve labeled $|E_v|$ ($\alpha = 0$) in Figure 3.25. Thus for $k_{11}L = 0.502$ an absorption of approximately 1.2 db results. The absorption for the two 10" lengths separated by the slotted hexagonal waveguide is 2.4 db. Power converted from the vertically polarized to the horizontally polarized composite modes by the transition and straight sections on the generator side of the slotted waveguide is absorbed by the slotted hexagonal waveguide. Power converted by the transition and the straight sections on the output side of the slotted waveguide is not detected by the holey top wall probe, and is absorbed in the multi-mode load located beyond the probe. Thus, 2.4 db of the4.5db mode absorption measured with all slots covered must be attributed to the lossless hexagonal waveguide mode of operation. This means that a mode absorption of only 2.1 db occurred due to the slotted hexagonal waveguide mode of operation, compared to a maximum possible value of 8 db obtained when $\alpha = 2k_{11}$. Evidently, the condition $\alpha = 2k_{11}$ was not met at the frequencies at which measurements were made. From Section 3.22 it can be concluded that α was too high. This reduced the amount of power transfer per unit

length which could occur between the vertically and horizontally polarized composite modes in the slotted hexagonal waveguide.

The following table gives the effective length of lossless hexagonal waveguide as a function of the number of slots covered. This also gives the value of $k_{11}L$ and the mode absorption for the TE_{11}, TM_{11} composite mode pair at 9.0 GHz.

Table 3.2

No. of Slots Covered	Effective Length of Hexagonal Waveguide (inches)	$k_{11}L$ (radians)	TE_{11}, TM_{11} Mode Absorption (db)
0	10	0.502	2.4 db
37	24.8	1.25	11
50	30	1.51	>25
65	36	1.81	16

In Table 3.2 the effective lengths refer to the lengths on the generator side of the slotted waveguide. A fixed 10" length of lossless waveguide was assumed on the load end of the slotted waveguide which produced a fixed value of absorption equal to 1.2 db. The data for the calculated mode absorption given in Table 3.2 show that a maximum mode absorption should occur for 50 holes covered. This agrees well with the experimental data given in Figure 3.24. Reasonably good agreement between the theoretical and experimental results was also obtained for 37 and 50 holes covered. These results seem to verify the fundamental idea that the coupling coefficient, k_{mn} is given by the difference in propagation constants between the TE_{mn} and TM_{mn} modes comprising the coupled composite modes.

3.2.5 A CONFIGURATION FOR A MODE ABSORBER EMPLOYING LOSSLESS HEXAGONAL WAVEGUIDE

Figure 3.27 shows a configuration for a mode absorber which employs lossless hexagonal waveguide in conjunction with rectangular waveguides having slotted side walls. This is designed to absorb both the vertically and horizontally polarized composite TE_{mn}, TM_{mn} modes incident on either end. For example, the horizontally polarized modes, E_h, which enter the mode absorber are absorbed immediately in the slotted rectangular waveguide sections placed on both ends of the mode absorber. A vertically polarized composite mode, E_v, which enters the mode absorber passes by the slotted rectangular waveguide section without loss. As this mode passes through the lossless hexagonal waveguide section, however, it is transformed to the horizontally polarized mode in accordance with equations 3.6 and 3.7. The horizontally polarized mode is then absorbed in the slotted rectangular waveguide at the output end of the mode absorber.

The slotted rectangular waveguides contain slots on both side walls. Transverse slots are placed at distances equal to b/4 from the center of the side wall where b is the width of the side wall. Slots located in this manner will provide absorption for both the TE_{11}, TM_{11} and the TE_{12}, TM_{12} horizontally polarized composite modes. In the case of the TE_{11}, TM_{11} modes the absorption with the pair of slots is approximately the same as with a single centered slot. From the data given in Section 3.2.2 it can be seen that approximately 20 slot pairs are required on each side wall in order to obtain 20 db absorption. With a slot spacing of 0.400" in the axial direction the length of each of the slotted rectangular waveguides, therefore, is approximately 8".

The absorption of the desired TE_{10} mode by the slots is very small, since this mode has no longitudinal current anywhere on the side walls. It should be

noted that in the case of the slotted hexagonal waveguide, only centered transverse slots could be employed, since the longitudinal current for the TE_{10} mode is zero only along the center of the side wall of the hexagonal waveguide. In this case the slotted hexagonal waveguide mode absorber could not absorb the TE_{1n}, TM_{1n} composite modes for which n is even.

The possibility of lower loss for the desired TE_{10} mode and the ability to absorb the TE_{12}, TM_{12} composite modes represent important advantages for the configuration shown in Figure 3.27. The question arises, however, as to whether the length of the lossy hexagonal waveguide section can be selected in order to permit absorption of both the TE_{11}, TM_{11} and the TE_{12}, TM_{12} composite modes. For this to occur it must be possible to select the values of kL for these modes so that cos kL (equation 3.6) is small for both modes. Using the data in Table 3.1 it can be shown that $k_{11}\lambda$ and $k_{12}\lambda$ have values of 0.066 and 0.1855, respectively, at 9.0 GHz. The ratio k_{12}/k_{11} is therefore equal to 2.81. It is seen, therefore, that if $k_{11}L$ is made equal to $\pi/2$ (L = 31.3", if f = 9.0 GHz), in order to obtain high absorption of the TE_{11}, TM_{11} composite mode, the value of $k_{12}L$ would be equal to 4.41 radians or 253 degrees. In this case cos $k_{12}L$ would be equal to 0.282 corresponding to an absorption of 11 db for the TE_{12}, TM_{12} composite mode. Since k_{mn} is approximately proportional to λ, high absorption for both modes would occur over a relatively broad frequency bandwidth.

One further point should be made concerning the configuration shown in Figure 3.27. Since the hexagonal waveguide is no longer required to be slotted in order to provide absorption for the TE_{mn}, TM_{mn} composite modes, the possibility now suggests itself of incorporating the TE_{mn}, TM_{mn} and TE_{30} mode absorbers into a single structure. It may be possible to couple the hexagonal waveguide to narrower waveguides having width equal to approximately a/3 in

order to absorb the TE_{30} mode. Since the narrower width waveguides have low loss, and are much narrower than the hexagonal waveguide, the wavelengths of the horizontally polarized TE_{mn}, TM_{mn} composite modes in the hexagonal waveguide may not be significantly perturbed by the presence of the slots. In this case the horizontally and vertically polarized composite modes would remain essentially degenerate and equations 3.6 and 3.7 would still apply.

4.0 RESONANT RING DEVELOPMENT

A -17 db side wall directional coupler between two waveguides having width a= to 2.800" and height b= 2.500" was designed and fabricated. Coupling is achieved through full height slots formed with strips having thickness t = 0.100" and a minimum width w = 0.100". The strip width w is varied along the 30" long coupling region in order to produce a sinusoidal coupling distribution. With these strip dimensions it will be possible to water-cool the strips in order to realize the design objective of 1.0 megawatt of CW power at X-band. It is planned to use the compact H-plane bends[1] having (R/a = 1.48 for the resonant ring. These bends have low mode conversion over a 5% frequency bandwidth centered at $a/\lambda = 2.0$.

The -17 db coupler described above was assembled in the directional coupler test fixture (Figures 2.15a and b of Reference 2) and tested for VSWR, coupling, and spurious mode generation over the frequency band from 7.5 to 9.5 GHz. Measured VSWR was below 1.02, and the coupling was approximately -16.5 db. The measured TE_{30} mode level was below -24 db in the above frequency range. The measured TE_{20} mode level, however, was approximately -15 db in the region near 9.0 GHz and decreased steadily to -22 db near 7.5 GHz. Calculations based on loose coupling theory now show that the theoretical spurious mode conversion for the TE_{20} mode which is a function of the variable θ/π (1,9) has one of its maxima in the above frequency range. The function can be shifted off this maximum by a small fractional change in the length of the coupling region, or by a change in the coupling distribution. This can be readily accomplished with the directional coupler test fixture and the adjustments will be further expedited with the aid of the mode selective directional couplers (Section 2.2).

An analysis has been performed of a resonant cavity configuration employing a directional coupler as a coupling element. The results of the analysis show

the effect of coupler losses on cavity resonance buildup. The characteristics of the resonant cavity which can be readily assembled with existing components are similar to those of a resonant ring, and it is planned to perform a few simple experiments with the resonant cavity configuration in order to determine losses and tuning characteristics. These experiments will be performed before the design of the coupler for the resonant ring is finalized. Results will be presented in the next report.

5.0 CONCLUSIONS AND RECOMMENDATIONS

5.1 -3 db MULTI-HOLE COUPLER DEVELOPMENT

During the past period it was demonstrated that the tapers employed to reduce the waveguide width along the coupling region (in order to obtain higher coupling per unit length) are the principal source of spurious mode conversion. Techniques were developed for reducing the spurious mode conversion from this source. These techniques employ tapered dielectric and metal wedges placed on the side walls to transform the wavefronts from planar to cylindrical. The use of canted input waveguides for accomplishing this same purpose was also demonstrated. Using these techniques spurious mode amplitudes in all ports were reduced to -22 db or lower over the frequency band from 7.5 to 8.7 GHz. These represent preliminary results, and it is hoped that the spurious modes can be reduced to even lower levels with more refined adjustments.

5.2 MODE ABSORBER DEVELOPMENT

Experimental results obtained with the mode absorber for the TE_{30} mode demonstrated that it is possible to couple the TE_{30} mode from the main waveguide with only small effect on the desired TE_{10} mode. It was shown that the relatively small insertion loss experienced by the TE_{10} mode was caused mostly by dissipation effects, mode conversion loss being negligible. Q measurements indicate an insertion loss of 0.03 db for the mode absorber, whereas smooth unperturbed waveguide of the same length and material (aluminum) as the mode absorber would have 0.01 db insertion loss due to dissipation. It should be noted that the experiments were performed with a mode absorber assembly which was bolted together all along its 36" length. The top and bottom walls of the main waveguide in this assembly were aluminum, and the side walls were the

coupling gratings which were made from brass. It is believed that a copper electroformed model would exhibit substantially lower insertion loss for the TE_{10} mode.

The experimental results obtained with the hexagonal waveguide mode absorber for the TE_{mn}, TM_{mn} composite modes have shown close agreement with theory. In particular the results verify the theoretical analysis which showed that the coupling coefficient k_{mn} between the vertically and horizontally polarized composite TE_{mn}, TM_{mn} modes is equal to the propagation constant difference between the TE_{mn} and the TM_{mn} modes comprising the composite modes.

A new configuration for the hexagonal waveguide mode absorber has been defined which employs unslotted hexagonal waveguide in conjunction with short lengths of slotted rectangular waveguide connected to each end of the hexagonal waveguide through transitions. This new configuration has important advantages over the previously proposed configuration employing slotted hexagonal waveguide. The advantages are lower loss for the desired TE_{10} mode, and the ability to absorb all of the TE_{mn}, TM_{mn} composite modes. Further work will be directed towards combining the TE_{30} mode absorber and the TE_{11}, TM_{11} mode absorber into a single structure.

5.3 RECOMMENDATIONS FOR FURTHER WORK ON OVERSIZED WAVEGUIDE SYSTEMS BEYOND PRESENT CONTRACT

It now appears that under the present contract AF 30 (602) -3682 a successful design will be achieved for the -3 db directional coupler. Successful designs will also be achieved for mode absorbers for the TE_{30} mode and the TE_{11}, TM_{11} composite modes. These components will represent important additions to the list of oversized rectangular waveguide components available for systems use of oversized rectangular waveguides. The list of components that will be available stands as follows:

1. Tapers
2. Bends
3. -20 db Multi-Hole Directional Coupler
4. Spark Gap Switches
5. Mica Pressure Windows
6. Matched Power Divider - Oversized Rectangular Waveguide to 8 Standard Size Rectangular Waveguides
7. Mode Absorbers
8. -3 db Multi-Hole Directional Coupler

Under Contract AF30(602)-3682 work will also be directed towards development of a resonant ring capable of carrying 1.0 megawatts of CW power, and a -3 db compact quasi-optical coupler.

The number and variety of the available components listed above suggests that one avenue for future work beyond the present contract AF30(602)-3682 should be the demonstration of systems in which several oversized components are employed together to achieve higher power levels than can be achieved with standard size components. One relatively simple system could be a narrow pulse generator employing the spark gap switch and the -3 db coupler to discharge a resonant cavity formed with oversized rectangular waveguide.

The spark-gap switches were developed under contract AF30(602)-3544 to the point where they are now satisfactory for systems use. Higher operating powers could be achieved, however, by pressurizing with clean dry gas at slightly above atmospheric pressure in order to prevent spurious triggering effects. Very high operating power levels could be achieved by operating the spark gap switch at high pressure. In either case the switch could be pressurized with the simple mica window which has been tested under contract AF30(602)-3682 (see Reference 2). The use of tungsten electrodes for achieving longer switch life should also be investigated. It now appears that it should be possible to generate narrow X-band pulses of at least 10 megawatts peak power without pressurization using the spark-gap switch and the -3 db coupler. Even higher powers should be possible with pressurization.

Further work should also be carried out on the low pressure gaseous electronics switch employing a Penning electrode configuration. Switches of this type were also investigated under contract AF30(602)-3544. These investigations were exploratory in nature, and were confined to cold cathode configurations in standard size WR112 waveguide at 9.0 GHz with miliwatt power levels.

Although high plasma densities and lower switching times may be expected with hot cathodes and high microwave power levels, the results obtained with the cold cathode Penning switch at low microwave power levels were surprisingly good. Using hydrogen gas in the micron pressure range, and a magnetic field of approximately 5000 gauss, reflection coefficients ranging from -2 to -1.0 db and switch isolation greater than 24 db were obtained. Switching times ranged between 50 and 100 nonoseconds. This performance compares favorably with that reported previously[13] for the hot cathode thyratron at high microwave power levels, and strengthens the prediction that the hot cathode Penning discharge will result in an ultra-low loss microwave switch.

Further work on the Penning switch should be directed along the following lines:

a. Test the cold cathode switch in WR112 waveguide with high microwave power levels. This switch with associated vacuum system which was developed under contract AF30(602)-3544 is still in place, and only a minimum bake out effort would be required to restore the system to its original condition. The results of the high power tests would show whether hot cathodes are actually required in order to attain ultra low reflection loss and very short switching times. If hot cathodes are not actually required, a truly rugged switch configuration will have been attained. It should be noted that such a switch would find application in standard size as well as oversized waveguide systems.

b. Further development efforts should also be directed towards realizing a Penning discharge switch in oversized rectangular waveguide with hot or cold cathodes depending on the results of item a above. One of the major problems to be solved with the oversized waveguide switch is the control of spurious modes. The use of two or more plasma columns in a single transverse plane in the oversized waveguide, however, shows promise of providing a satisfactory solution to this problem.

6.0 LIST OF REFERENCES

1. J. P. Quine, C. Younger, J. W. Maurer, "Ultra High Power Transmission Line Techniques," RADC-TR-65-164 Final Report Contract AF 30(602)-2990; September 1965

2. Progress Report No. 1 (March 16 to September 16, 1965) "Ultra High Power Transmission Line Techniques", Contract AF 30(602)-3682

3. M. P. Forrer and K. Tomiyasu, "Determination of Higher Order Propagating Modes in Wave-Guide System", Journal of Applied Physics, July 1958, Vol. 29, No. 7, pp. 1040-1045

4. Y. Klinger, "The Measurement of Spurious Modes in Over-Moded Waveguides," Proc. IEE Part B Supplement, Convention on Long Distance Transmission by Waveguide, Jan. 1959, pg. 89

5. RADC-TDR-64-414, Fifth Quarterly Report for Contract AF 30(602)-2990, "Ultra High Power Transmission Line Techniques", October 1964

6. S. B. Cohn, "Microwave Coupling by Large Apertures, Proc. IRE June 1952, pp. 696-698

7. S. Silver, "Microwave Antenna Theory and Design," MIT Radiation Laboratory Series, Vol. 12, McGraw-Hill 1949; pp. 291-295

8. V. G. Price, R. H. Stone, V. Met, "Harmonic Suppression by Leaky-Wall Waveguide Filter," 1959 IRE WESCON Convention, San Francisco, Aug. 18-21, 1959

9. S. E. Miller, "Coupled Wave Theory and Waveguide Applications", Bell System Technical Journal, Vol. 33, May 1954

10. L. Solymar, "Design of a Conical Taper in Circular Waveguide System Supporting H_{01} Mode", PROC, IRE, March 1958, pp. 618-619

11. L. Solymar, "Mode Conversion in Pyramidal-Tapered Waveguides", Electronic and Radio Engineering, Dec. 1959, pg. 461

12. J. P. Quine, "E and H-Plane Bends for Oversized Rectangular Waveguide", IEEE Transactions on Microwave Theory and Techniques, Vol. MIT-13, Jan. 1965

13. H. Goldie, "A Fast Broad Band High-Power Microwave Switch", Research Report No. PIB MRI-1111-63, Contract AF 30(602)-2135, Feb. 1963

Appendix 1

Spurious Mode Conversion Produced by Tapers and Methods for Compensation

First, the spurious mode conversion produced by the taper discontinuities will be calculated. Figure A1 shows the tapered coupler. As is well-known an arbitrary excitation of the input ports 1 or 2 can be resolved into modes having even and odd symmetry about the plane of the coupling grating. Consider first the even modes. Figure A1a shows the even component of the incident TE_{10} mode on either port 1 or 4. The transverse field distributions of the even modes excited in the taper region depend on the coupling per unit length resulting from the coupling grating. Figures A1b and A1c show the limiting forms for the transverse field distribution for the desired even mode and the first two higher order spurious even modes. Thus, in Figure A1b, for loose coupling, the coupling grating closely approximates a perfectly conducting wall. In this case the desired mode is equivalent to the TE_{10} mode, and the first two spurious modes are equivalent to the TE_{20} and TE_{30} modes in unperturbed waveguide of width equal to a. On the other hand, in Figure A1c, for very tight coupling, the common wall is essentially completely removed. In this case the desired mode is equivalent to the TE_{10} mode, and the first two spurious modes are equivalent to the TE_{30} and TE_{50} modes in unperturbed waveguide of width equal to 2a.

For the modes having odd symmetry about the grating plane, this plane is a plane of zero tangential electric field, and can, therefore, be replaced with a perfectly conducting plane without disturbing the odd modes. On either side of the grating plane, therefore, the odd modes have the same transverse field distributions as the even modes under loose coupling conditions.

It can be seen therefore that the spurious mode conversion coefficients should be calculated for the two extreme cases represented by Figures Alb and Alc. For the odd modes, or for the even modes under very loose coupling, the mode conversion coefficients can be calculated from the following formula.

$$\frac{E_{mo}}{E_{10}} = \frac{2a}{\pi\lambda}\left(\frac{a_2-a_1}{T}\right)\frac{4m}{(m^2-1)^2} \qquad \text{(a1)}$$

Equation a1 was derived by a method employed by Solymar[10] to derive the spurious mode conversion coefficients in tapered circular waveguide carrying the TE_{01} mode. In equation a1 the mode index m can take on the integer values, m = 2, 3, 4, 5 · · ·), and the factors a_1, a_2 and T are defined in Figure A1. The factor a, without subscript, is equal to a_1 or a_2, depending on whether the mode conversion is being calculated at the interface between taper and rectangular waveguide of width a_1 or a_2. In deriving this formula, it was assumed that the modes being considered were for above cutoff. It is believed that the mode conversion coefficient for a spurious mode near cutoff is lower than the value calculated from equation a1.

The spurious mode conversion coefficients for the even modes in the limit of very tight coupling (Figure Alc) can be calculated from formulas published by Solymar[1,11] for rectangular waveguide tapers. In this case the mode conversion coefficient for the spurious TE_{30} mode in the double width waveguide can be calculated from the following formula derived from Solymar's results.

$$\frac{E_{30}}{E_{10}} = (0.152)\ \frac{\pi}{4}\ \frac{a}{\lambda}\left(\frac{a_2-a_1}{T}\right) \qquad \text{(a2)}$$

Note that the even modes of Figure Alc transform into the corresponding even modes of Figure Alb as they travel into regions of looser coupling. For this reason the TE_{30} mode in the double width waveguide can be considered to be a "distorted" TE_{20} mode of the single width waveguide. Using this point of view

the TE_{20} mode can be considered the strongest spurious mode for all values of coupling.

As an example of the use of the above formulas, consider the following case.

$a_1 = 2.800$ $\qquad$ t = grating thickness = 0.100"

$a_2 = 2.050"$ $\qquad$ $\lambda = 1.313"$ (9.0 GHz)

$T = 15.000"$

Using equation a1 there results

$$\left(\frac{E_{20}}{E_{10}}\right)_{a = 2.80"} = -24.4 \text{ db}$$

$$\left(\frac{E_{20}}{E_{10}}\right)_{a = 2.05"} = -27.34 \text{ db}$$

For this case equation a1 shows that the TE_{30} mode in the single width waveguide is -13.5 db relative to the TE_{20} mode.

Using equation a2 there results

$$\left(\frac{E_{30}}{E_{10}}\right)_{a = 5.700"} = 25.74 \text{ db}$$

$$\left(\frac{E_{30}}{E_{10}}\right)_{a = 4.200"} = -28.4 \text{ db}$$

In this case a has been set equal to 5.700" and 4.200" to account for the double width waveguide plus the grating thickness. Equation a2 actually applies only at the a_1 taper cross section, since loose coupling is always employed near the a_2 cross section.

The above calculated values of mode conversion for the individual taper discontinuities appear reasonable when compared with the measured results obtained with four taper discontinuities (Figures 2.4, 2.9).

The above calculations show that the taper discontinuities generate predominantly the TE_{20} spurious mode for all values of the grating coupling, and that the TE_{30} mode is of the order of 13 db below the TE_{20} mode. Any device that is employed to compensate the taper discontinuities must have similar characteristics. Figure A2 shows a method for generating predominantly TE_{30} or TE_{20} modes which employs metal or dielectric wedges on the side walls of the rectangular waveguide. The wedges are tapered as shown in order to minimize back scattering. In Figure A2a identical wedges, either metal or dielectric, are placed on the two side walls. This results in the generation of only the TE_{30} mode, the TE_{20} mode being suppressed by symmetry. One can also argue that the two wedges in Figure A2a generate equal TE_{30} modes which add constructively in phase to produce a net TE_{30} mode output. On the other hand, each of the two wedges generate equal TE_{20} modes which add destructively in phase to produce a net TE_{20} mode amplitude equal to zero. It should be noted that the TE_{20} and TE_{30} modes generated by each of the wedges is approximately 90° out of phase with the incident TE_{10} mode. This is true, provided the length of the wedge in the axial direction is a small fraction of a beat wavelength. The TE_{20} and TE_{30} modes lead the incident TE_{10} mode by 90° in the case of a metal wedge, and lag by 90° in the case of a dielectric wedge.

From the above discussion it can be seen that it should be possible to employ a combination of a metal and a dielectric wedge as shown in Figure A2b in order to generate predominantly a TE_{20} mode. Of course the relative sizes of the metal and dielectric wedges must be adjusted to obtain exact cancellation of the TE_{30} mode generated by the two wedges in combination. Since the TE_{20} mode generated by the wedges is approximately 90° out of phase with respect to the incident TE_{10} mode, it can be seen that the net result is to tilt the wavefront toward the dielectric wedge. This is what is required in order to reduce the spurious modes generated at an abrupt change in the angle of a straight taper.

Appendix 2

TE_{1n}, TM_{1n} Mode Generating Wedge

Figure A3 shows the dimensions of the E-plane wedge. The mode conversion coefficient k_{on} between the TE_{10} mode and the TE_{1n}, TM_{1n} composite mode can be determined by assuming that the wedge is equivalent to a short E-plane bend. In this case equation 12 of Reference 12 applies. For operation far above cutoff this becomes (for n odd only),

$$k_{on}z = \frac{4\sqrt{2}bz}{n^2\pi R\lambda} \qquad a3$$

For even values of n, k_{on} is zero. For $b/\lambda = 2$, $z/R = 1/6$ there results

$$k_{on}z = \frac{8\sqrt{2}}{n^2 6\pi} = \frac{0.6}{n^2} \qquad a4$$

The normalized voltage E_{11} for the TE_{11}, TM_{11} composite mode at the output of the wedge can be calculated approximately by assuming that this mode is degenerate with the TE_{10} mode. In this case,

$$|E_{11}| = \sin k_{01}z = \sin 0.6 = 0.565$$

The normalized voltage F_{10} for the TE_{10} mode is

$$|E_{10}| = \cos k_{01}z = \cos 0.6 = 0.8251$$

$$\left|\frac{E_{11}}{E_{10}}\right| = \tan 0.6 = 0.6847 = -3.28 \text{ db}$$

The measured value of E_{11}/E_{10} was approximately -2 db which is fair agreement with the calculated value. Measured values of the TE_{12}, TM_{12} and TE_{13}, TM_{13} composite mode voltages were of the order of -20 db or less relative to the TE_{10} mode.

Appendix 3

CORRECTIONS TO PROGRESS REPORT NO. 1 OF CONTRACT AF30(602)-3682

1. In Section 2.31 equation 2.92 should have the following form

$$c_{pm} = \frac{V_p}{V_m} \sqrt{\frac{G_p}{G_m}} \quad \frac{2}{1 + \frac{I_m}{G_m V_m}}$$

2. In Section 2.42, the second sentence of paragraph 2 should be modified to read: It is seen that the large fluctuations in coupling obtained with the 1.000" spacings are not obtained with the 0.600" spacing, except at approximately 10 Gc which represents the aTE_{10} mode resonance.

3. In Figure 2.4a delete a/d = 2.800 and add $d/\lambda = 0.7861$.

4. In Section 2.41, the first sentence of paragraph 2 should read: Figures 2.17a, b, c and d show the results obtained with 30 holes having d = 1.000", t = 0.100", w = 0.100" and a = 2.800". In the third sentence of this paragraph Figure 2.17 should be substituted for Figure 2.8.

5. In Section 3.11 the last sentence in the first paragraph (just below equation 3.2) should read: For a slot on each side wall of the main waveguide the coupling is equal to $\sqrt{2}$ times the value given by equation (3).

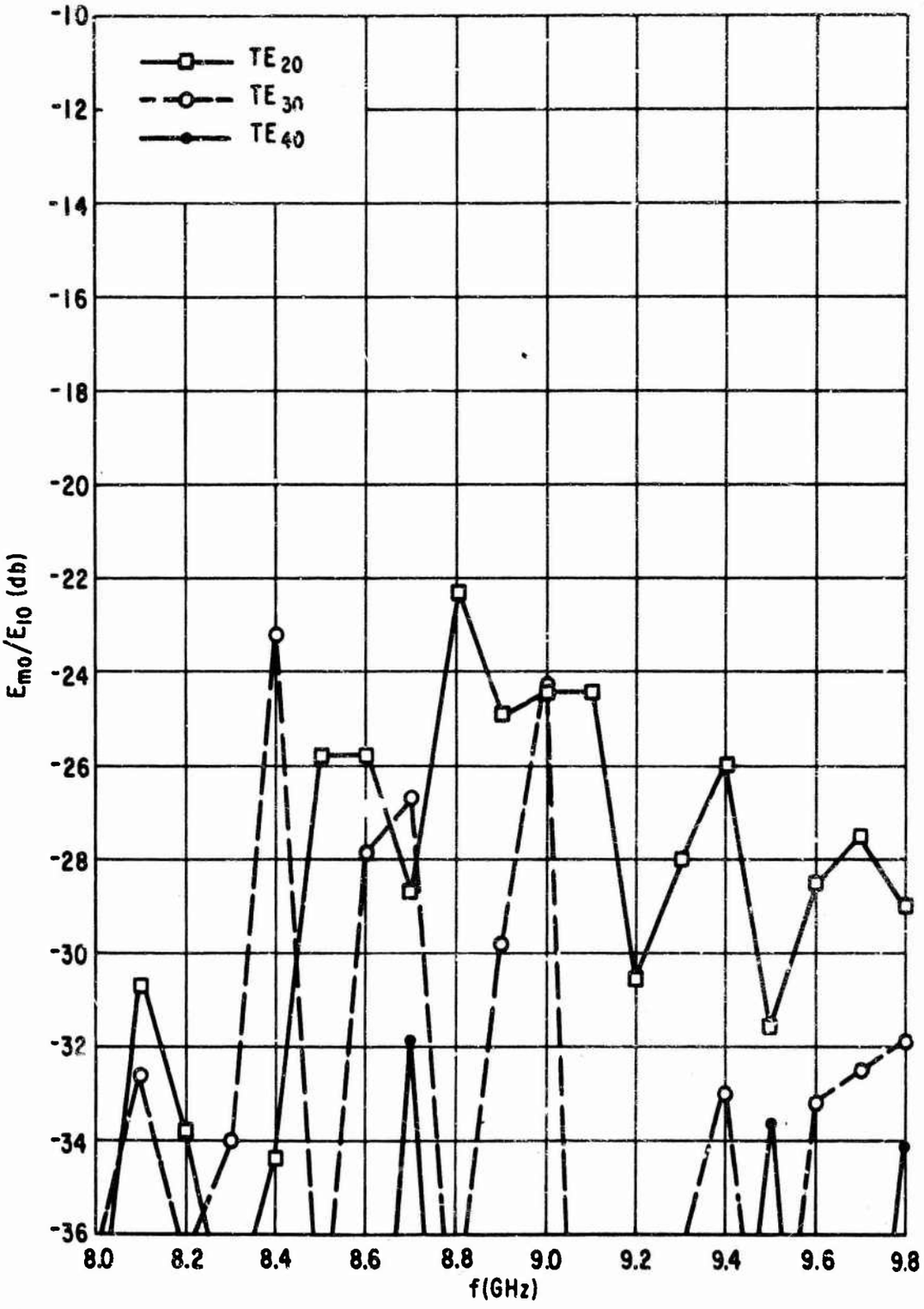

FIGURE 2.1 MEASURED SPURIOUS MODE CONVERSION FOR PAIR OF 22" VARIABLE TAPERS.

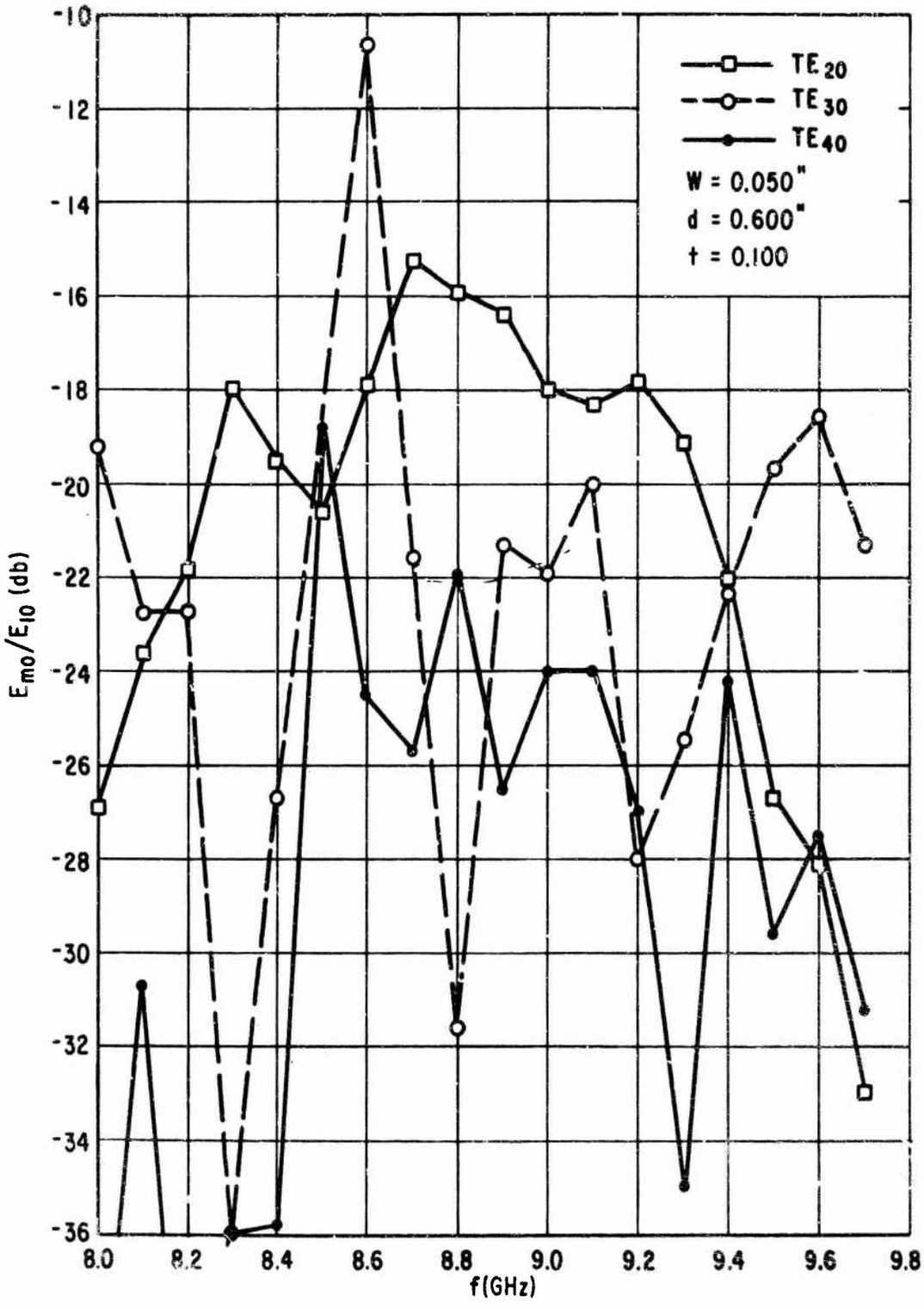

FIGURE 2.2 MEASURED SPURIOUS MODE CONVERSION FOR VARIABLE TAPERED COUPLER - PORT 3

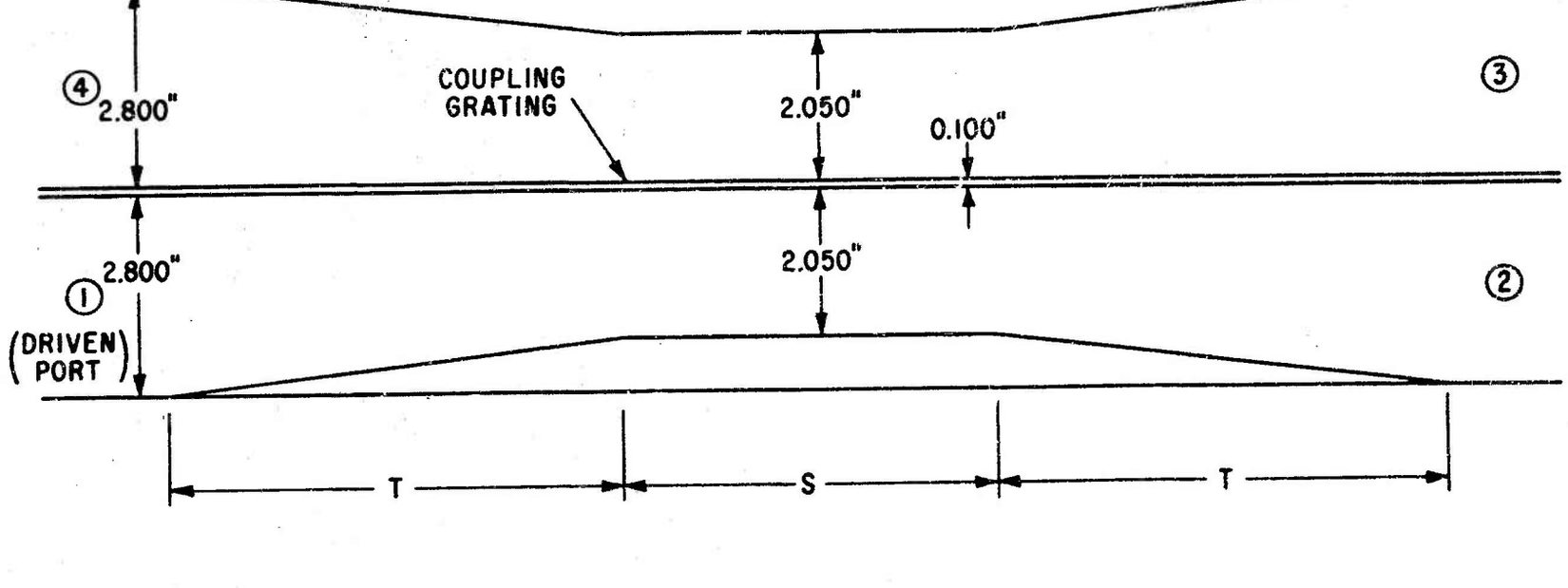

FIGURE 2.3 STRAIGHT TAPERS FOR REDUCING WAVEGUIDE WIDTH IN DIRECTIONAL COUPLER.

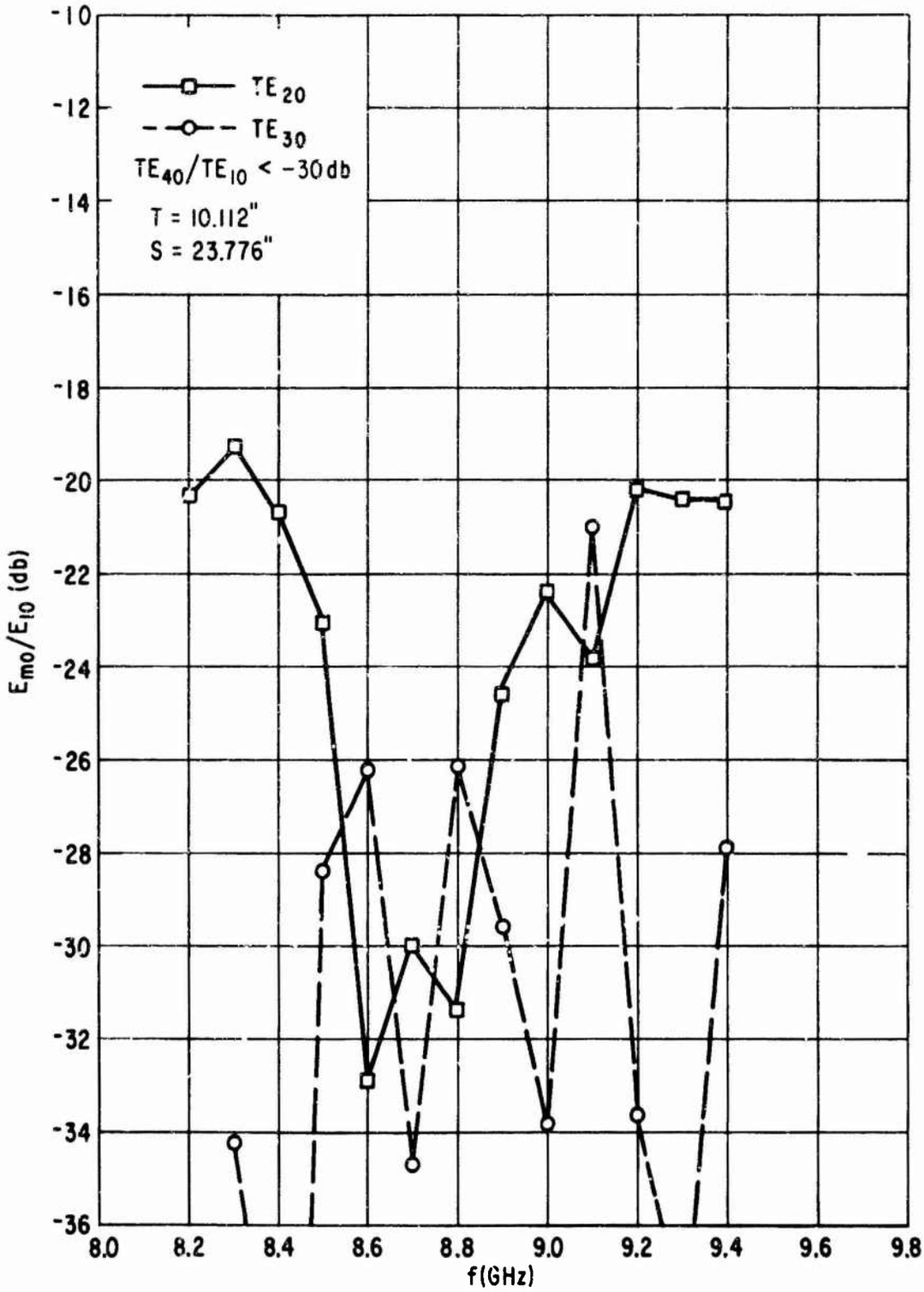

FIGURE 2.4 MEASURED SPURIOUS MODE CONVERSION FOR PAIR OF STRAIGHT TAPERS

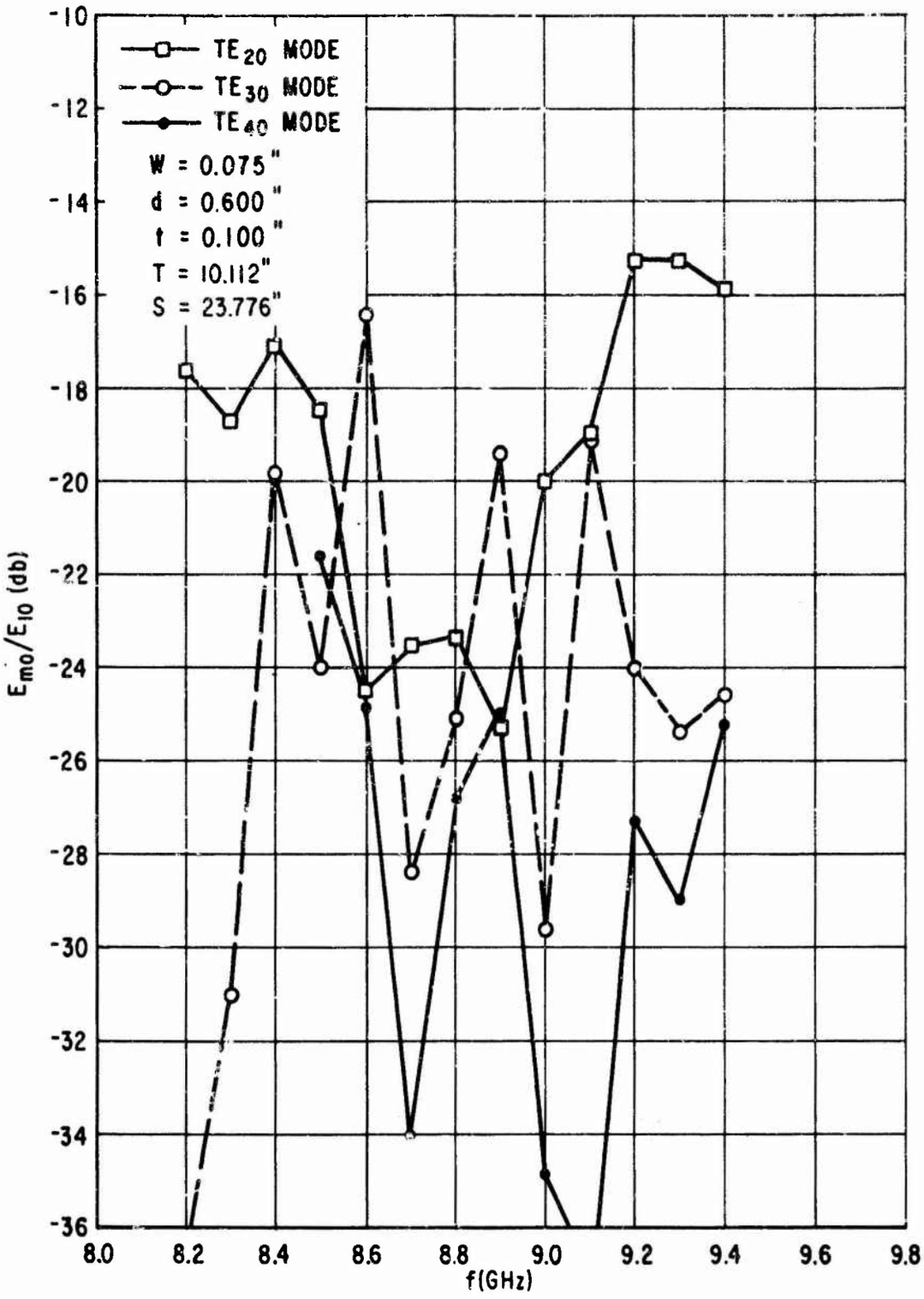

FIGURE 2.5 MEASURED SPURIOUS MODE CONVERSION FOR STRAIGHT TAPERED COUPLER – PORT 2

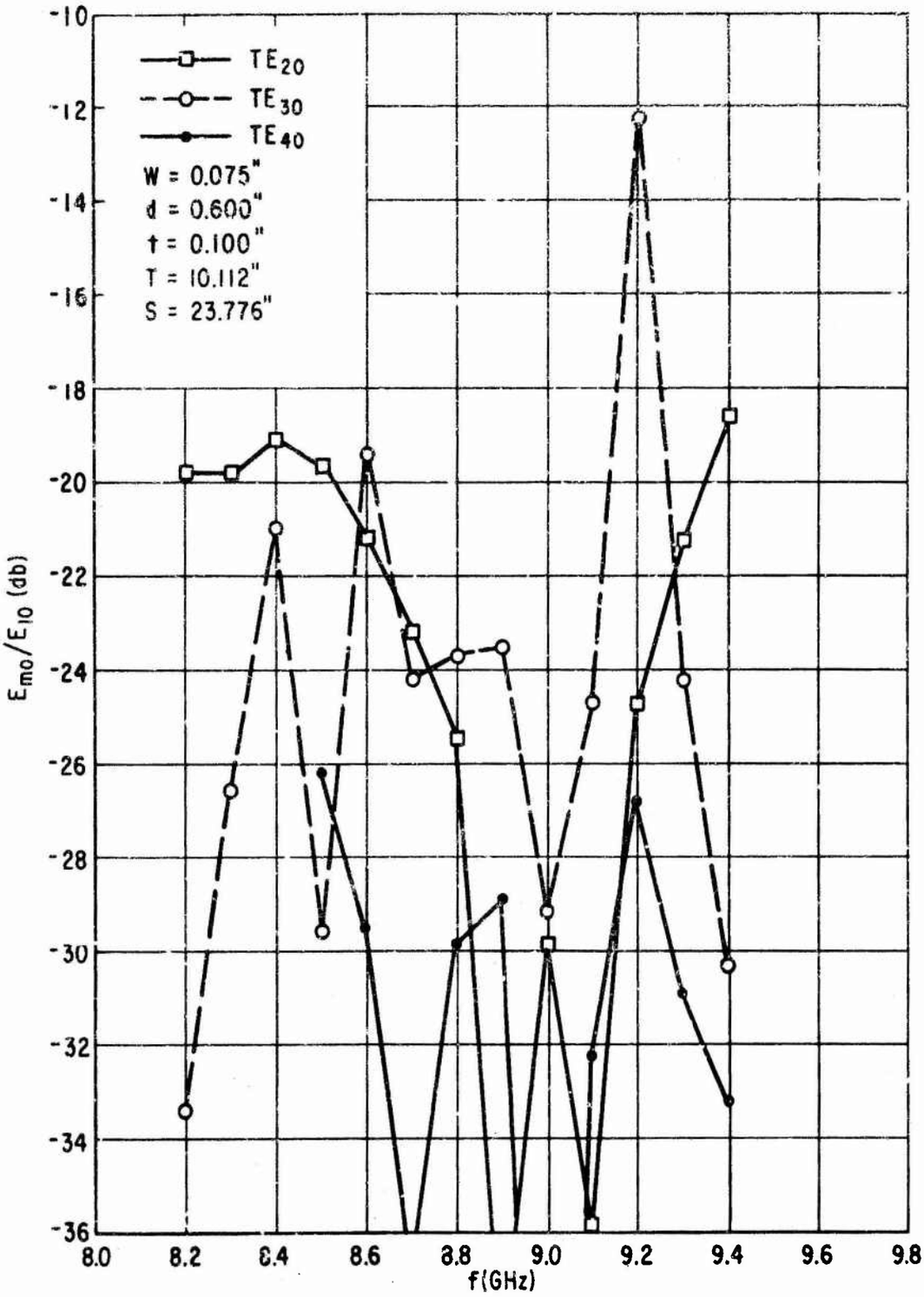

FIGURE 2.6 MEASURED SPURIOUS MODE CONVERSION FOR STRAIGHT TAPERED COUPLER – PORT 3

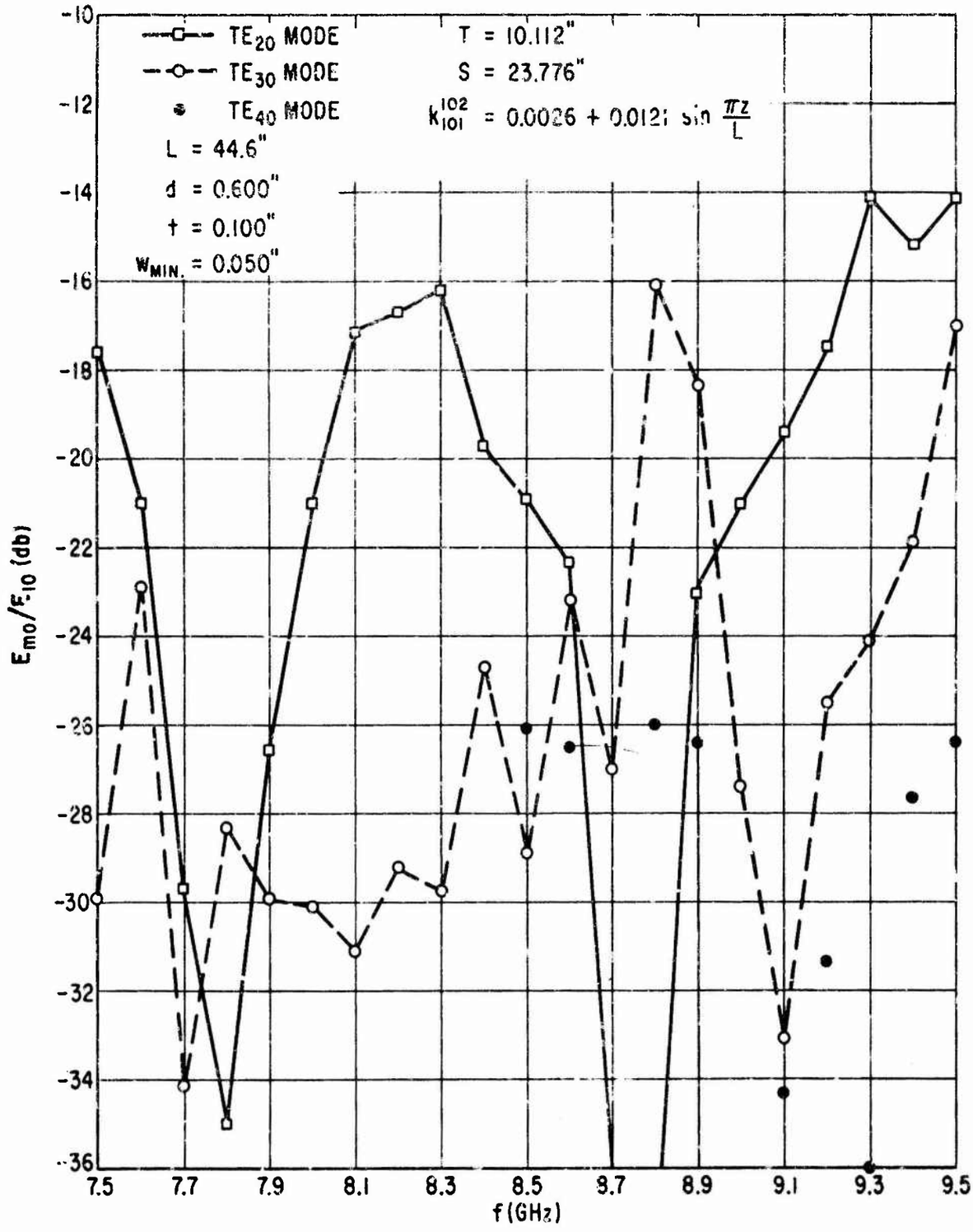

FIGURE 2.7 MEASURED SPURIOUS MODE CONVERSION FOR STRAIGHT TAPERED COUPLER - PORT 2.

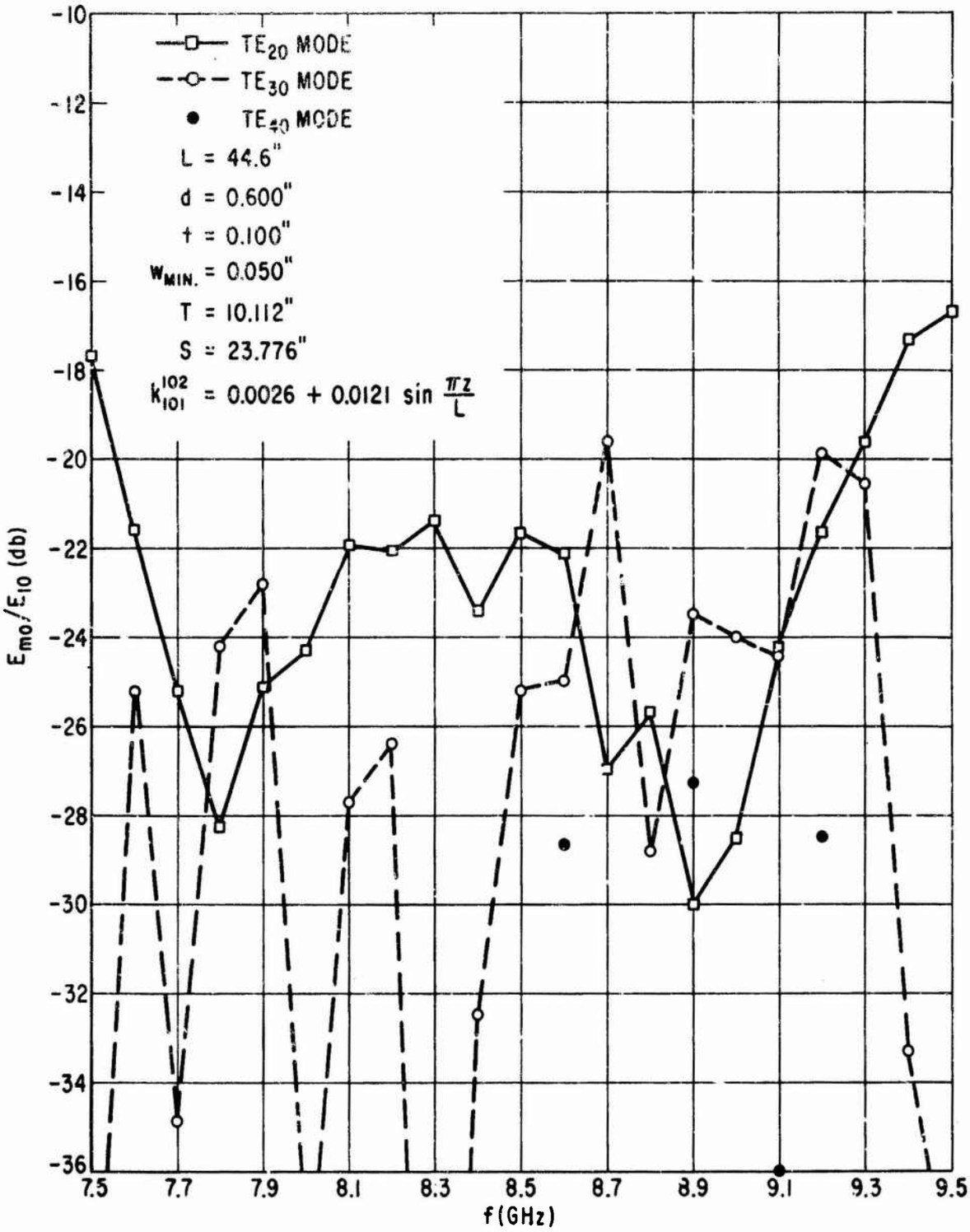

FIGURE 2.8 MEASURED SPURIOUS MODE CONVERSION FOR STRAIGHT TAPERED COUPLER - PORT 3.

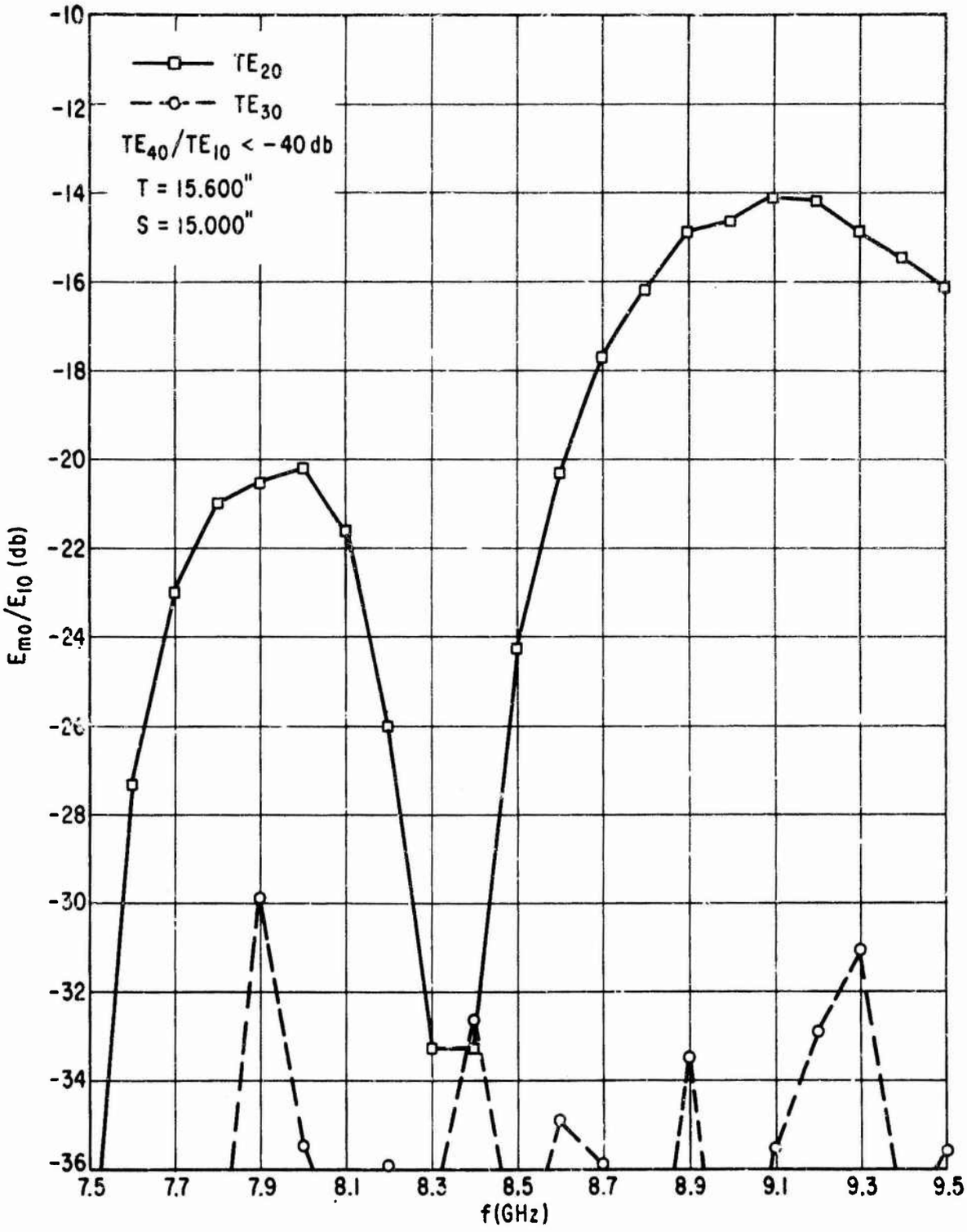

FIGURE 2.9 MEASURED SPURIOUS MODE CONVERSION FOR PAIR OF STRAIGHT TAPERS.

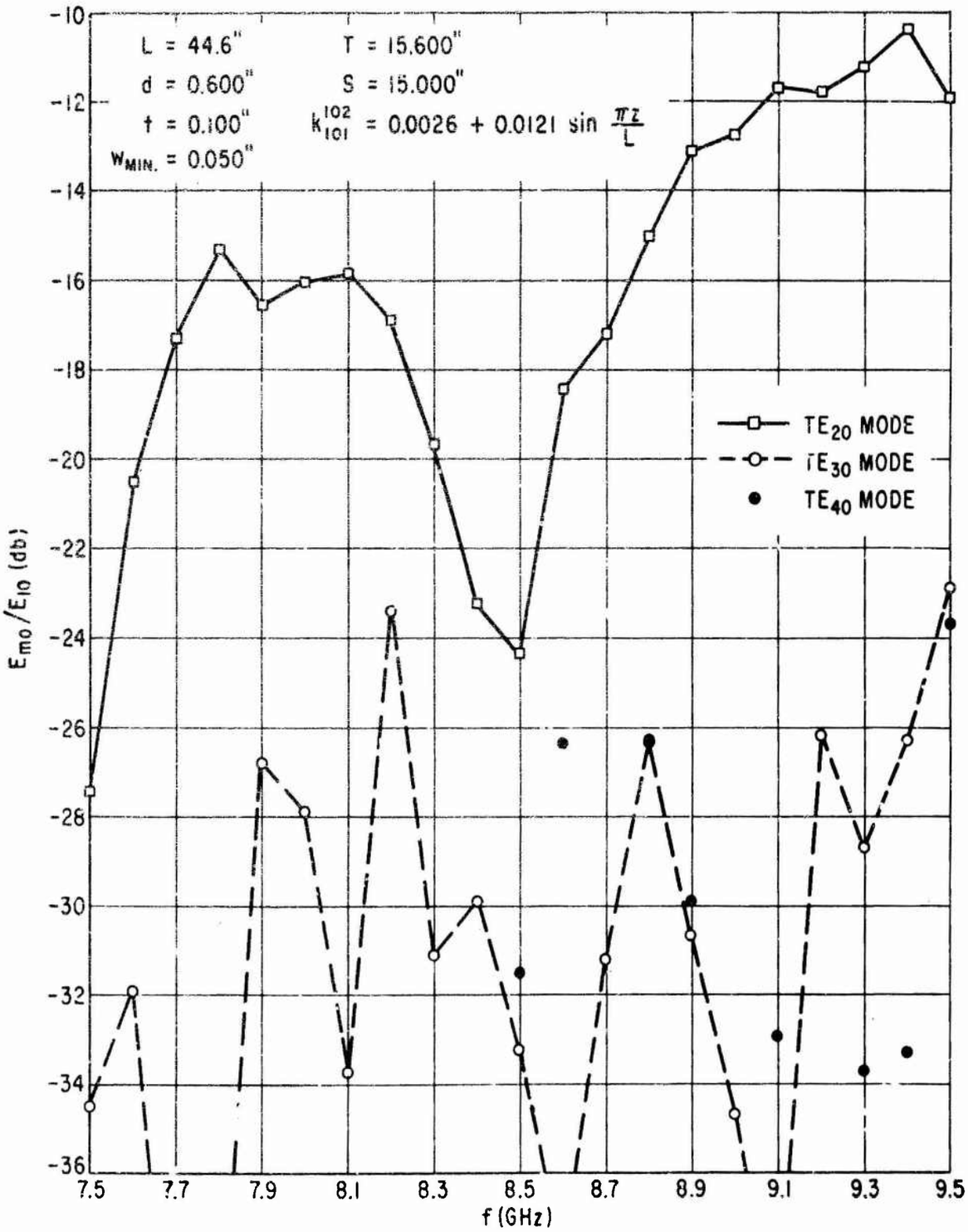

FIGURE 2.10 MEASURED SPURIOUS MODE CONVERSION FOR STRAIGHT TAPERED COUPLER - PORT 2.

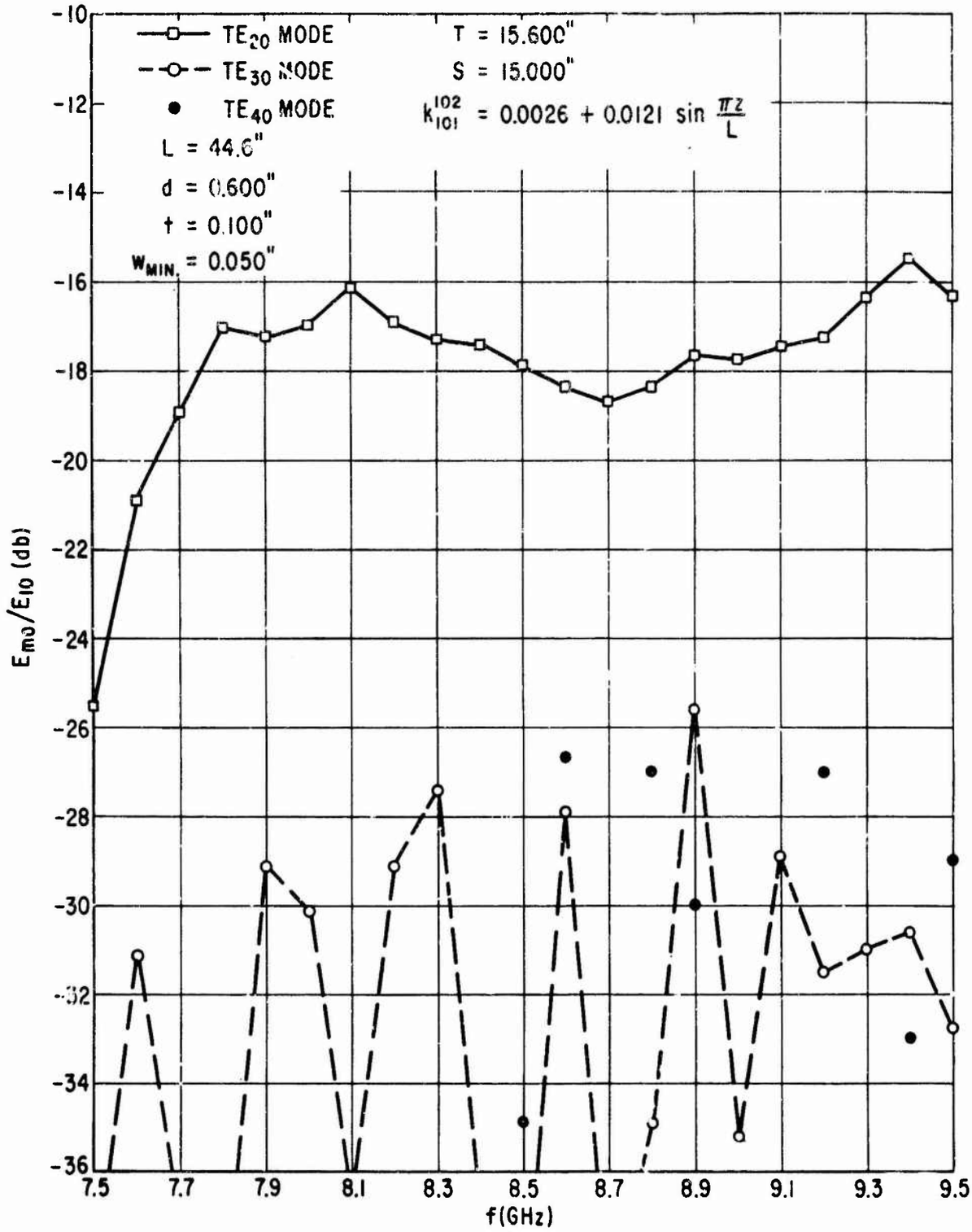

FIGURE 2.11 MEASURED SPURIOUS MODE CONVERSION FOR STRAIGHT TAPERED COUPLER - PORT 3.

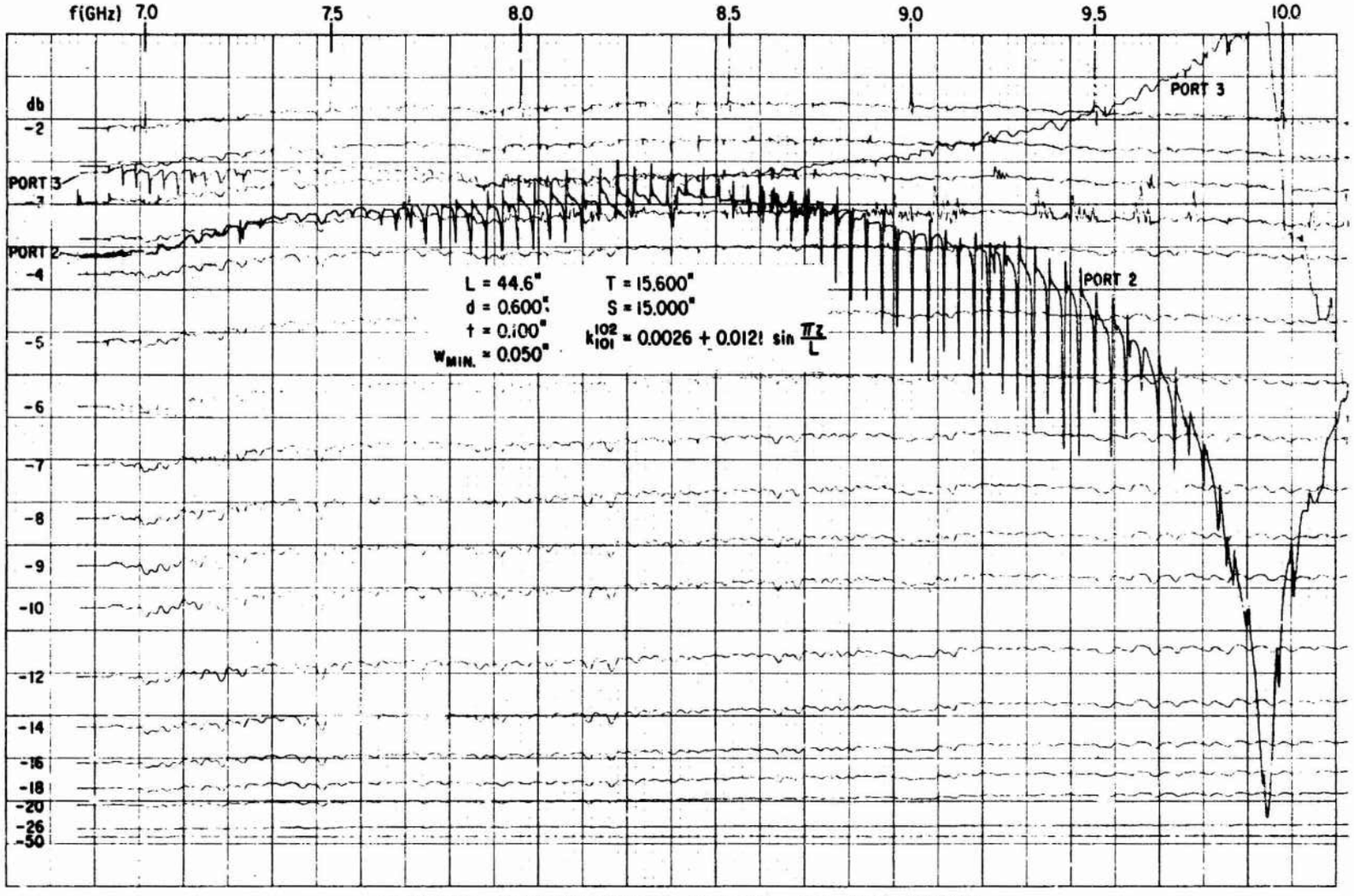

FIGURE 2.12 STRAIGHT TAPERED COUPLER – NO COMPENSATION

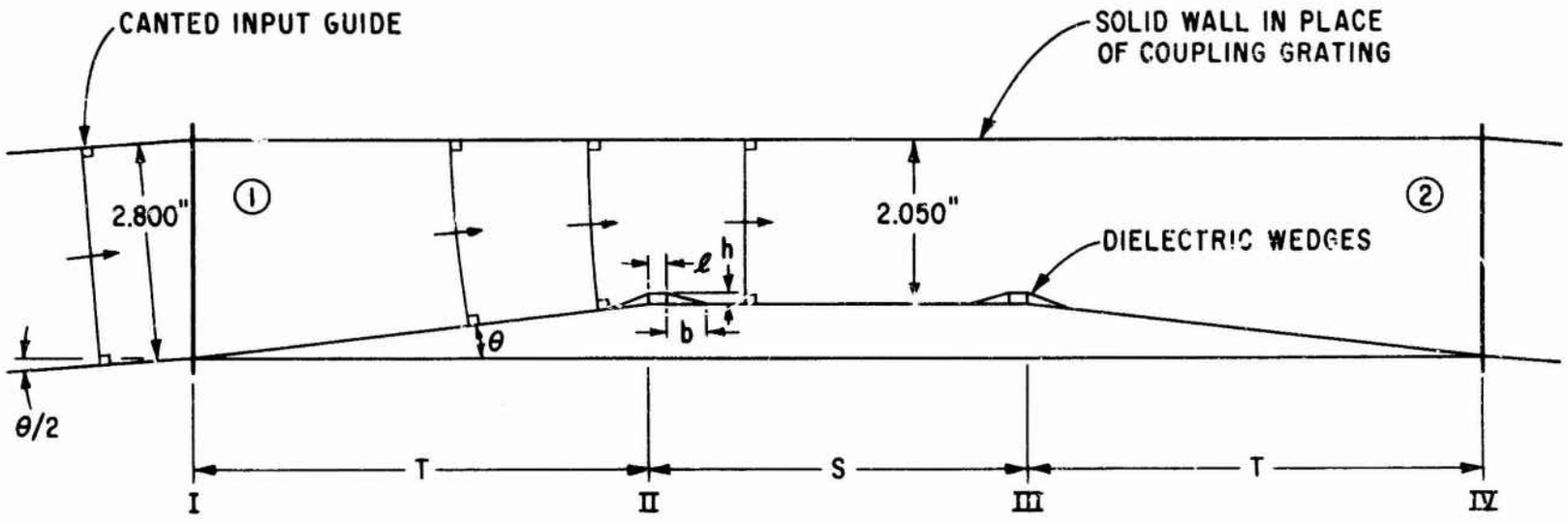

FIGURE 2.13 COMPENSATION OF STRAIGHT TAPERS ALONE

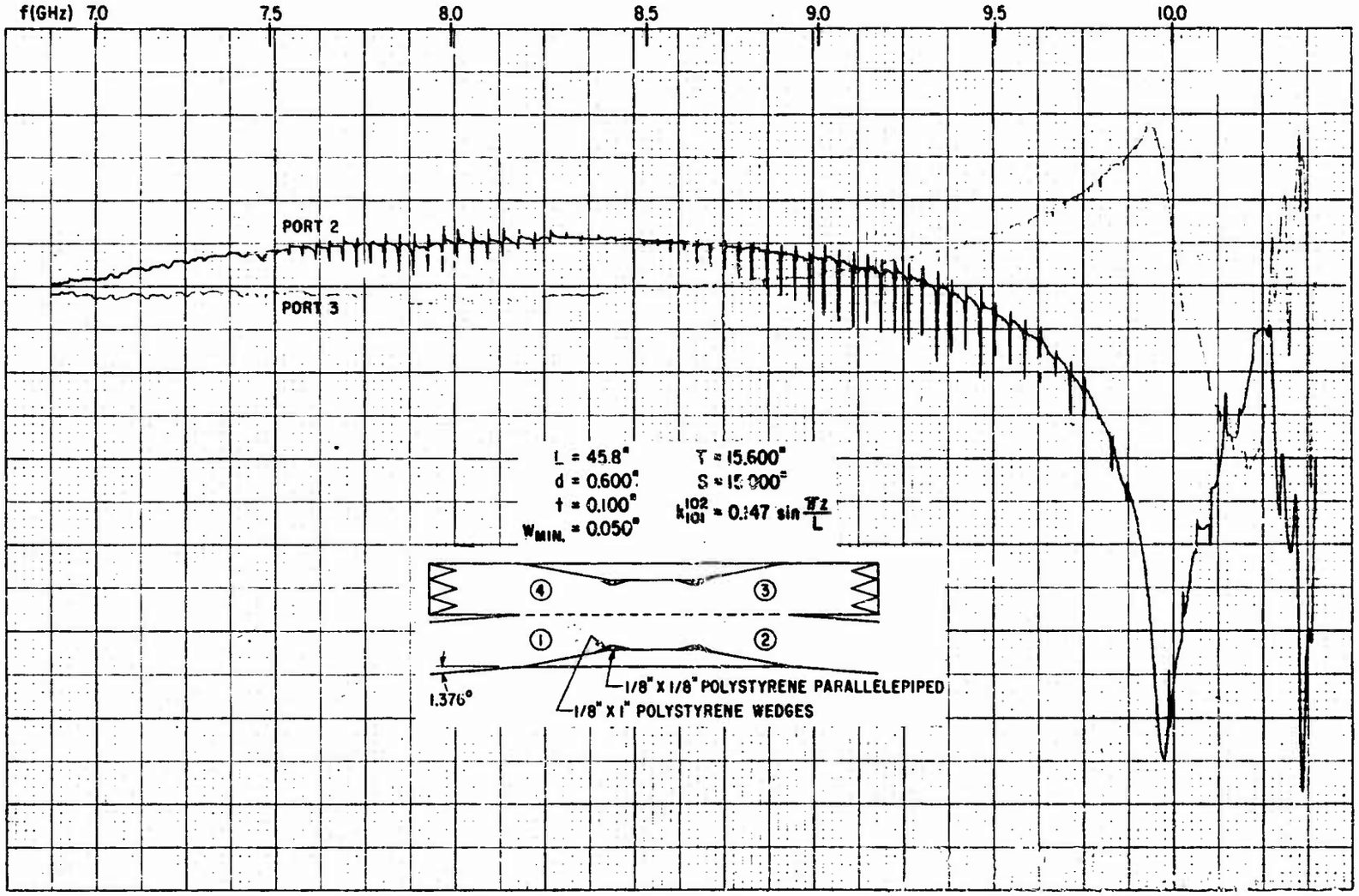

FIGURE 2.14a STRAIGHT TAPERED COUPLER – AS COMPENSATED WITHOUT COUPLING HOLES

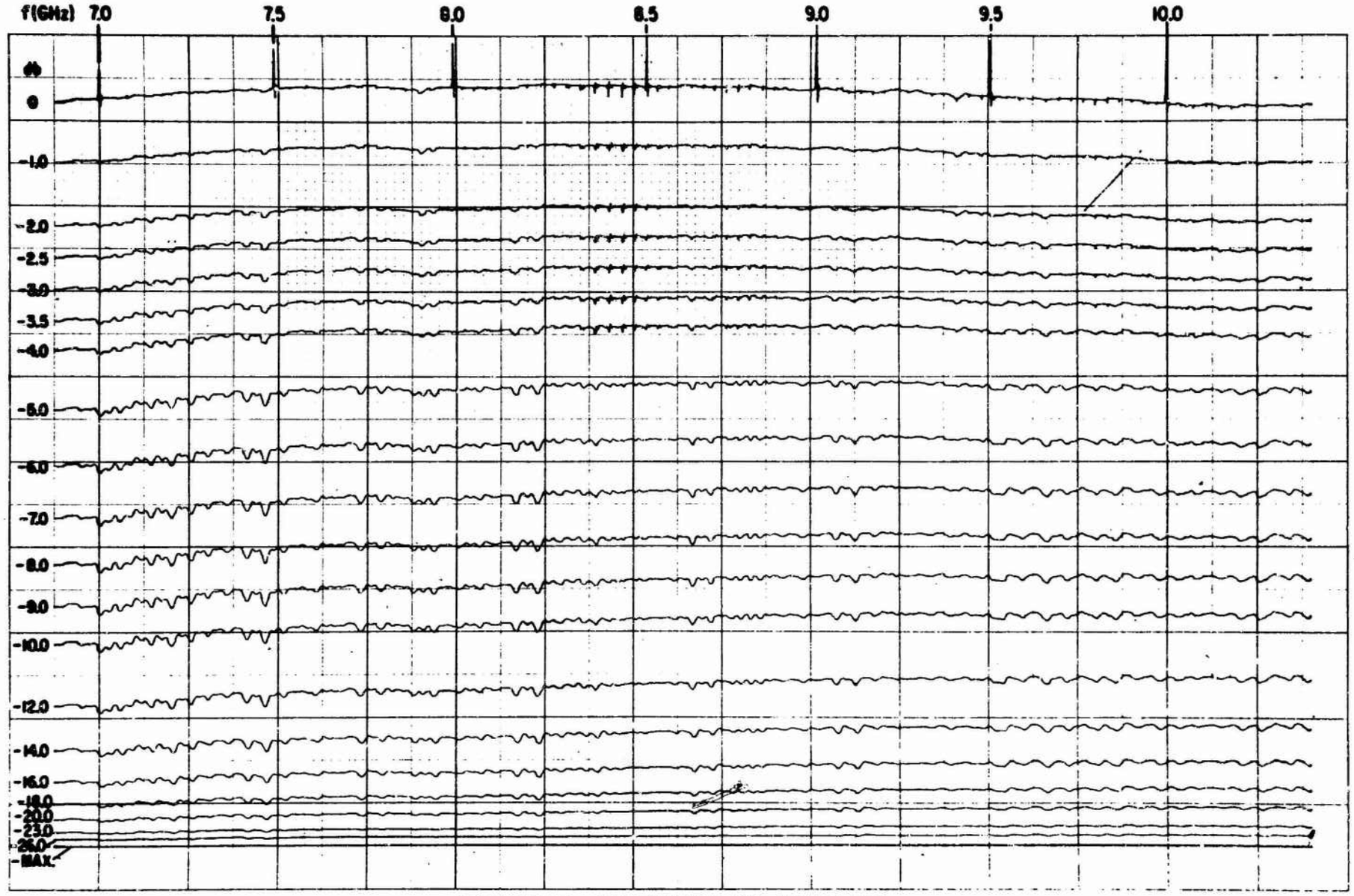

FIGURE 2.14b CALIBRATION FOR FIGURE 2.14a

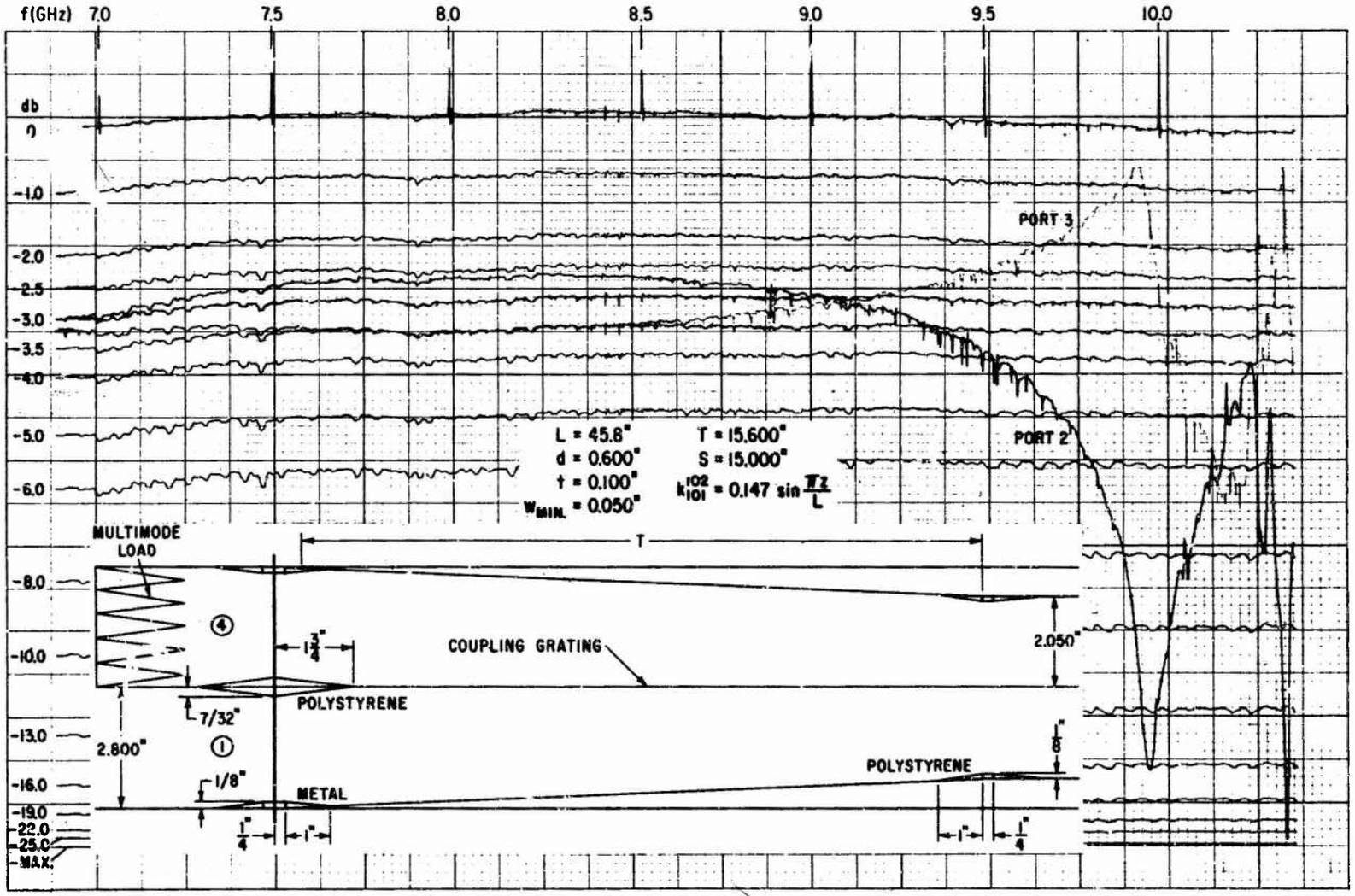

FIGURE 2.15 STRAIGHT TAPERED COUPLER WITH ALL WEDGE COMPENSATION

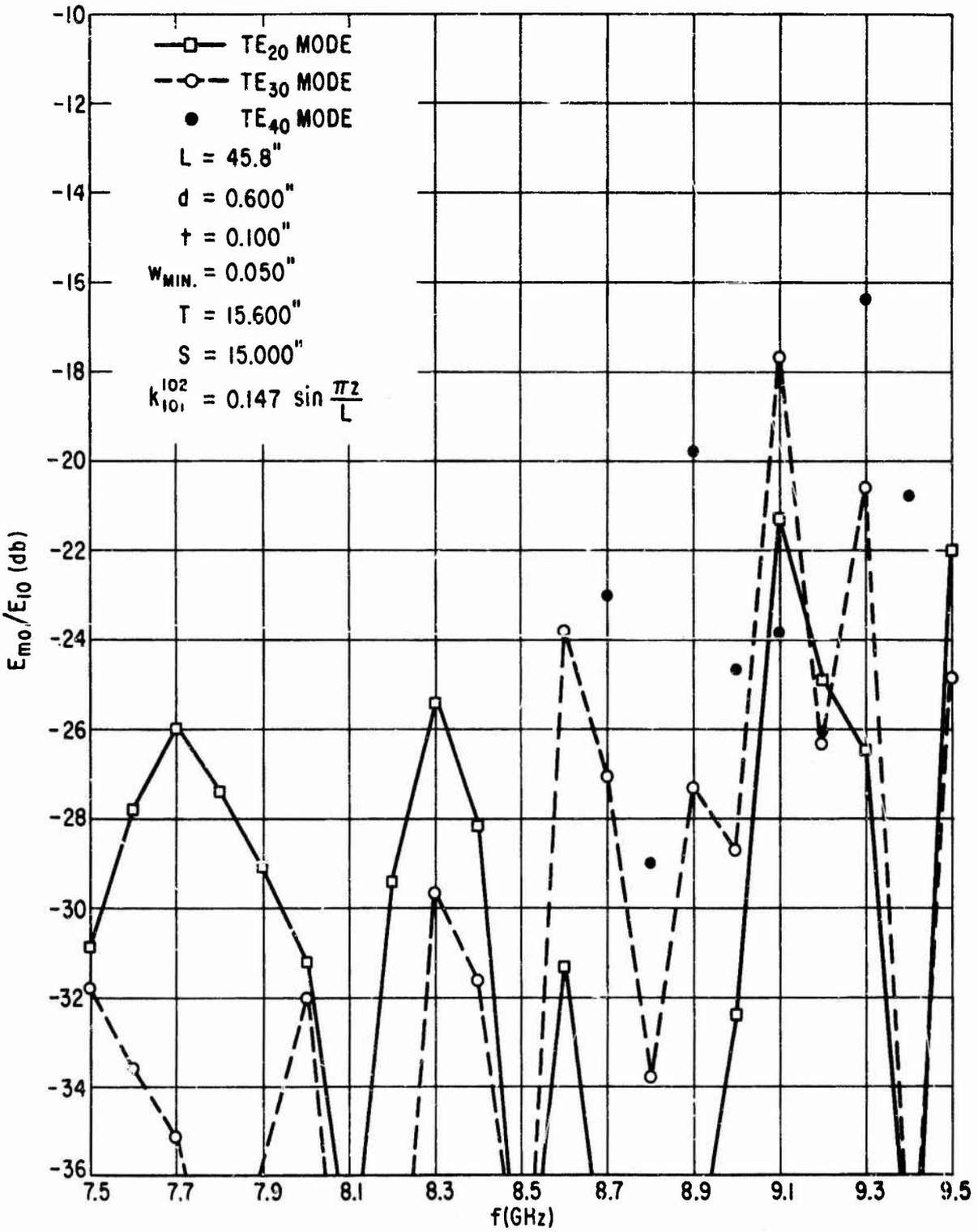

FIGURE 2.16 MEASURED SPURIOUS MODE CONVERSION FOR STRAIGHT TAPERED COUPLER WITH ALL WEDGE COMPENSATION - PORT 2.

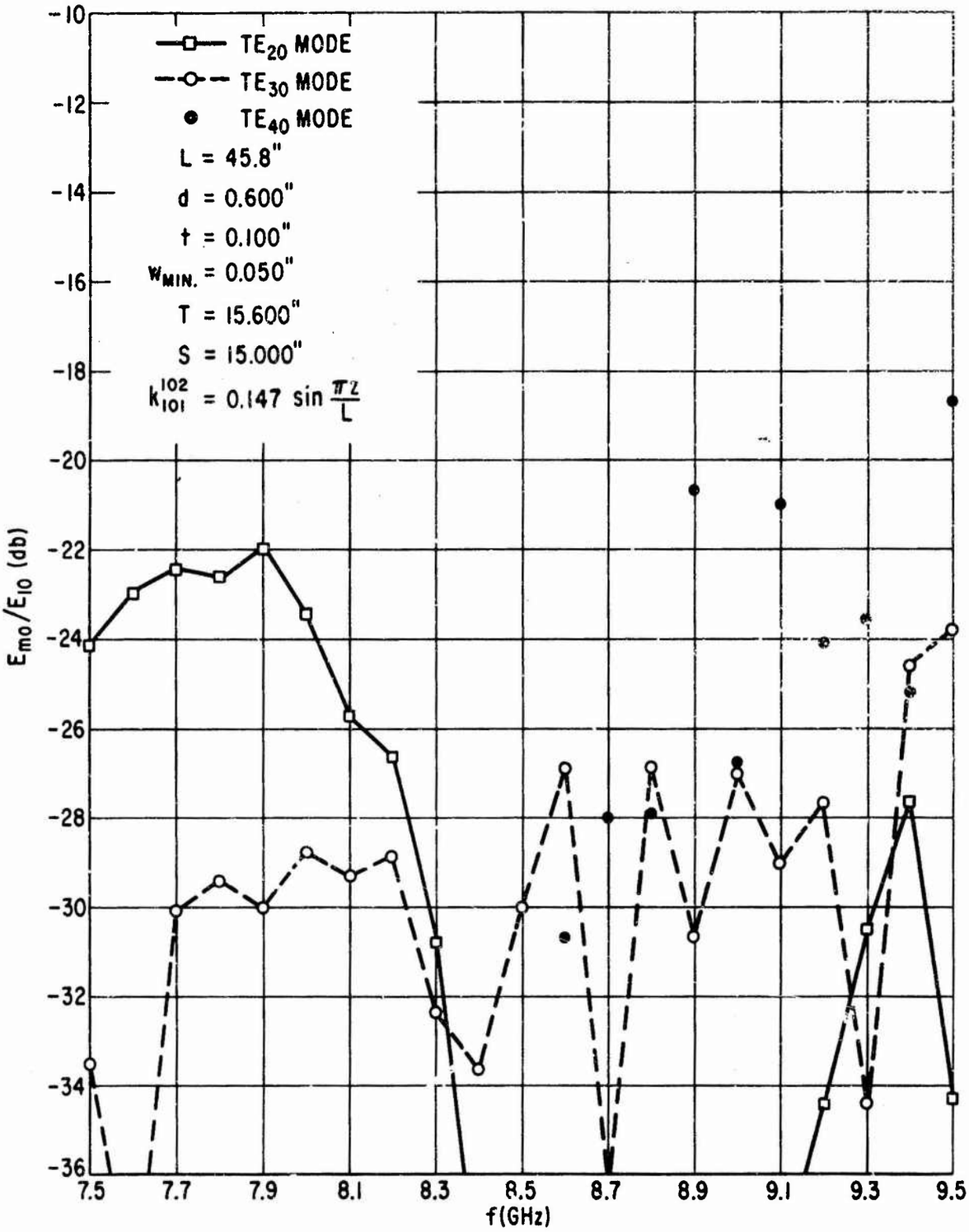

FIGURE 2.17 MEASURED SPURIOUS MODE CONVERSION FOR STRAIGHT TAPERED COUPLER WITH ALL WEDGE COMPENSATION - PORT 3.

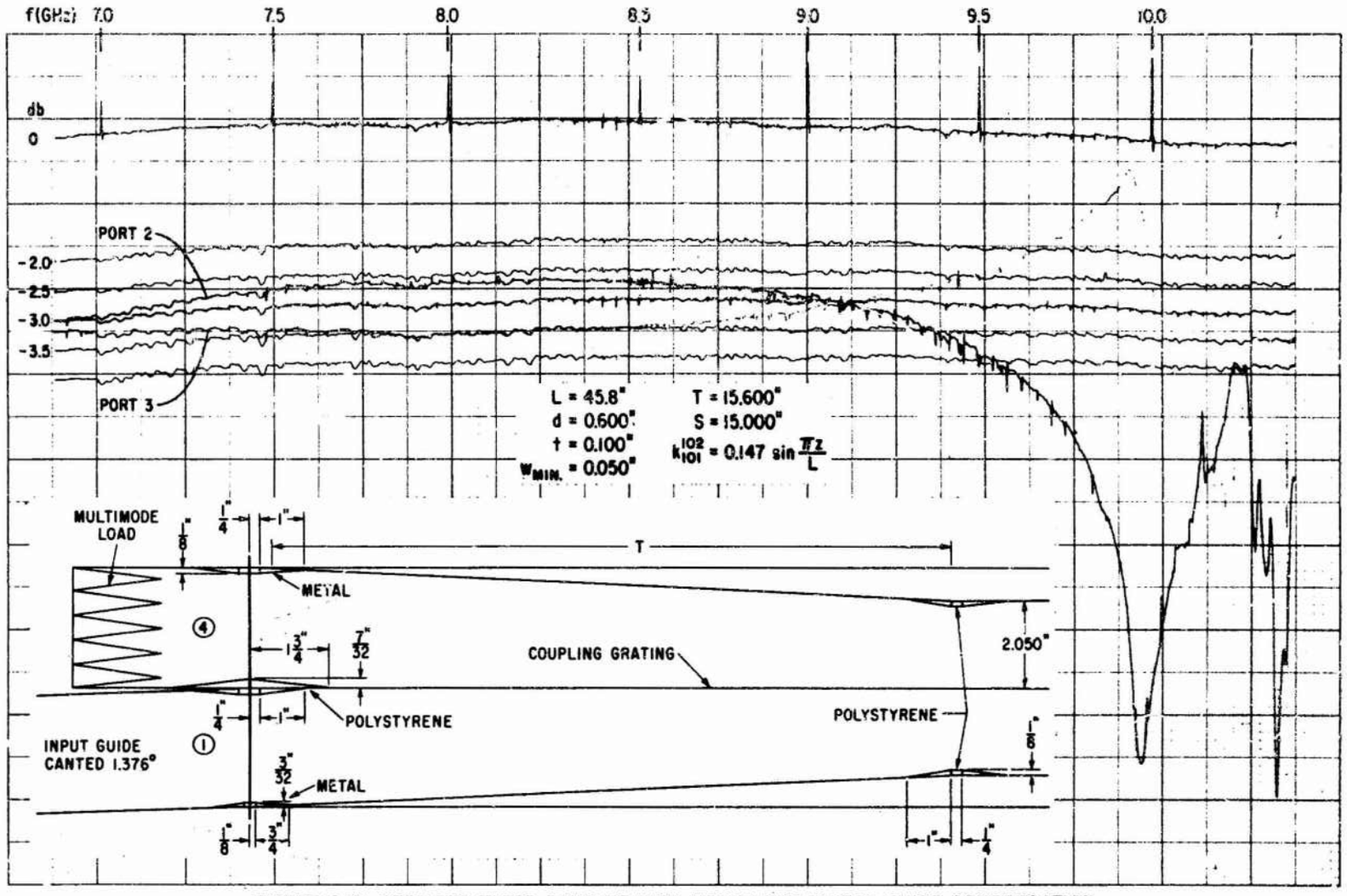

FIGURE 2.18 STRAIGHT TAPER COUPLER WITH WEDGE AND CANTED GUIDE COMPENSATION

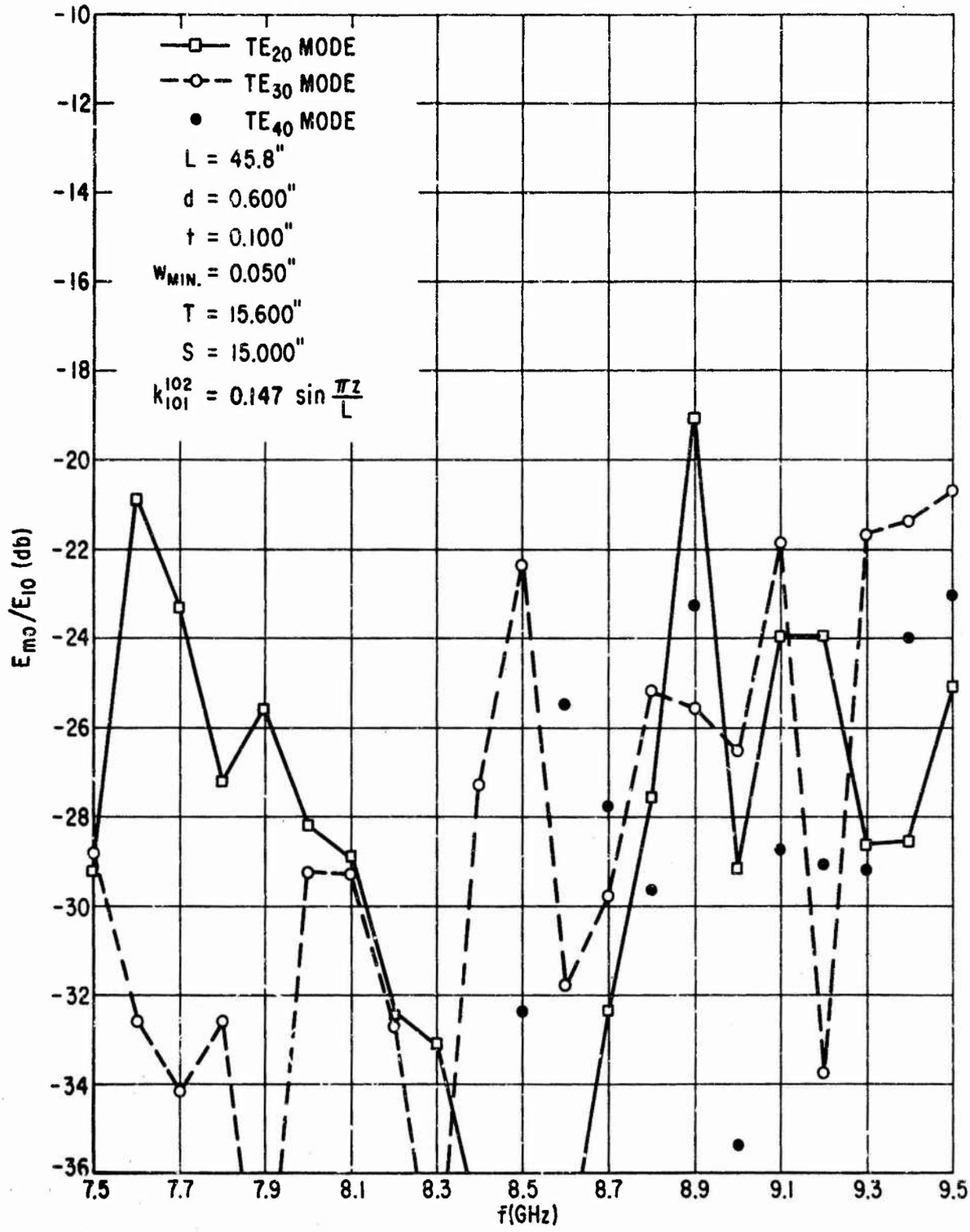

FIGURE 2.19 MEASURED SPURIOUS MODE CONVERSION FOR STRAIGHT TAPERED COUPLER WITH WEDGE PLUS CANTED GUIDE COMPENSATION - PORT 2.

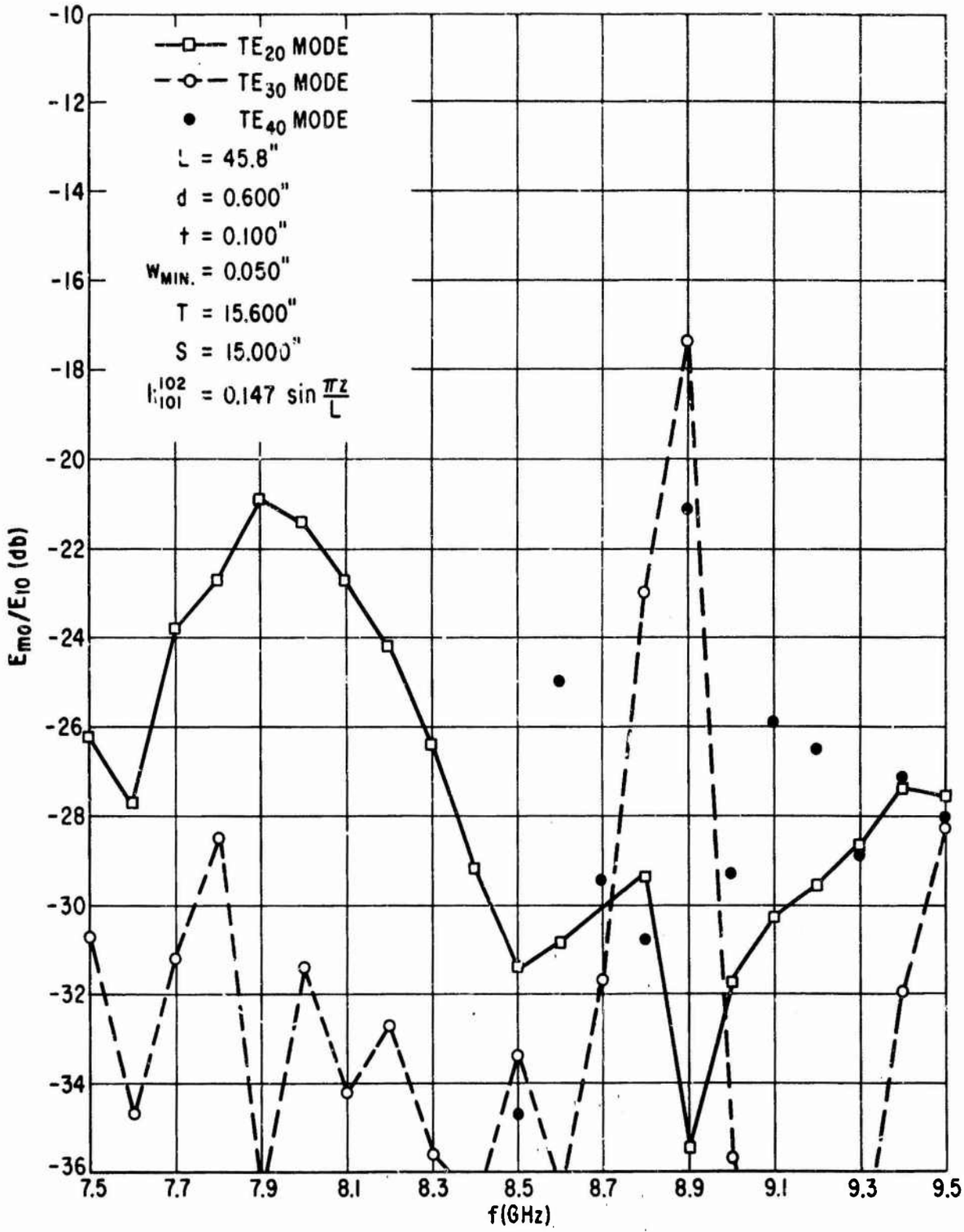

FIGURE 2.20 MEASURED SPURICUS MODE CONVERSION FOR STRAIGHT TAPERED COUPLER WITH WEDGE PLUS CANTED GUIDE COMPENSATION - PORT 3.

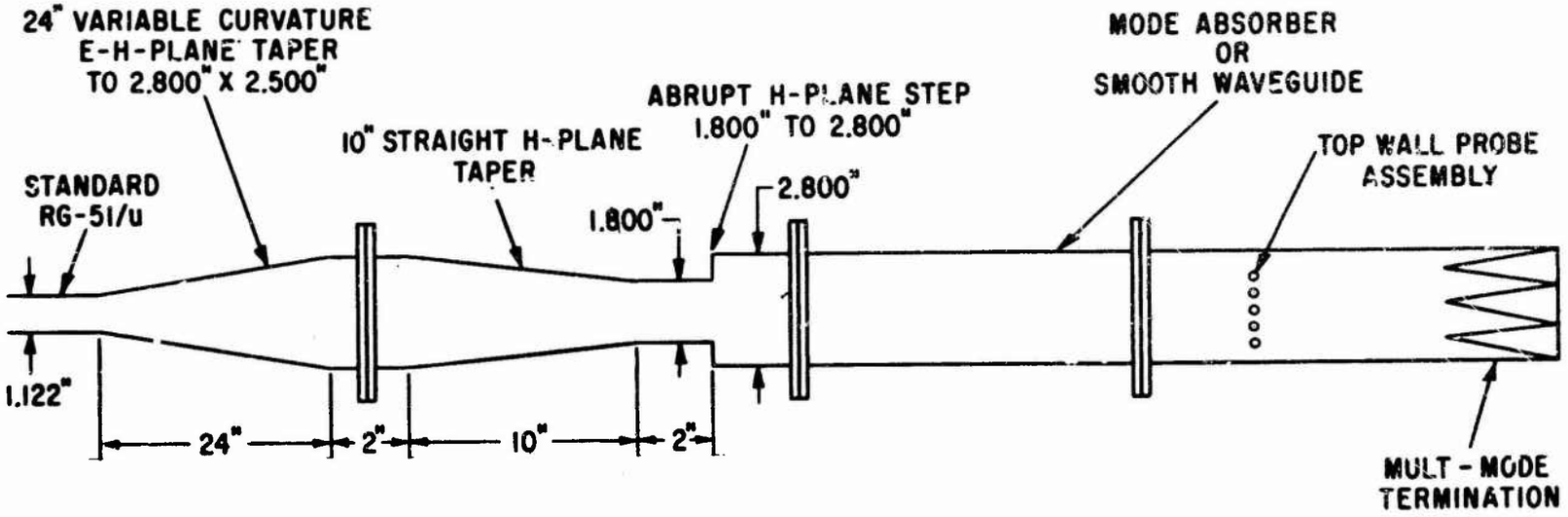

FIGURE 3.1 EXPERIMENTAL SETUP FOR MEASURING TE_{30} MODE ABSORPTION.

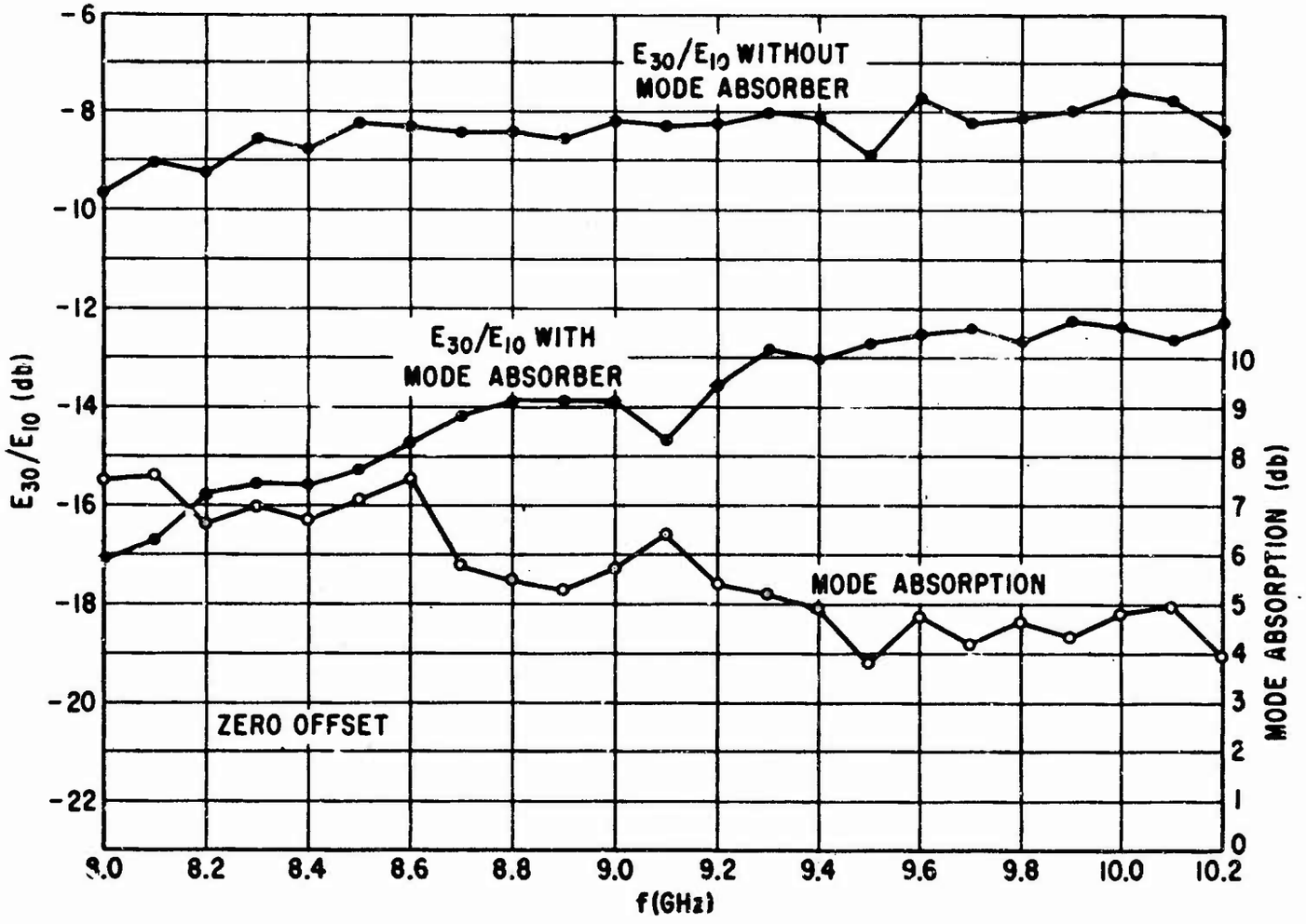

FIGURE 3.2 EFFECT OF MODE ABSORBER ON TE_{30} MODE.

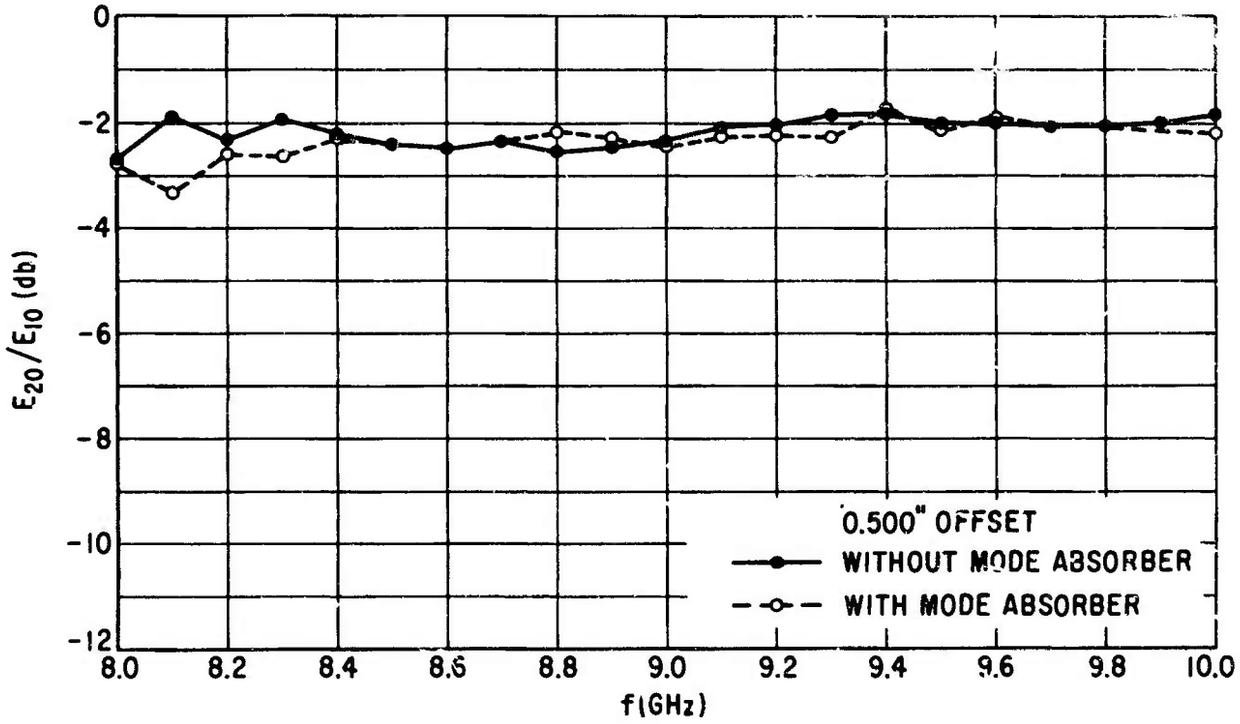

FIGURE 3.3 EFFECT OF MODE ABSORBER ON TE_{20} MODE.

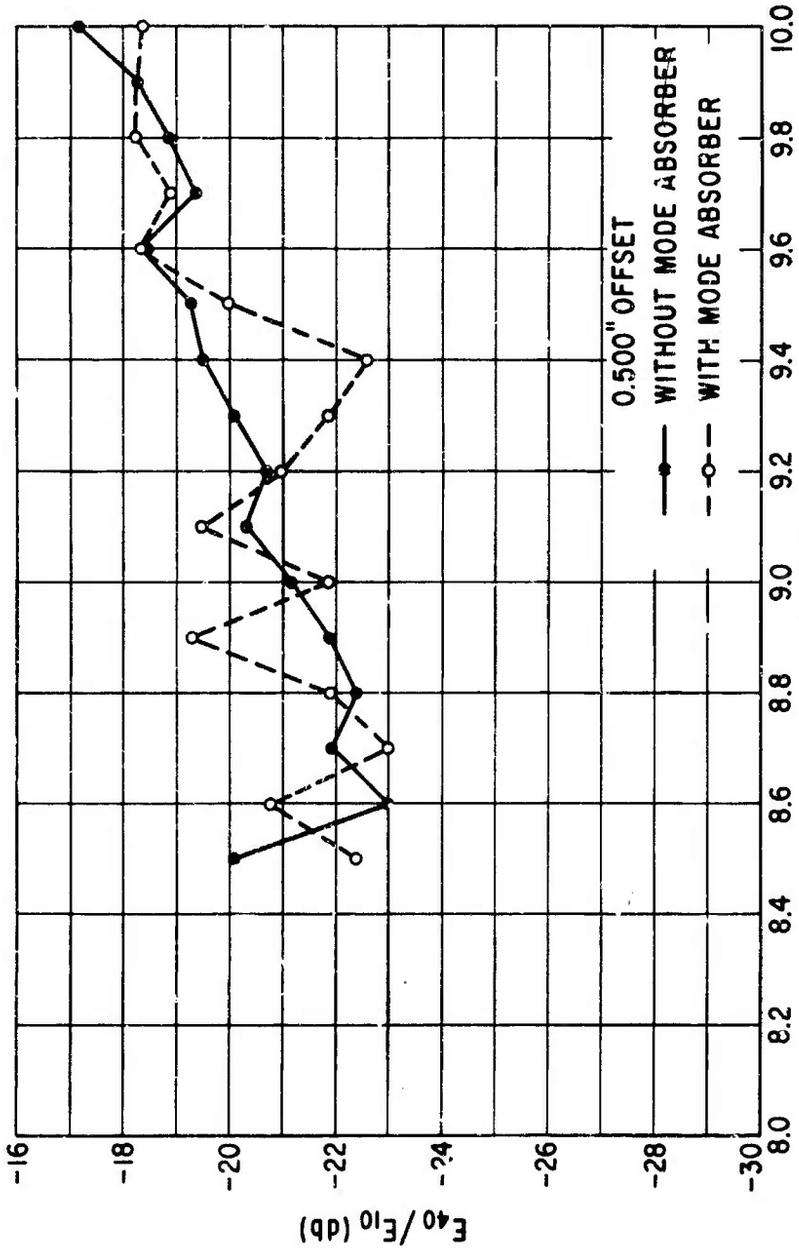

FIGURE 3.4 EFFECT OF MODE ABSORBER ON TE_{40} MODE.

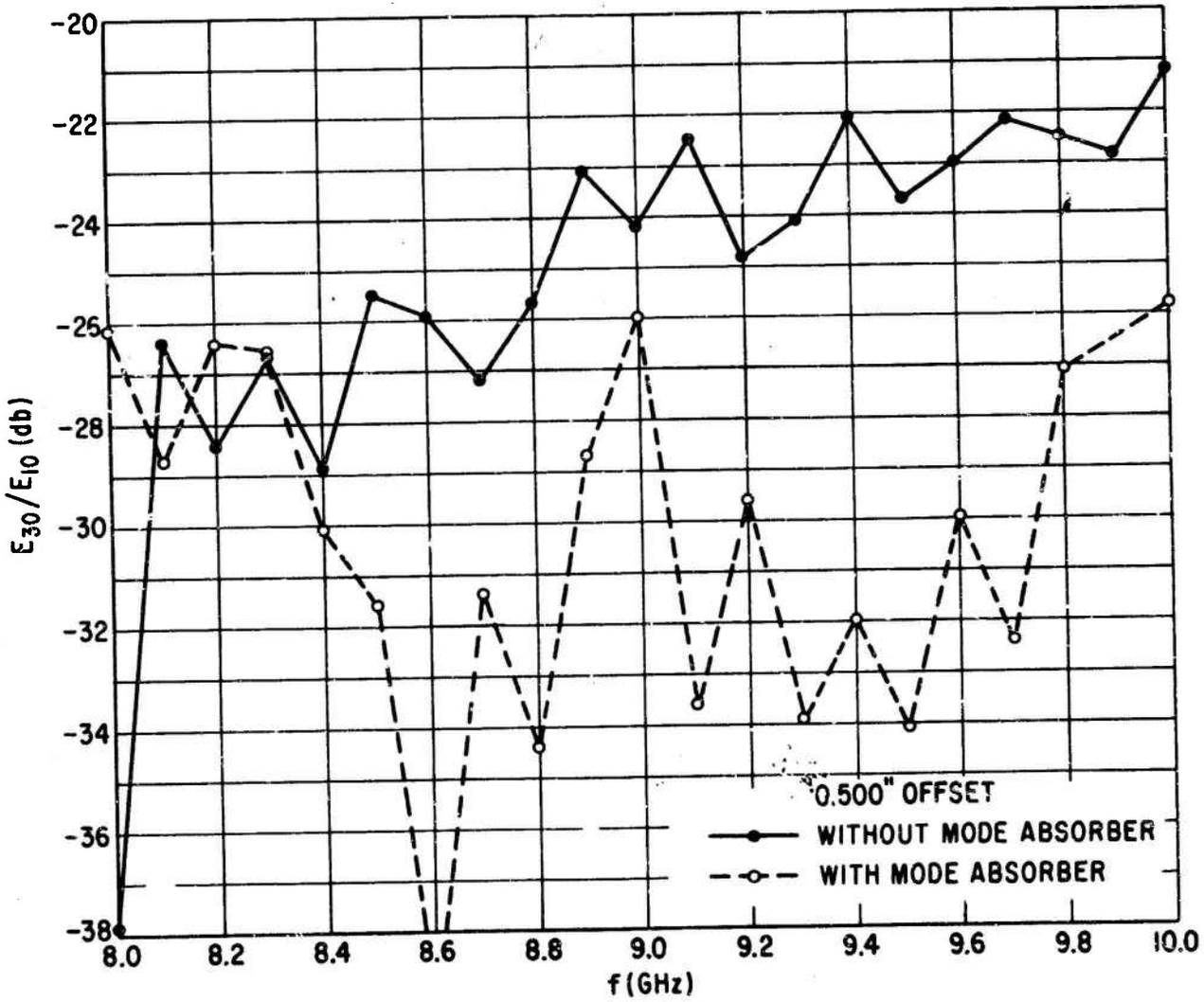

FIGURE 3.5 EFFECT OF MODE ABSORBER ON TE_{30} MODE.

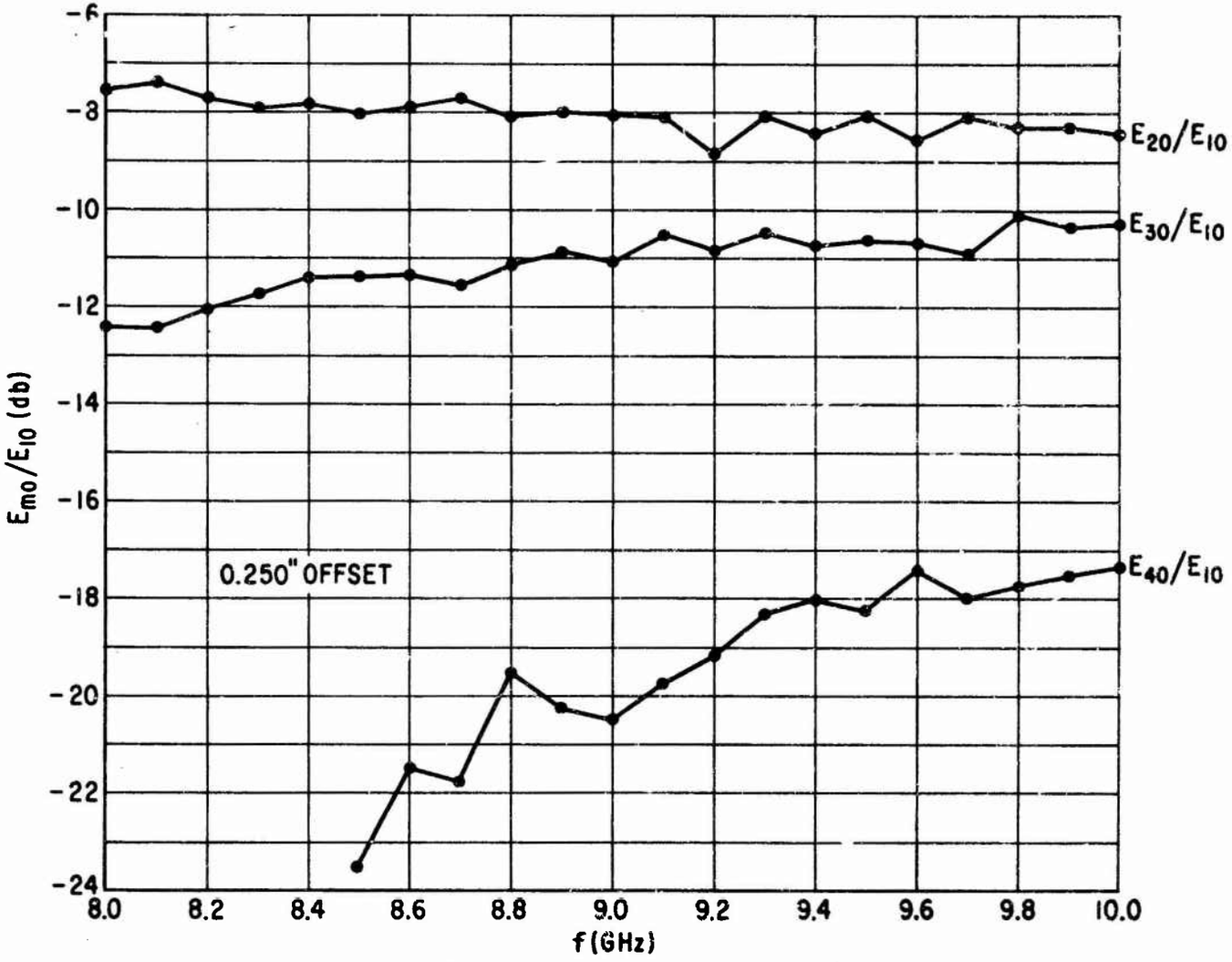

FIGURE 3.6 SPURIOUS MODES GENERATED WITH 0.250" OFFSET.

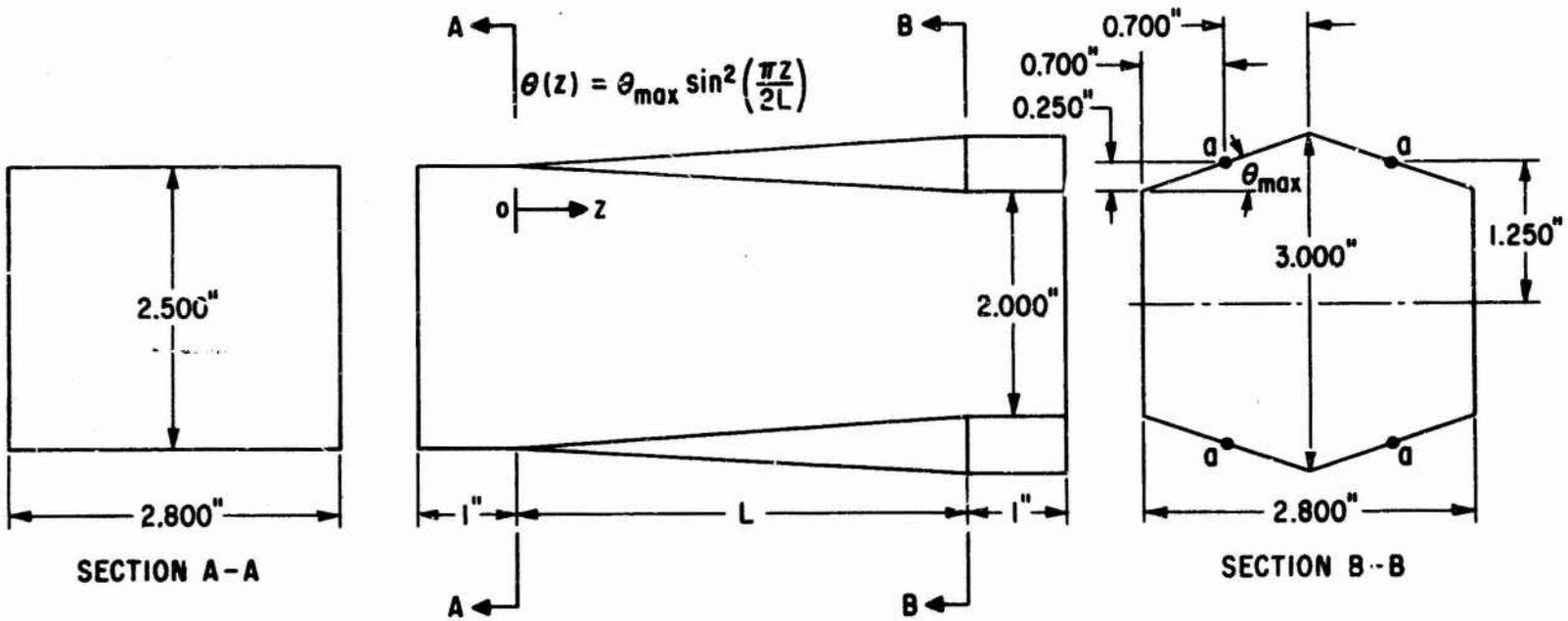

NOTES:

1- TOLERANCES ± 0.002"

2- 20 MICROINCH SURFACE

3- POINTS "a" ARE CENTERS OF ROTATION FOR GENERATING ELEMENT

FIGURE 3.7 RECTANGULAR TO HEXAGONAL WAVEGUIDE TRANSITION.

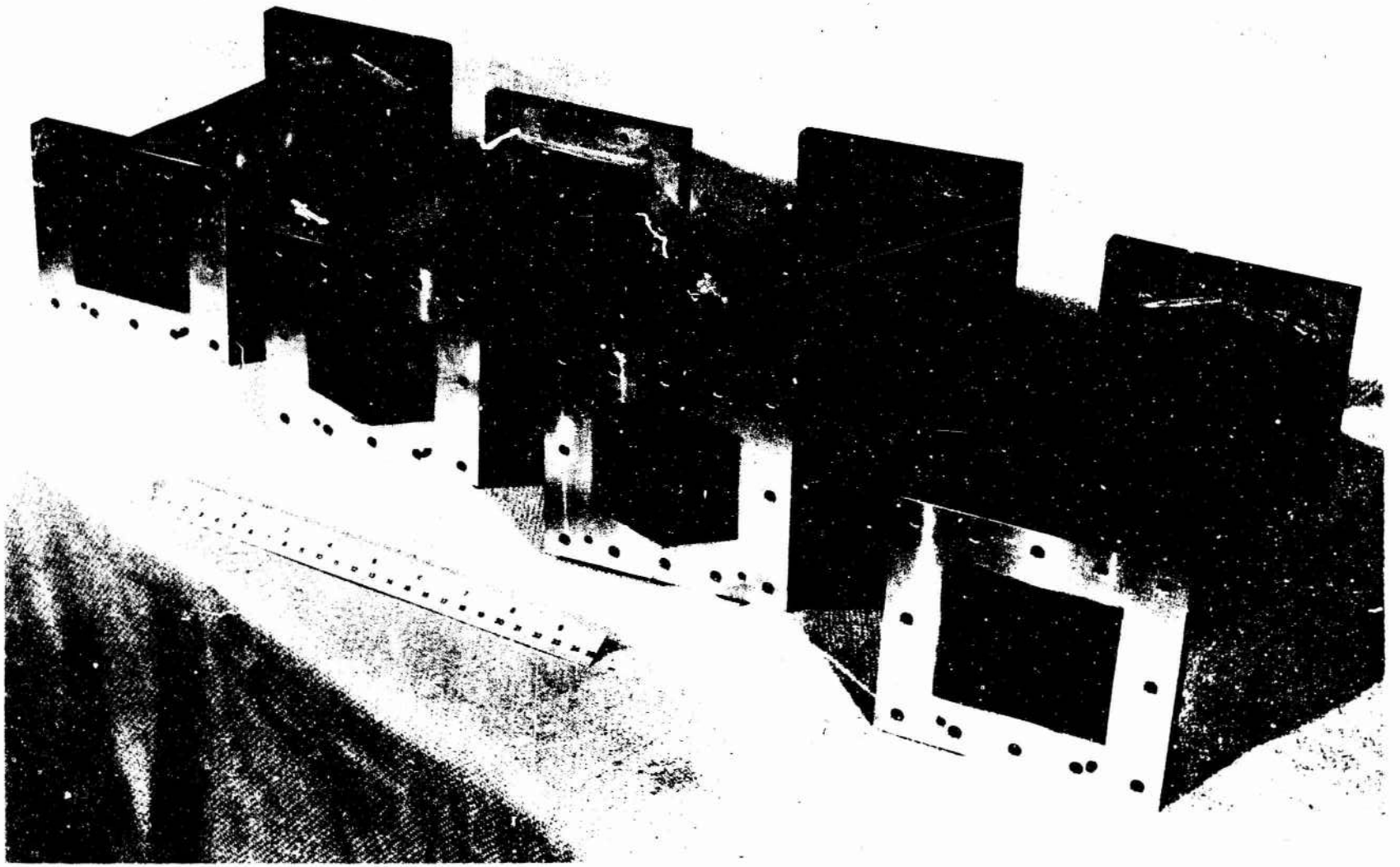

Figure 3.8. Rectangular to Hexagonal Transitions.

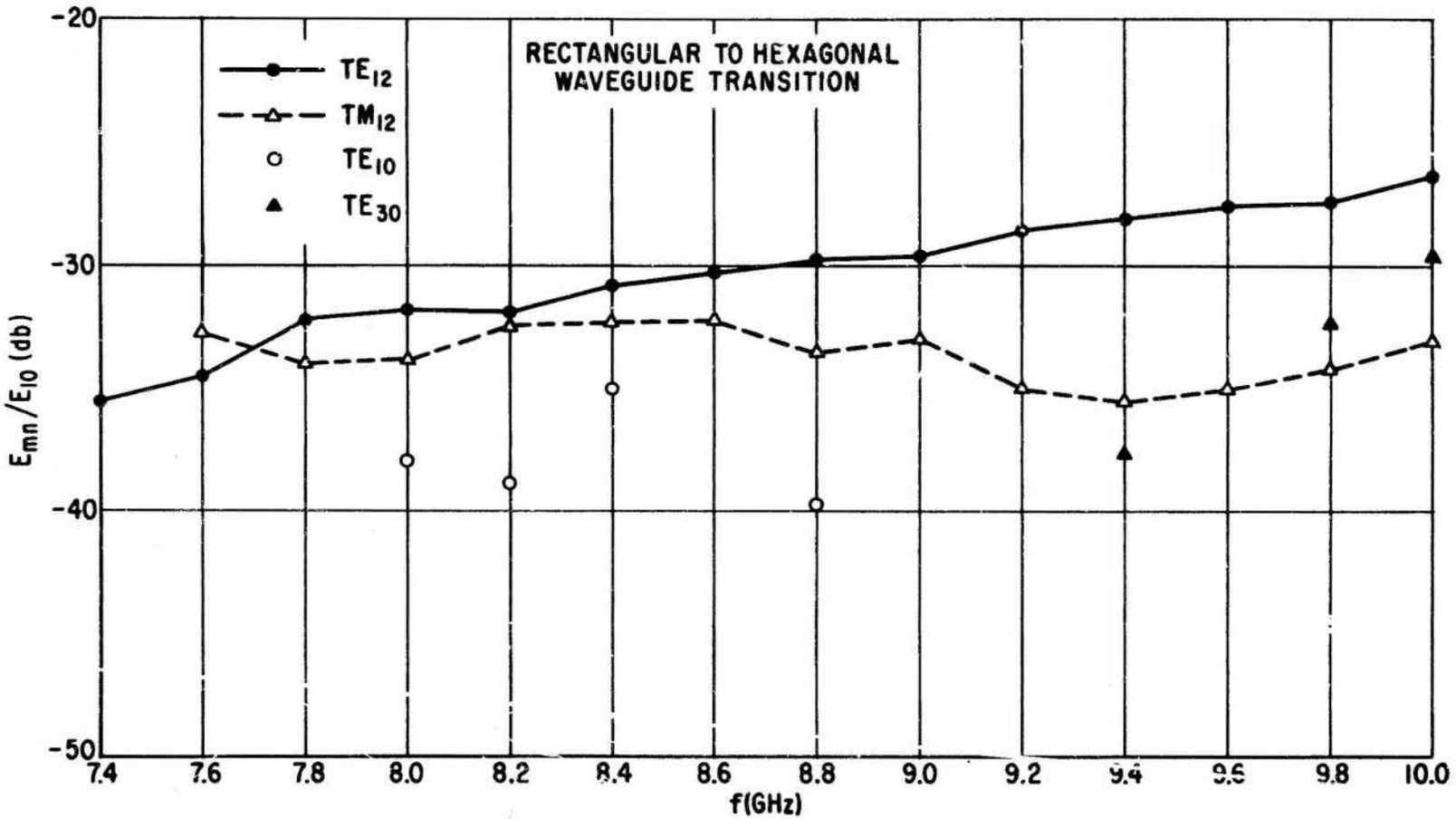

FIGURE 3.9 MEASURED SPURIOUS MODE CONVERSION FOR SINGLE 7" TRANSITION

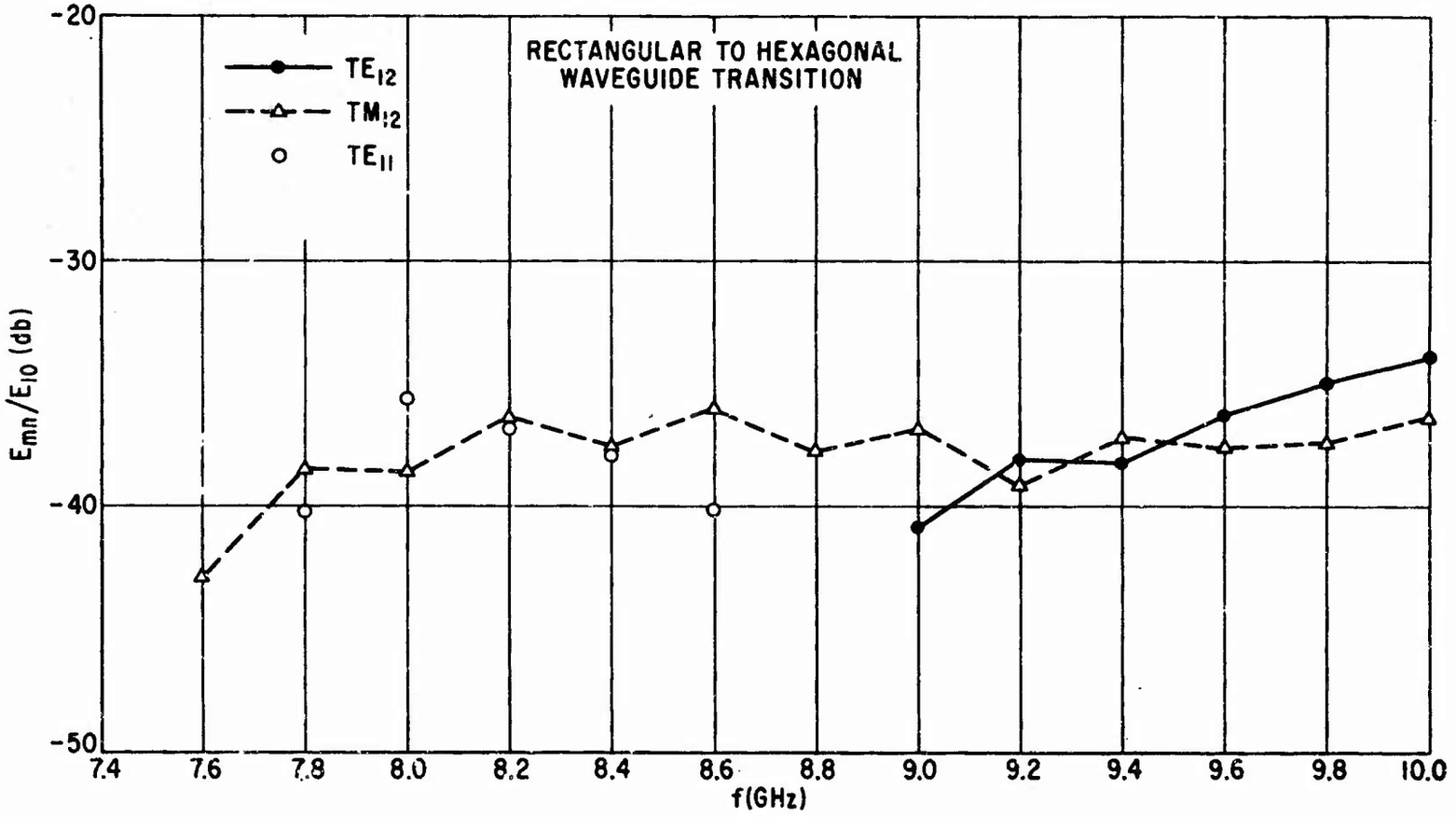

FIGURE 3.10 MEASURED SPURIOUS MODE CONVERSION FOR SINGLE 10" TRANSITION

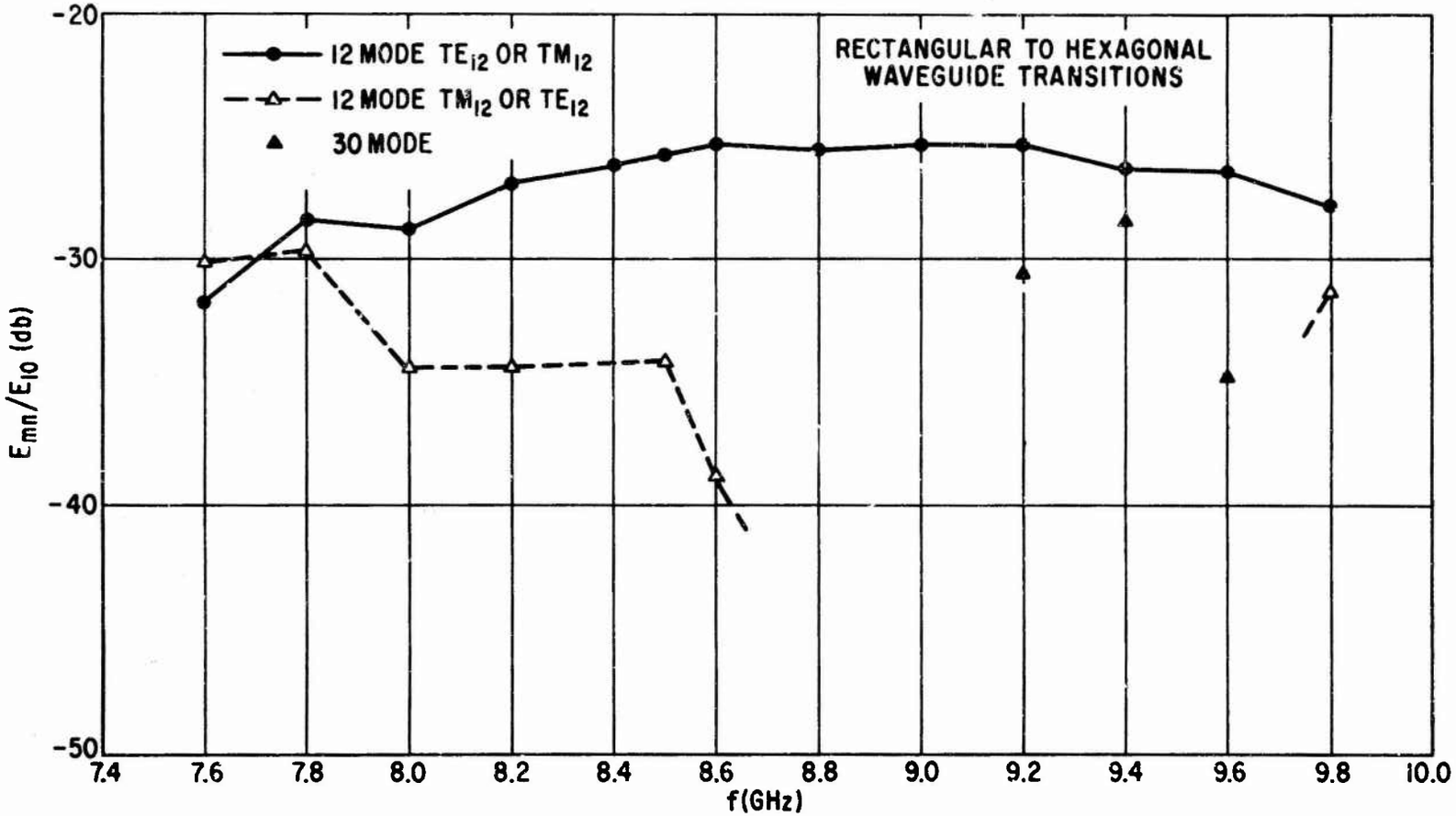

FIGURE 3.11 MEASURED SPURIOUS MODE CONVERSION FOR PAIR OF 7" TRANSITIONS

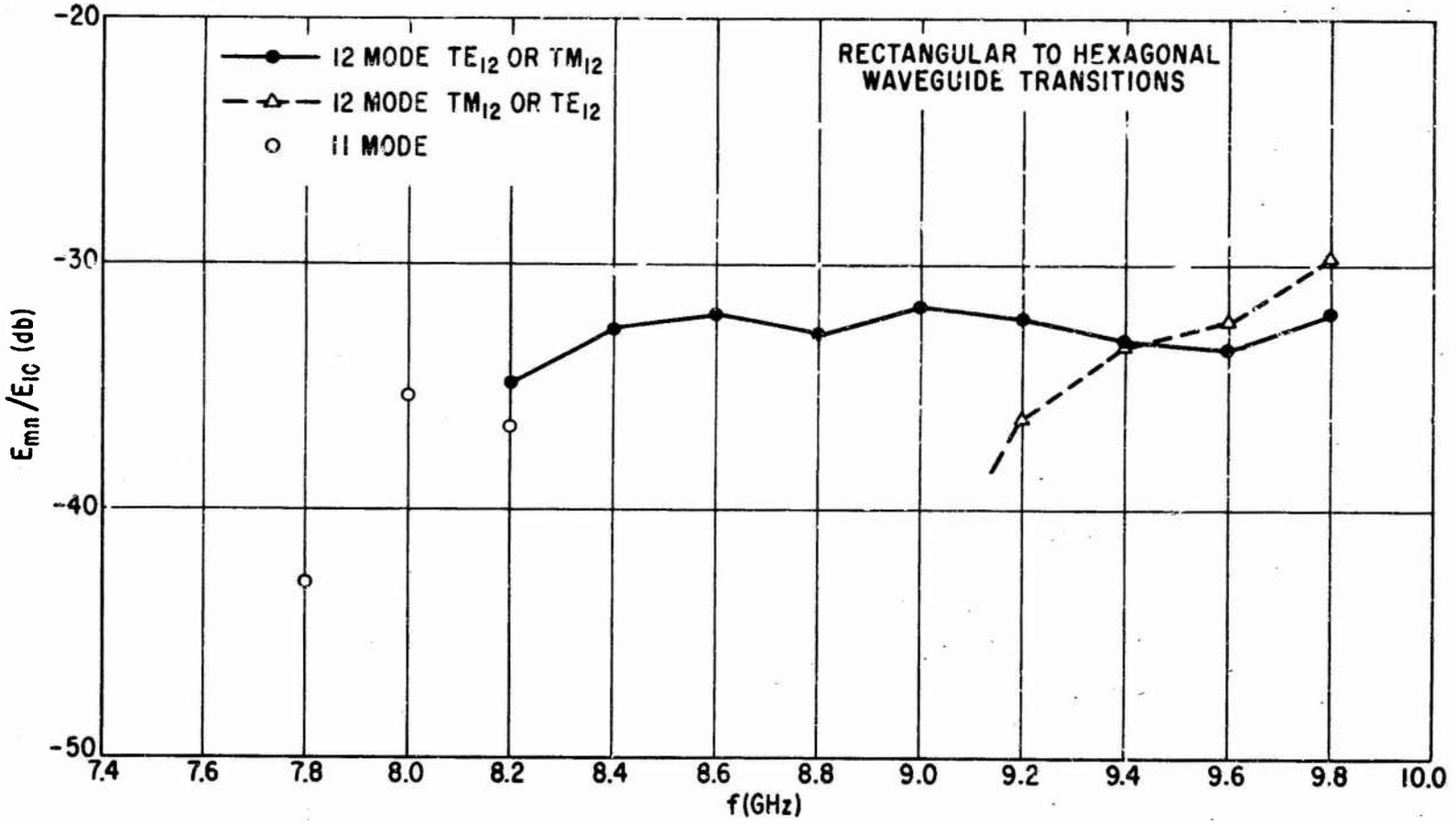

FIGURE 3.12 MEASURED SPURIOUS MODE CONVERSION FOR PAIR OF 10" TRANSITIONS

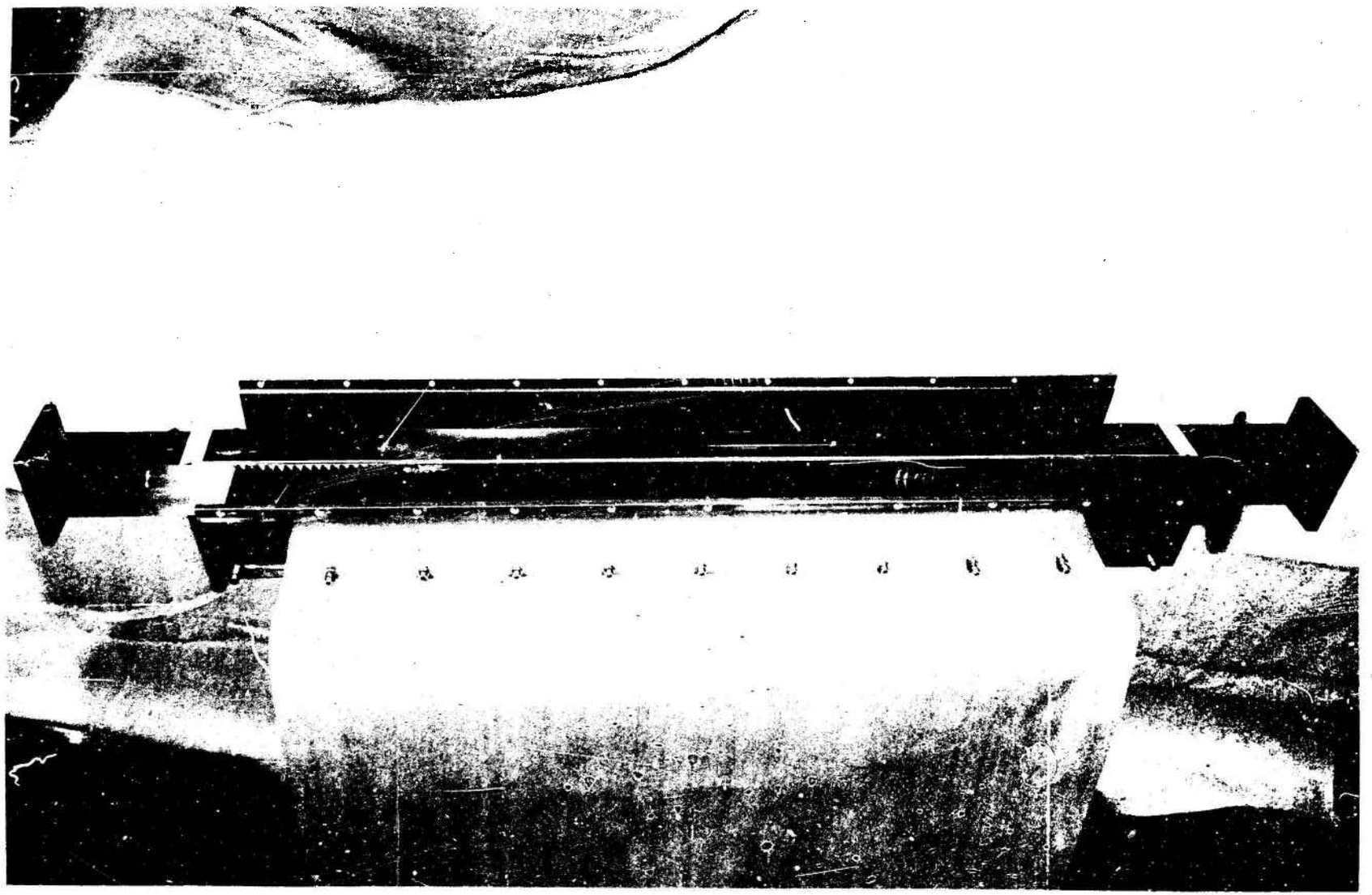

Figure 3.13. Partial Assembly of Slotted Rectangular Waveguide and Absorbing Loads.

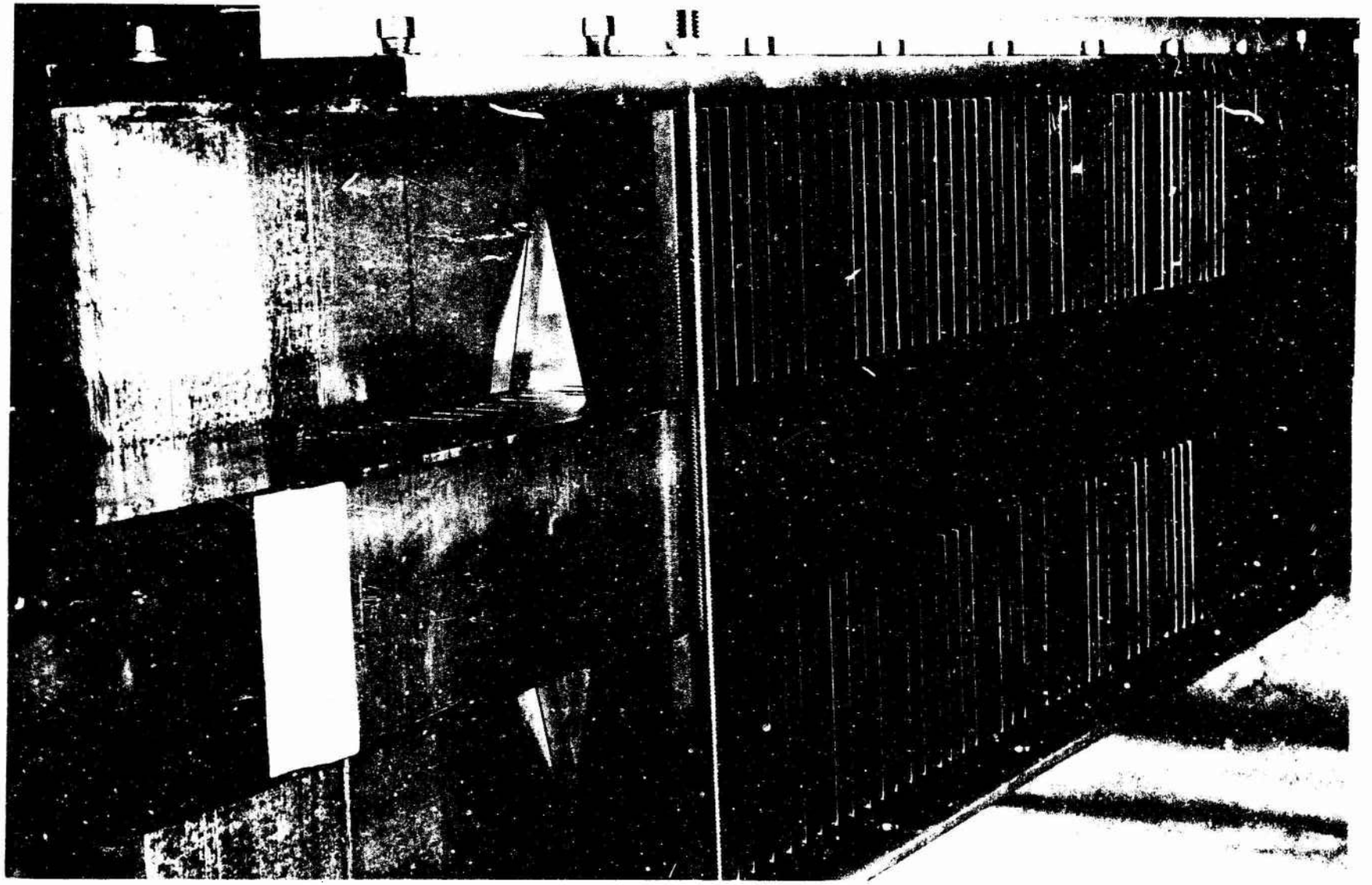

Figure 3.14. Close-up view of Slotted Rectangular Waveguide and Absorbing Loads.

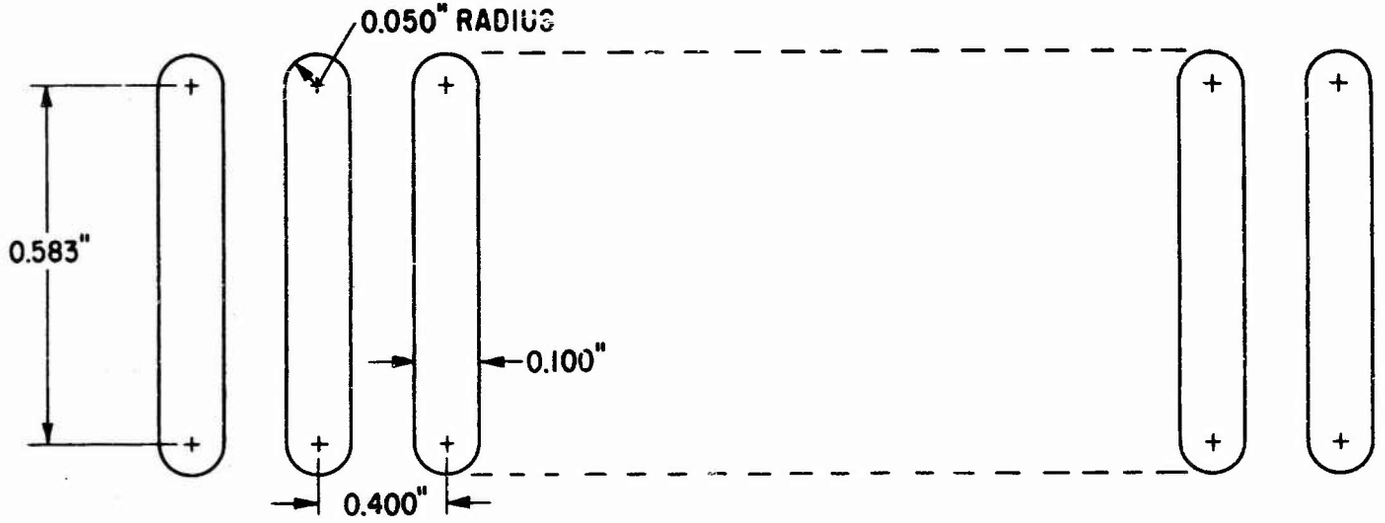

FIGURE 3.15 DIMENSIONS OF RESONANT SLOTS

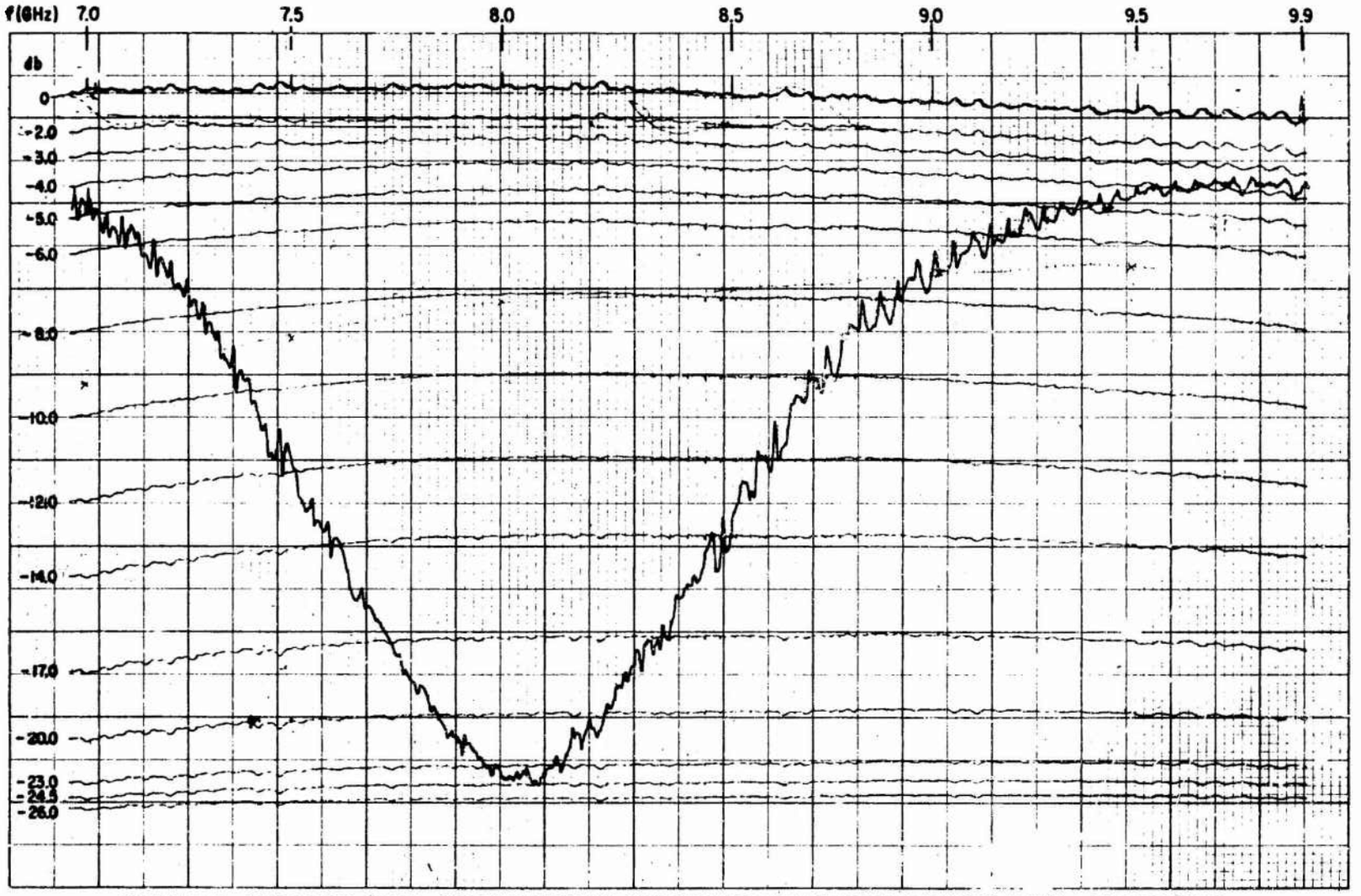

FIGURE 3.16 ABSORPTION OF TE_{10} MODE IN OVERSIZED RECTANGULAR WAVEGUIDE BY RESONANT SLOTS – 25 SLOT PAIRS

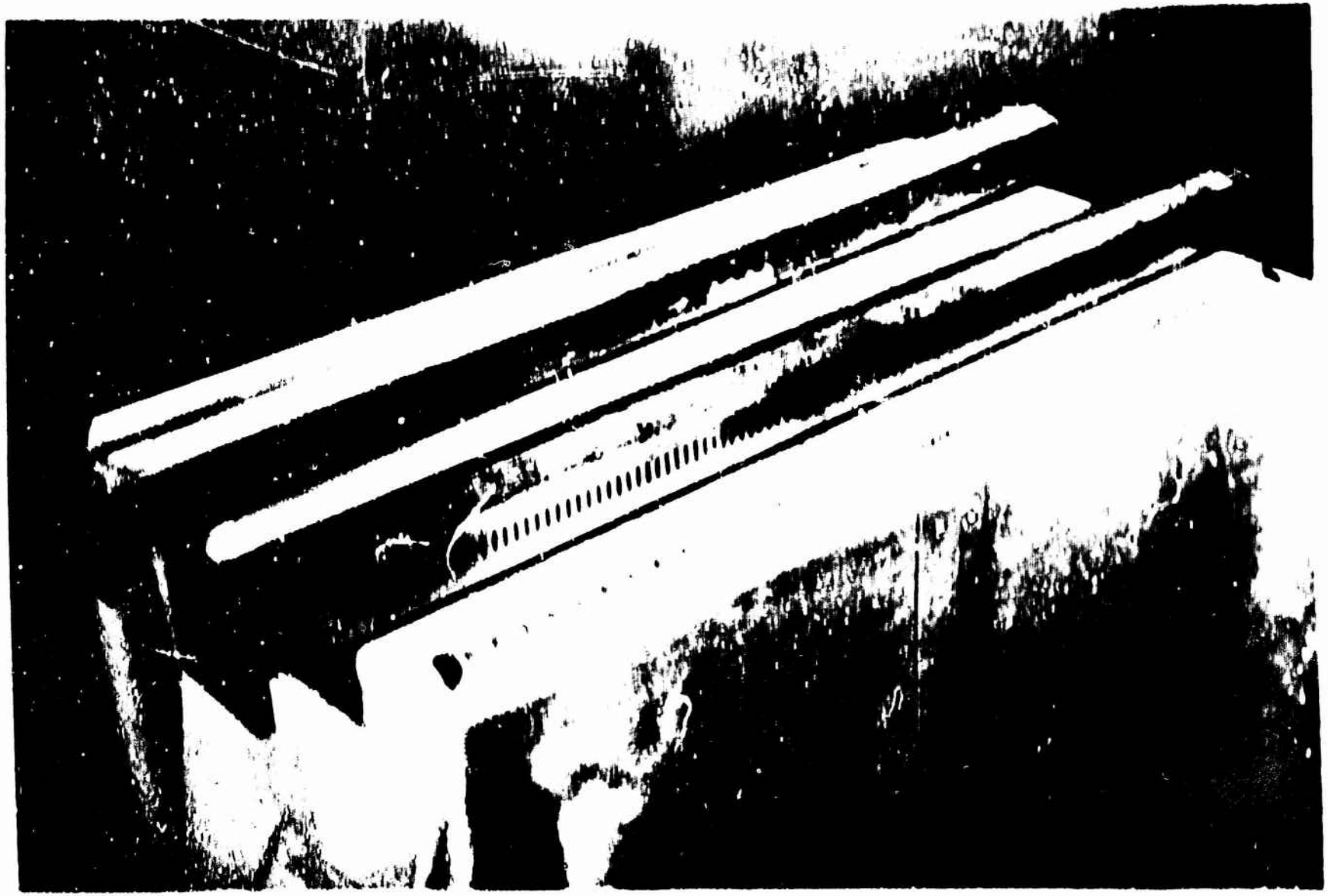

Figure 3.17. Electroformed Hexagonal Waveguides.

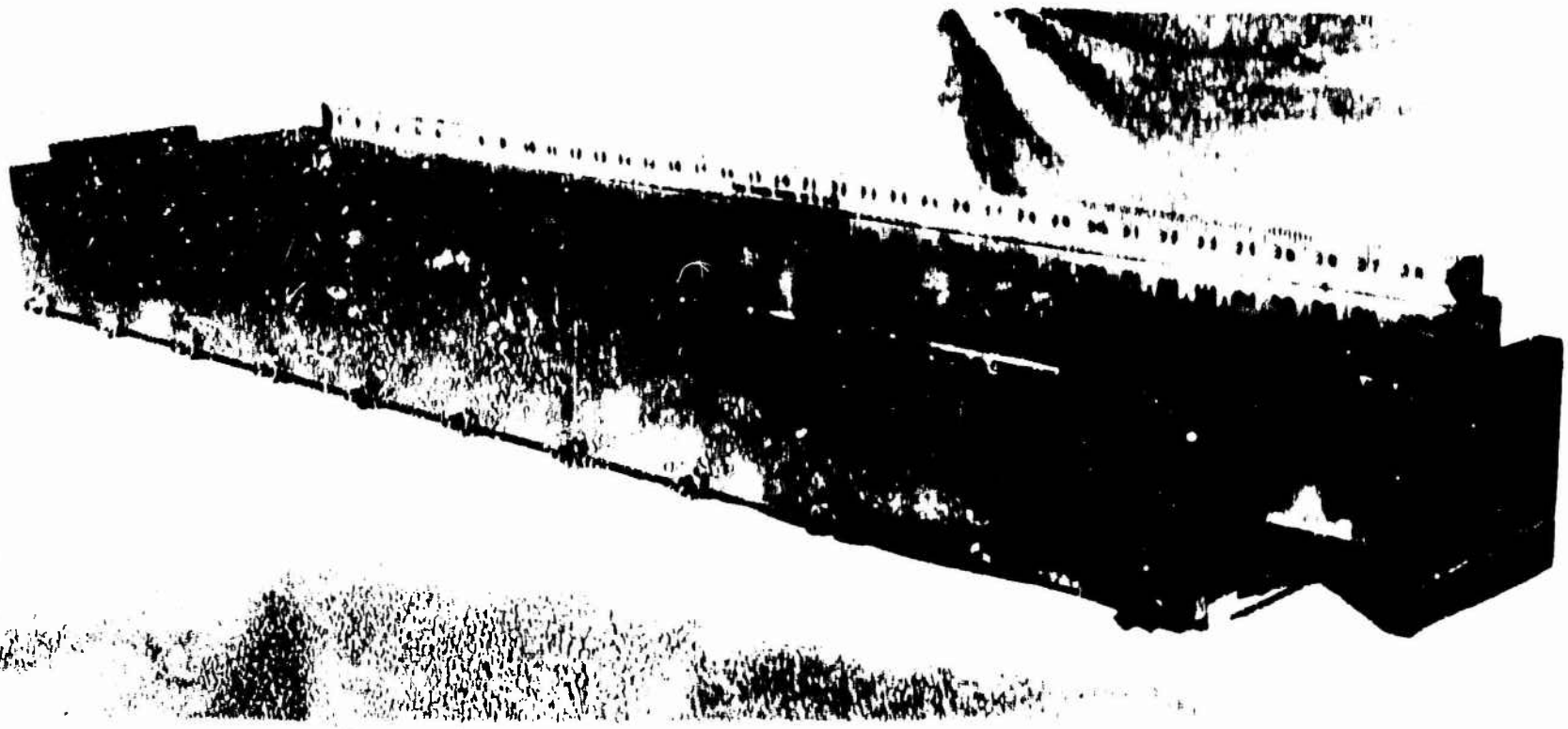

Figure 3.11. Hexagonal Waveguide Mode Absorber Assembly.

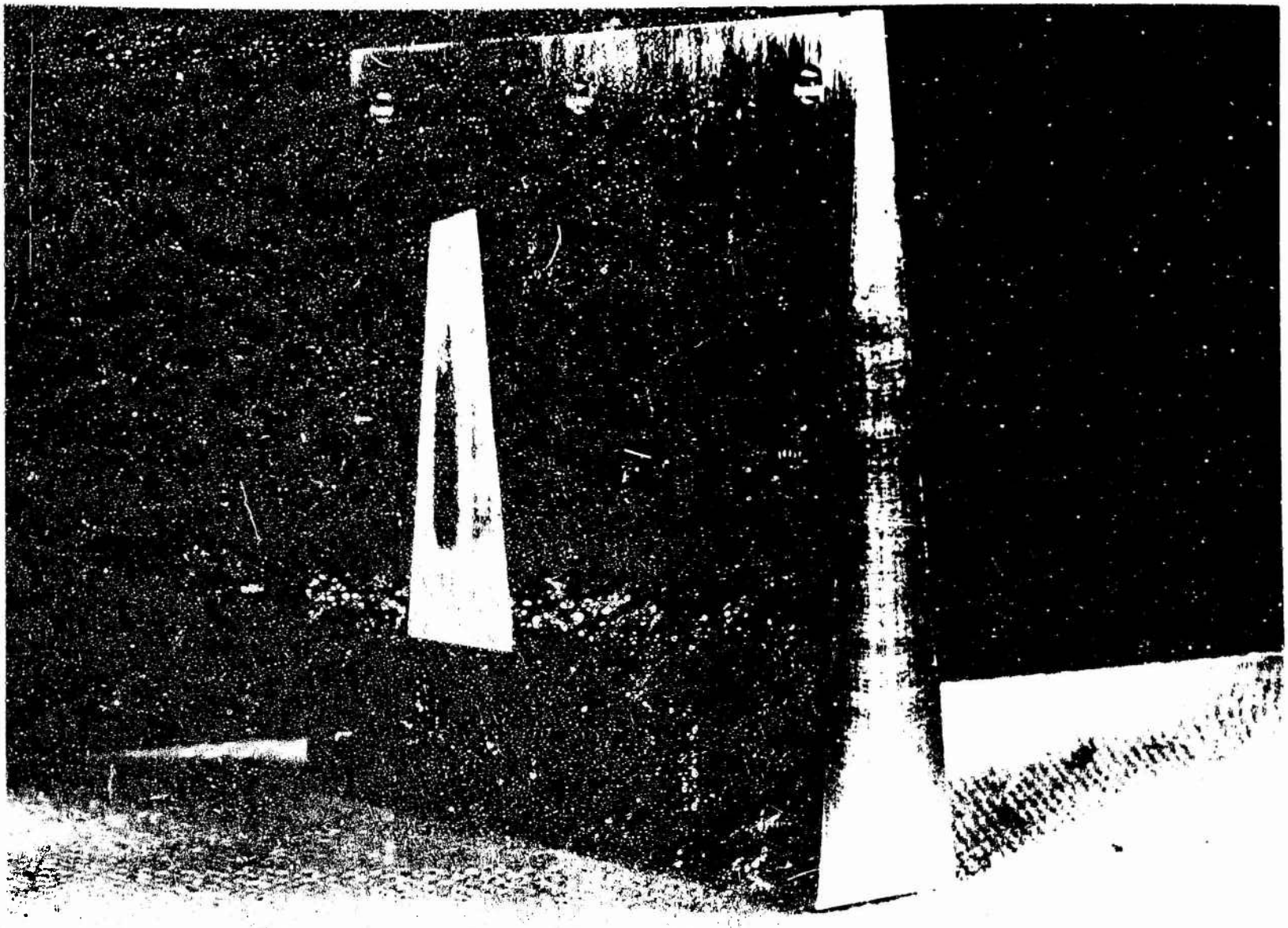

Figure 3.19. E-Plane Wedge for Spurious Mode Generation.

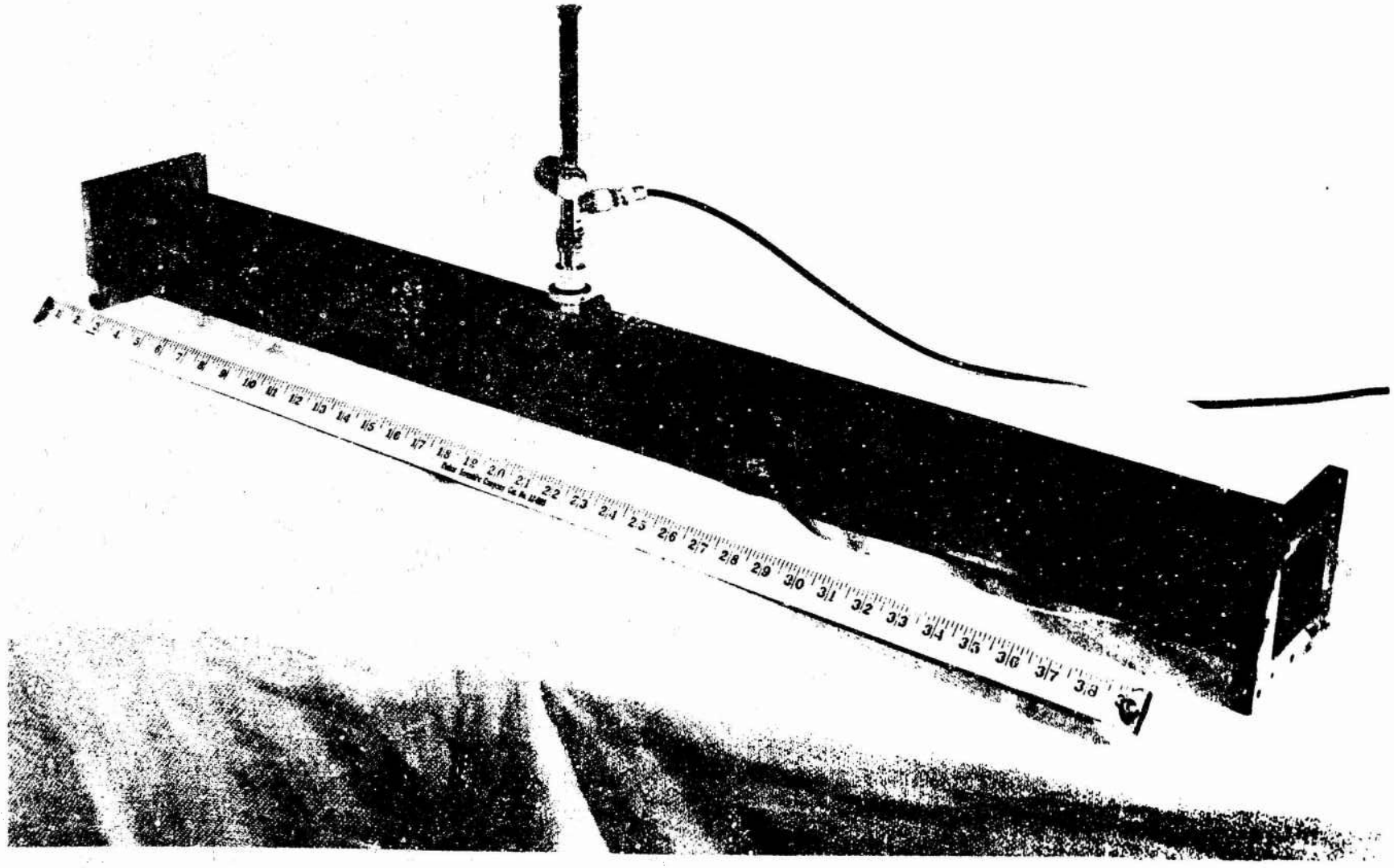

Figure 3.20. Holey Top Wall Waveguide for Field Probing.

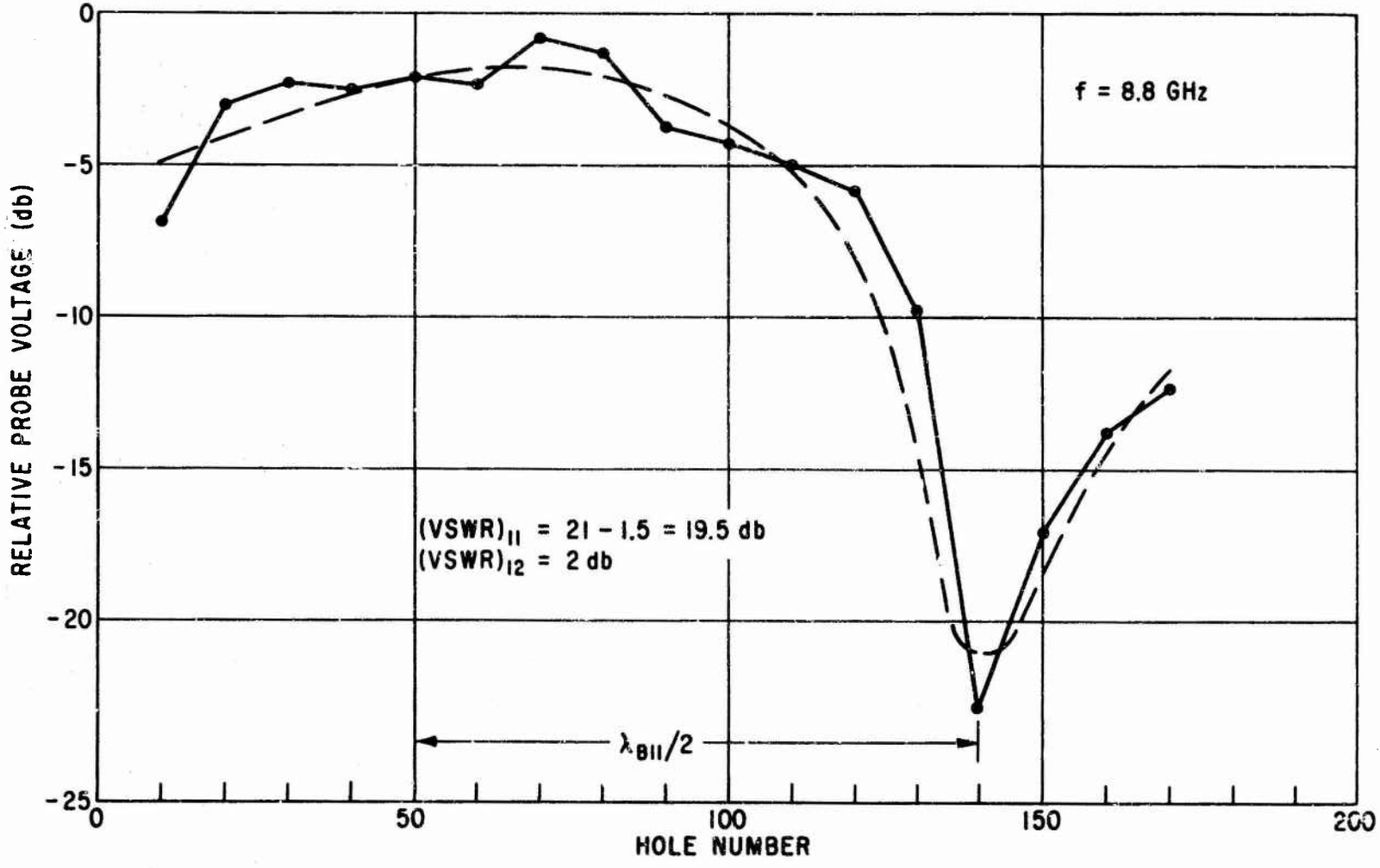

FIGURE 3.21 RELATIVE PROBE VOLTAGE - MODE ABSORBER REMOVED

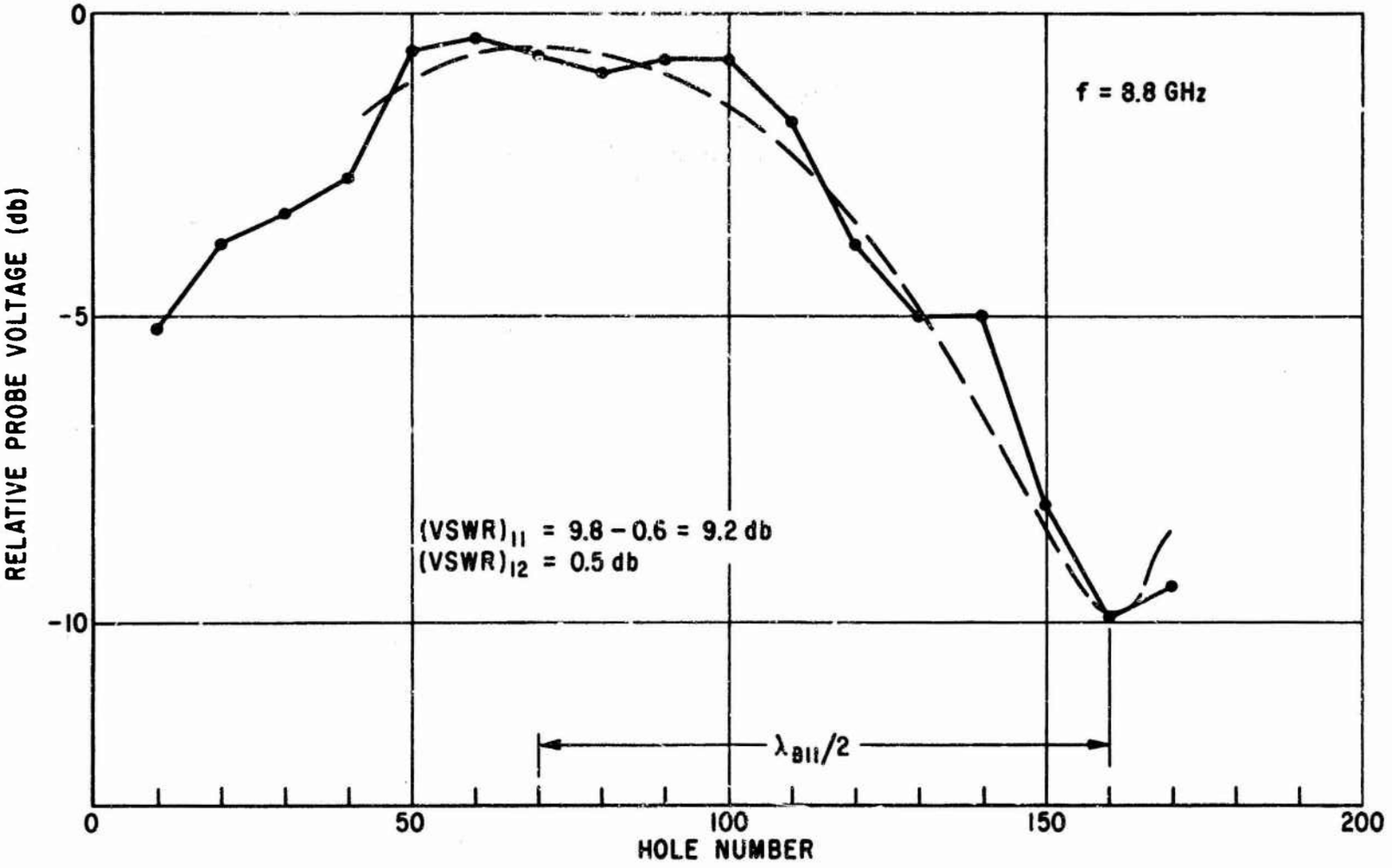

FIGURE 3.22 RELATIVE PROBE VOLTAGE – MODE ABSORBER IN PLACE WITH 100 SLOTS EXPOSED

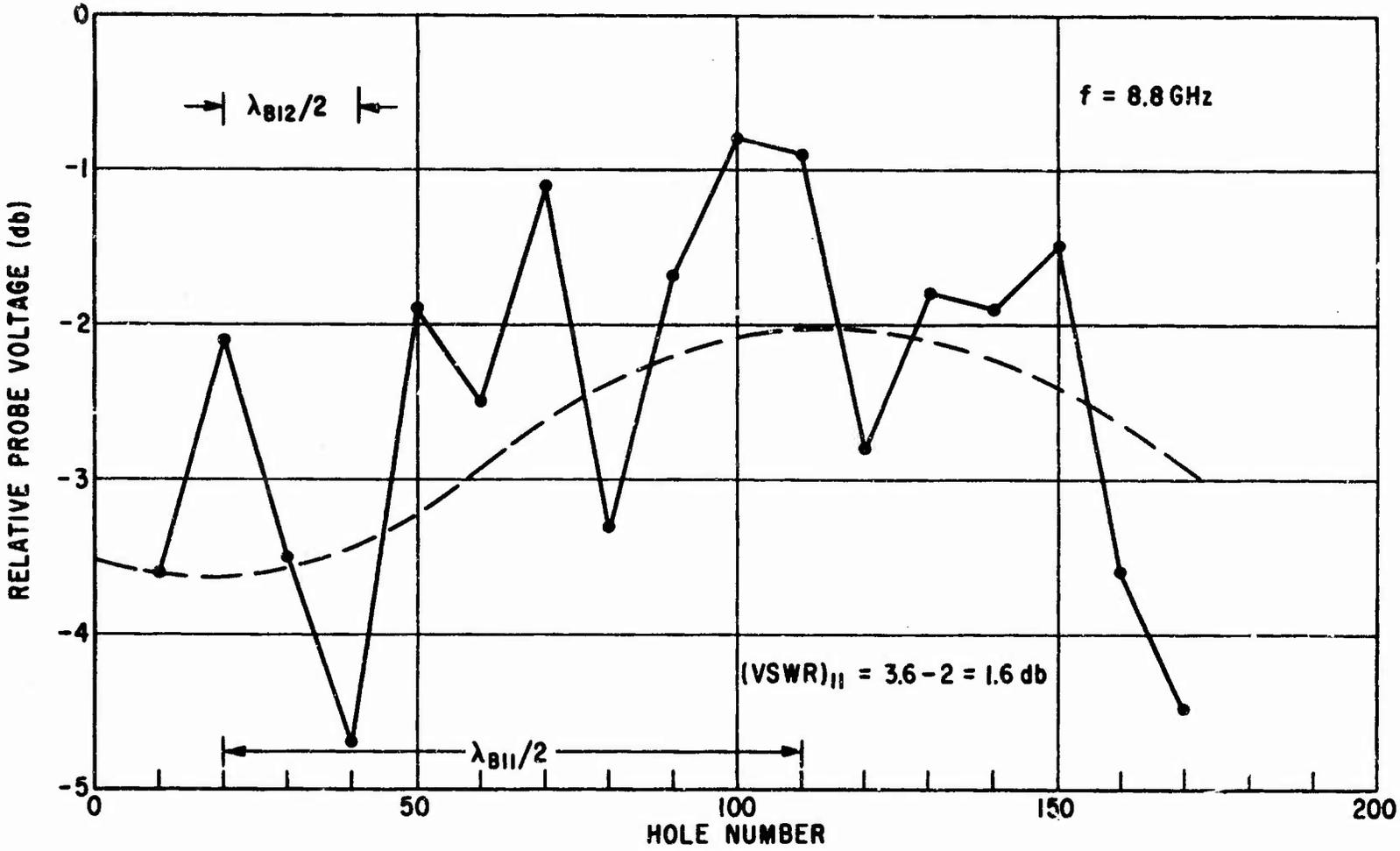

FIGURE 3.23 RELATIVE PROBE VOLTAGE - MODE ABSORBER IN PLACE WITH 50 SLOTS EXPOSED

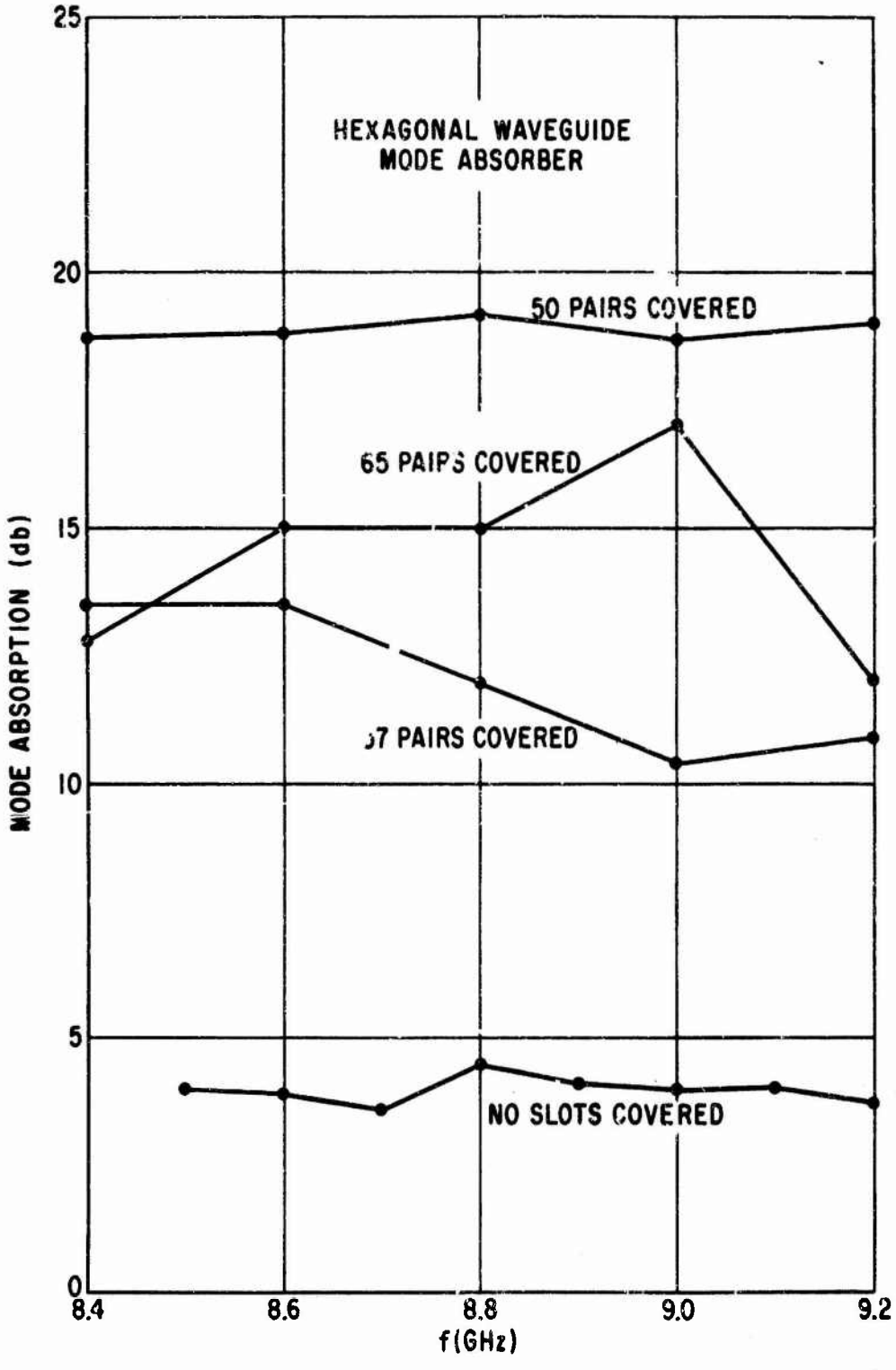

FIGURE 3.24 MEASURED ABSORPTION OF TE_{11}/TM_{11} TOPWALL SPURIOUS MODE PAIR

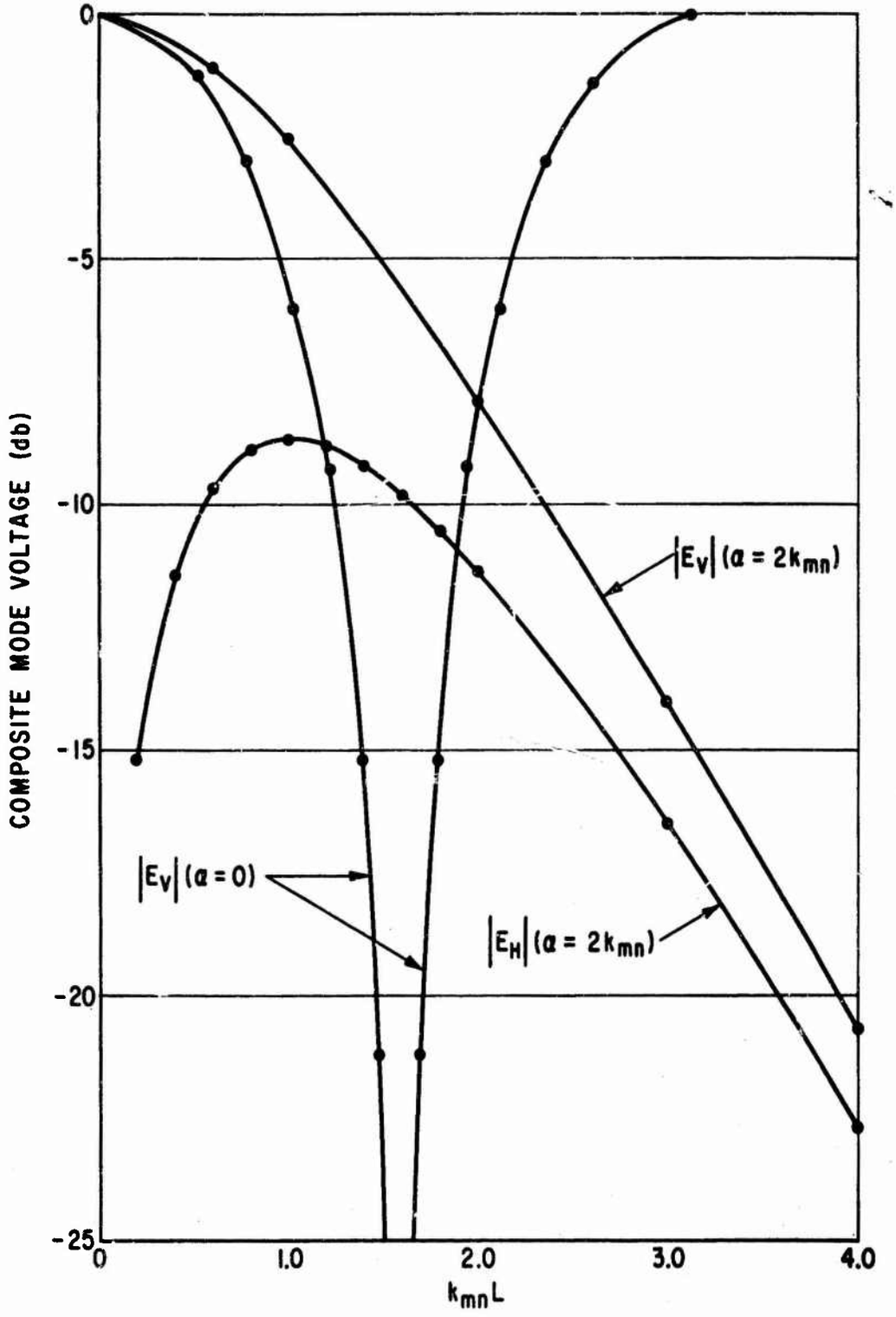

FIGURE 3.25 VARIATION OF COMPOSITE MODE VOLTAGES ALONG LENGTH OF HEXAGONAL WAVEGUIDE

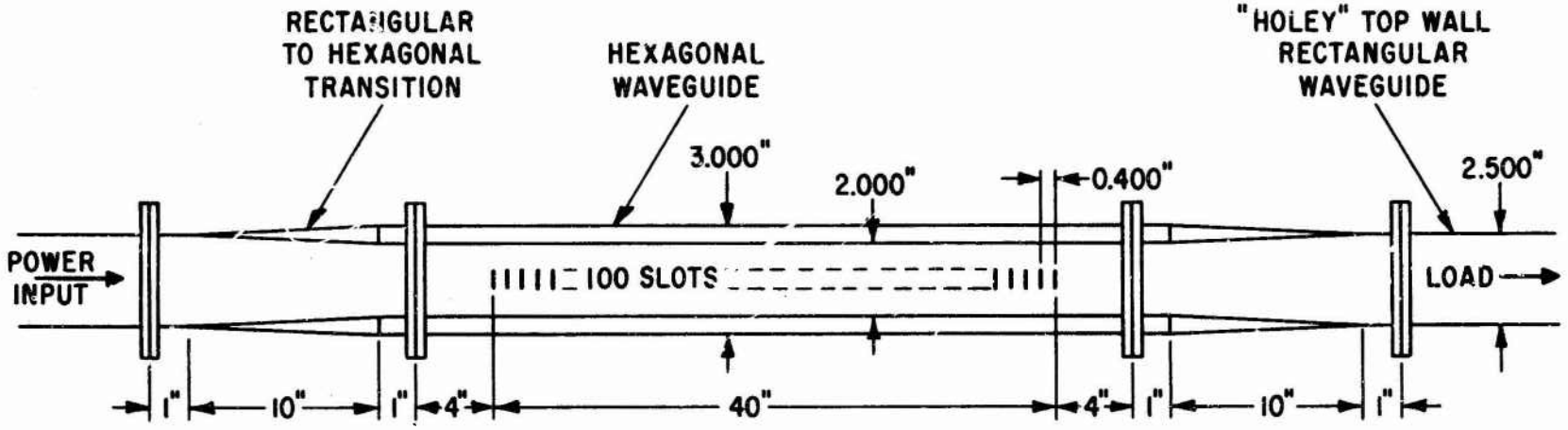

FIGURE 3.26 COMPONENT DIMENSIONS FOR MODE ABSORBER EXPERIMENTS

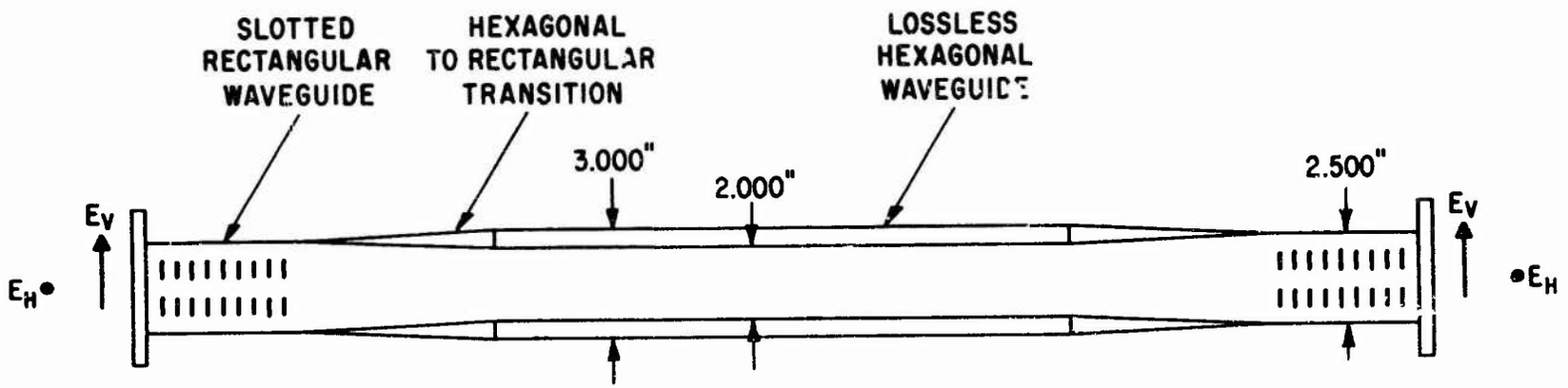

FIGURE 3.27 CONFIGURATION FOR MODE ABSORBER FOR TE_{mn}, TM_{mn} MODES EMPLOYING LOSSLESS HEXAGONAL WAVEGUIDE

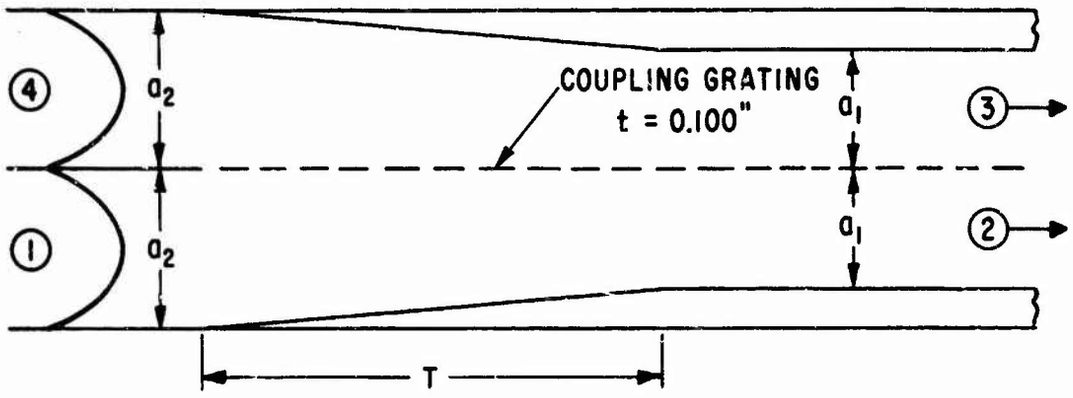

(a) INCIDENT EVEN MODE IN INPUT WAVEGUIDE

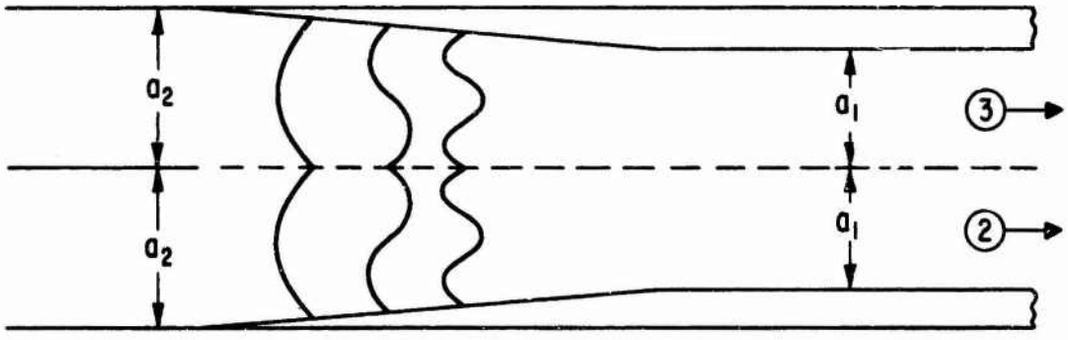

(b) EVEN MODES IN TAPER REGION - LOOSE COUPLING CONDITIONS

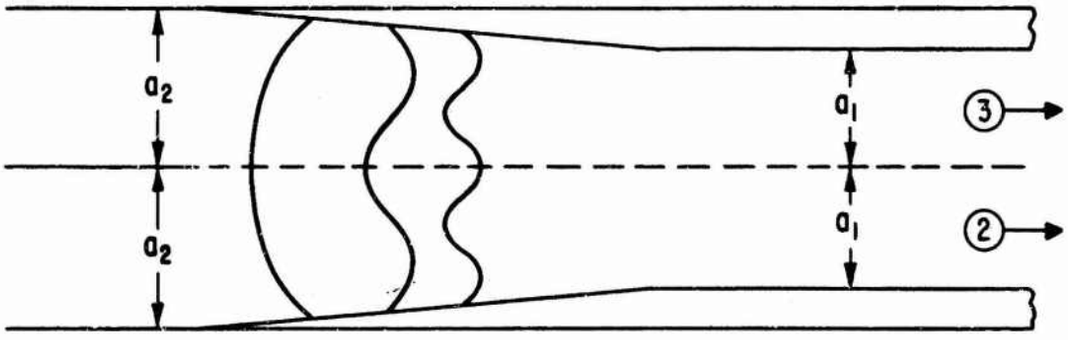

(c) EVEN MODES IN TAPER REGION - TIGHT COUPLING CONDITIONS

FIGURE A1 EVEN MODES IN TAPERED COUPLER

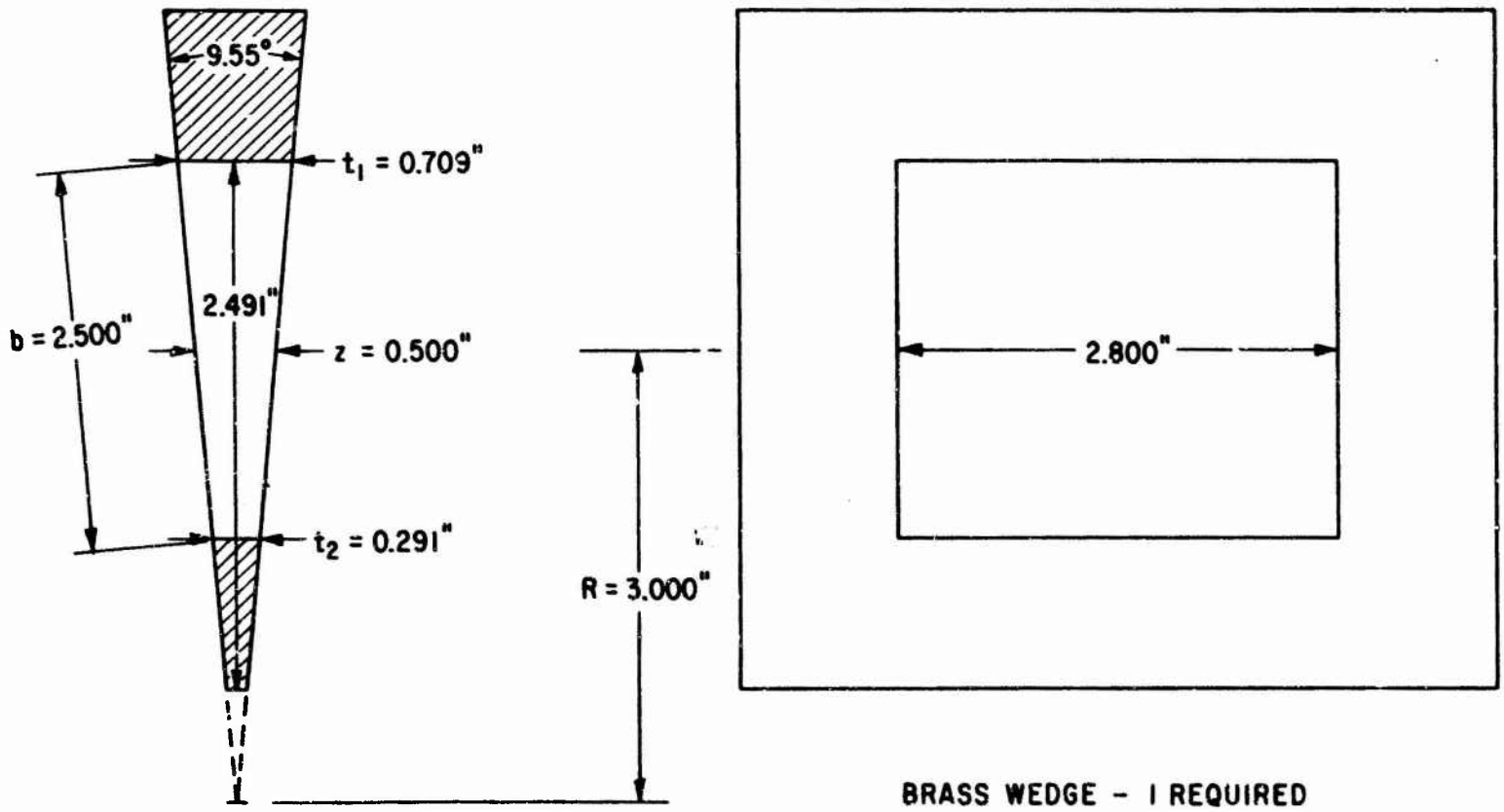

FIGURE A3 TE_{mn}, TM_{mn} MODE GENERATING WEDGE

Unclassified

Security Classification

DOCUMENT CONTROL DATA - R&D

(Security classification of title, body of abstract and indexing annotation must be entered when the overall report is classified)

1. ORIGINATING ACTIVITY (Corporate author)
General Electric Company
Schenectady, NY and Heavy Military Electronics Department
Syracuse, New York

2a. REPORT SECURITY CLASSIFICATION
Unclassified

3. REPORT TITLE

HIGH POWER MICROWAVE COMPONENTS IN OVERSIZED WAVEGUIDE

4. DESCRIPTIVE NOTES (Type of report and inclusive dates)
Interim, 17 Sep 65 to 17 Mar 66.

5. AUTHOR(S) (Last name, first name, initial)
Quine, John P.
Younger, Cousby
Jarek, J. J.

6. REPORT DATE	7a. TOTAL NO. OF PAGES	7b. NO. OF REFS
June 1966	116	13

8a. CONTRACT OR GRANT NO.	9a. ORIGINATOR'S REPORT NUMBER(S)
AF30(602)-3682	
b. PROJECT NO. 4506	
c. Task No. 450602	9b. OTHER REPORT NO(S) (Any other numbers that may be assigned this report)
d.	RADC-TR-66-305

10. AVAILABILITY/LIMITATION NOTICES
This document is subject to special export controls and each transmittal to foreign governments or foreign nationals may be made only with prior approval of RADC (EMATE).

11. SUPPLEMENTARY NOTES	12. SPONSORING MILITARY ACTIVITY
RADC Project Engineer Vincent C. Vannicola, 330-4251	Rome Air Development Center Techniques Branch (EMATE) Griffiss AFB, NY 13440

13. ABSTRACT

The purpose of this investigation is to develop components for oversized waveguide configurations for which a/λ and b/λ are in the range of 1.5 - 2.25 for the TE_{10} mode in rectangular waveguide and where D/λ is at least 1.7 for the TE_{01} mode in circular waveguide. The components considered shall include E- and H-plane bends, mode absorbers, 3 db directional couplers, pressure windows, resonant rings and rotary joints. Where necessary, the theoretical and computer studies shall be verified before design data is finalized. These components may be developed through whatever design concepts are necessary to assure high peak and high average power. The present report presents experimental results at X-band for -3 db multihole side wall directional couplers. These couplers employ tapers along the coupling region to reduce the waveguide width from 2.800" to 2.050". The reduction in width is necessary in order to increase the coupling per unit length. In this way a -3 db coupler having a length equal to 45" can be obtained. A method is described for cancelling the mode conversion caused by the tapers by means of metal and dielectric wedges placed on the side walls. Experimental results are presented for an X-band mode absorber in which the TE_{30} mode in the 2.800" wide oversized waveguide is coupled to 0.933" wide waveguide by means of side wall slots. Experimental results are also presented for a mode absorber for the TE_{mn}, TM_{mn} degenerate mode pairs. In this case a length of waveguide having an hexagonal cross section is employed to remove the degeneracy.

DD FORM 1 JAN 64 1473

Unclassified

Security Classification

Unclassified
Security Classification

14. KEY WORDS	LINK A		LINK B		LINK C	
	ROLE	WT	ROLE	WT	ROLE	WT
High Power Microwave Components Oversized Waveguide						

INSTRUCTIONS

1. ORIGINATING ACTIVITY: Enter the name and address of the contractor, subcontractor, grantee, Department of Defense activity or other organization *(corporate author)* issuing the report.

2a. REPORT SECURITY CLASSIFICATION: Enter the overall security classification of the report. Indicate whether "Restricted Data" is included. Marking is to be in accordance with appropriate security regulations.

2b. GROUP: Automatic downgrading is specified in DoD Directive 5200.10 and Armed Forces Industrial Manual. Enter the group number. Also, when applicable, show that optional markings have been used for Group 3 and Group 4 as authorized.

3. REPORT TITLE: Enter the complete report title in all capital letters. Titles in all cases should be unclassified. If a meaningful title cannot be selected without classification, show title classification in all capitals in parenthesis immediately following the title.

4. DESCRIPTIVE NOTES: If appropriate, enter the type of report, e.g., interim, progress, summary, annual, or final. Give the inclusive dates when a specific reporting period is covered.

5. AUTHOR(S): Enter the name(s) of author(s) as shown on or in the report. Enter last name, first name, middle initial. If military, show rank and branch of service. The name of the principal author is an absolute minimum requirement.

6. REPORT DATE: Enter the date of the report as day, month, year; or month, year. If more than one date appears on the report, use date of publication.

7a. TOTAL NUMBER OF PAGES: The total page count should follow normal pagination procedures, i.e., enter the number of pages containing information.

7b. NUMBER OF REFERENCES: Enter the total number of references cited in the report.

8a. CONTRACT OR GRANT NUMBER: If appropriate, enter the applicable number of the contract or grant under which the report was written.

8b, 8c, & 8d. PROJECT NUMBER: Enter the appropriate military department identification, such as project number, subproject number, system numbers, task number, etc.

9a. ORIGINATOR'S REPORT NUMBER(S): Enter the official report number by which the document will be identified and controlled by the originating activity. This number must be unique to this report.

9b. OTHER REPORT NUMBER(S): If the report has been assigned any other report numbers *(either by the originator or by the sponsor)*, also enter this number(s).

10. AVAILABILITY/LIMITATION NOTICES: Enter any limitations on further dissemination of the report, other than those imposed by security classification, using standard statements such as:

(1) "Qualified requesters may obtain copies of this report from DDC."

(2) "Foreign announcement and dissemination of this report by DDC is not authorized."

(3) "U. S. Government agencies may obtain copies of this report directly from DDC. Other qualified DDC users shall request through

_____."

(4) "U. S. military agencies may obtain copies of this report directly from DDC. Other qualified users shall request through

_____."

(5) "All distribution of this report is controlled. Qualified DDC users shall request through

_____."

If the report has been furnished to the Office of Technical Services, Department of Commerce, for sale to the public, indicate this fact and enter the price, if known.

11. SUPPLEMENTARY NOTES: Use for additional explanatory notes.

12. SPONSORING MILITARY ACTIVITY: Enter the name of the departmental project office or laboratory sponsoring *(paying for)* the research and development. Include address.

13. ABSTRACT: Enter an abstract giving a brief and factual summary of the document indicative of the report, even though it may also appear elsewhere in the body of the technical report. If additional space is required, a continuation sheet shall be attached.

It is highly desirable that the abstract of classified reports be unclassified. Each paragraph of the abstract shall end with an indication of the military security classification of the information in the paragraph, represented as *(TS), (S), (C), or (U)*.

There is no limitation on the length of the abstract. However, the suggested length is from 150 to 225 words.

14. KEY WORDS: Key words are technically meaningful terms or short phrases that characterize a report and may be used as index entries for cataloging the report. Key words must be selected so that no security classification is required. Identifiers, such as equipment model designation, trade name, military project code name, geographic location, may be used as key words but will be followed by an indication of technical context. The assignment of links, rules, and weights is optional.

SUPPLEMENTARY

INFORMATION

RADC-TR-66-305 June 1966

ERRATA - June 1967

The following corrections should be made to the Second Progress Report on AF 30(602)-3682, entitled "Ultra High Power Transmission Line Techniques."

1. In Figures 2.14a, 2.15, 2.16, 2.17, 2.18, 2.19, 2.20 and in the last line on page 8, change 0.147 sin $\frac{\pi z}{L}$ to 0.0147 sin $\frac{\pi z}{L}$.

2. Page 28 - Second line above equation 3.5 should read ---- be equal to $\Delta\beta/2$ where $\Delta\beta$ is the difference in the propagation constants of the ----.